Design, Synthesis and Applications of Dumbbell-Shaped Bipyridines as Ligands for Transition Metal Catalysis

ダンベル型ビピリジン配位子の設計、合成および遷移金属触媒反応への応用

Yongjoon Kim

2021

Contents

General Introduction

1. 2,2'-Bipyridine and 1,10 phenanthroline ligands

2,2'-bipyridine (bpy), 1,10 phenanthroline (phen) and their ring substituted derivates are classical chelating bidentate ligands, and they have been used in various field of coordination chemistry (Figure 1).[1,2] Bpy and Phen ligands have similar coordination properties, and both ligands form stable 5-membered ring with various transition metals through the biding of N,N'-chelating atoms. Bpy is slightly stronger σ-donor than phen because of the electron poor characteristic of phen heteroaromatic rings. Phen, however, binds metals more strongly than bpy since chelating nitrogen donors are preorganized. Both ligands have delocalized aromatic π* LUMO orbitals and act as a π-acceptor. In addition they are redox active ligands, and the metal-to-ligand charge transfer (MLCT) in their metal complexes is well studied in photocatalysis and luminescent molecular sensors.[3]

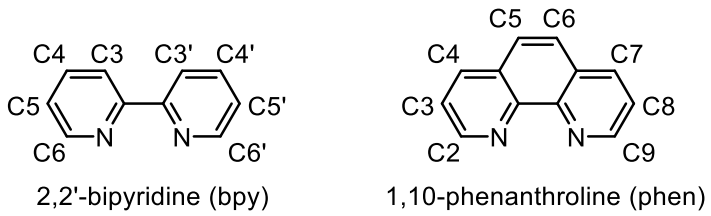

Figure 1. 2,2'-Biprydine and 1,10-phenanthrolines

1.1. Bpy and phen derivatives

Bpy and phen ligands have been widely used in various transition metal catalysis. Pursuing better catalytic properties of the metal complexes, they have been modified by introducing various substituents with different steric and electronic properties (Figure 2).

Bpys and phens functionalized at the N-α-positions (C6, C6' in bpy and C2, C9 in phen) are well employed in various purposes. Substituents at those positions greatly affect steric environments in the vicinity of the chelated metals. The steric hinderance in the vicinity of the nitrogen atoms, however, usually weakens stability of the complexes and makes substrate approach to the chelated metals difficult. 6,6'-Me_2bpy and 2,9-Me_2phen are often employed

in ligand screening for reaction development. The ligands with bulkier substituents such as phenyl (2,9-Ph_2phen) and mesityl (2,9-Mes_2phen) groups are often employed as well.[4] Development of the chiral bpy and phen ligands for asymmetric catalysis also have focused on functionalization of the N-α-positions.[5,6] One of the earliest examples developed by Bolm and coworkers (Figure 2, chiral bpy) was employed for the asymmetric addition of alkyl zinc reagents to aldehydes.[7]

Bpy and phen ligands functionalized at the N-β-positions (C5, C5' in bpy and C3, C8 in phen) are rarely used for catalytic applications as compared to those functionalized at the N-α- and N-γ-positions, because both steric and electronic effects are not significant in general. For a rare example, Hartwig and coworkers employed 3,8-disubstitued phenanthrolines (3,8-Mes_2phen[8] and 3,8-(3,5-$(CF_3)_2Ph)_2$phen[9]) for their application in C-H borylation reactions.

Bpys and phens functionalized at N-γ-positions (C4, C4' in bpy and C4, C7 in phen) have been well employed since these positions greatly change the electronic properties of the ligands while keeping the coordination steric properties. Frequently used examples are 4.4'-tBu_2bpy, 4,4'-$(OMe)_2$bpy and bathophenanthroline.

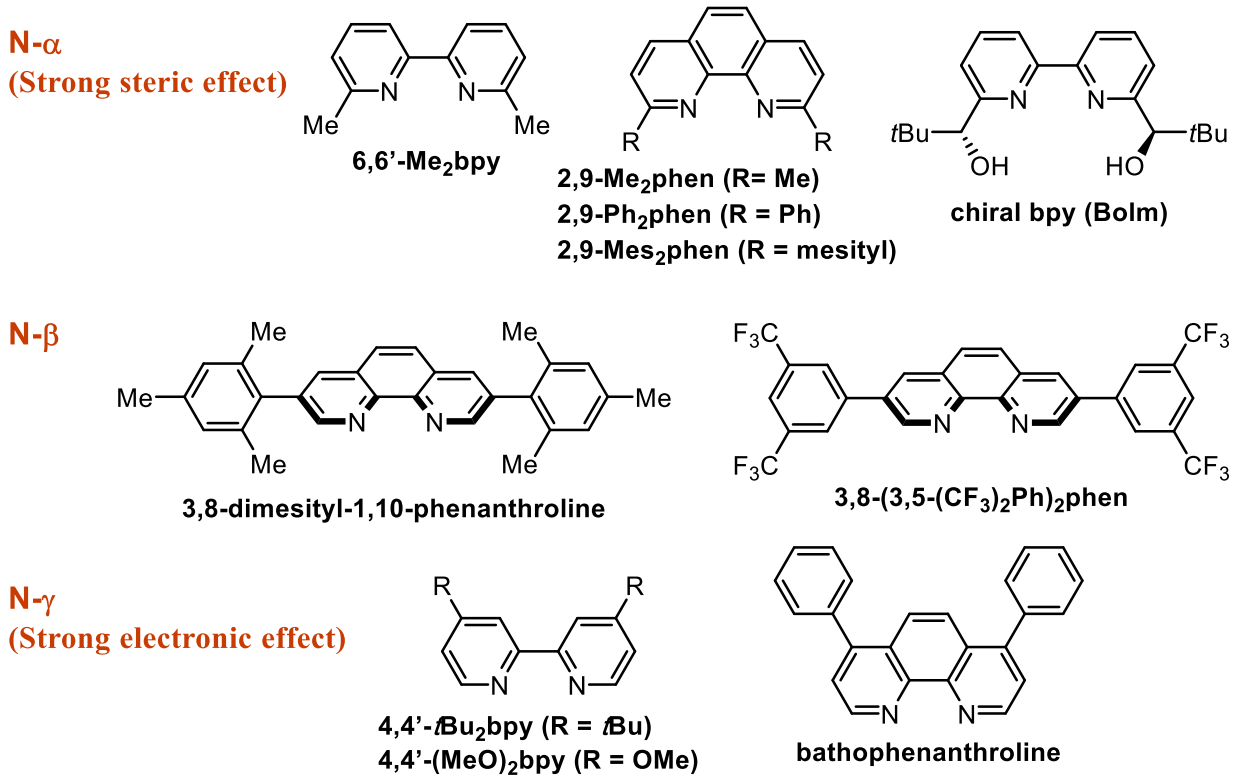

Figure 2. Examples of bpy and phen derivatives used in transition metal catalysis

1.2 Synthesis of bpy and phen derivatives

Numerous methods have been developed for the synthesis of various bpy and phen derivatives. [5, 10, 11] Among those, only a few of the synthetic methods will be briefly introduced herein. Common synthetic strategies for substituted bpys are annulation (Scheme 1, a), coupling of substituted pyridines (Scheme 1, b), and second functionalization of commercially available bipyridines (Scheme 1, c). The classic Kröhnke pyridine synthesis is well employed for the annulation method, where the 1,5-diketone intermediate produced by Michael addition cyclizes in the presence of NH_4OAc. 4,4'-*t*Bu_2bpy was traditionally synthesized by dehydrogenative homocoupling of 4-*t*Bu-pyridines[12], while Ullmann homocoupling of 4-*t*Bu-2-chloropyridines was also reported.[13] The chiral bpy developed by Bolm and coworkers was also synthesized by Ullmann homocoupling of the corresponding 2-halo-pyridines.[7] A chiral bipyridine, 6,6′-bis(4-(*S*/*R*)-isopropyl-2-oxazolinyl)-2,2′-bipyridine (Bipymox), was synthesized by the second functionalization of 6,6'-$(COOH)_2$bpy.[14]

The most prevalent strategies for constructing 1,10-phenanthrolines are the classic annulation reactions (Scheme 1, a) such as Friedländer reaction[15] and, Doebner-Miller reaction.[16] The second functionalization of commercially available phenanthrolines have also been well used for the synthesis of substituted phen derivatives (Scheme 1, c). 2,9-Ar_2phens were synthesized through Pd-catalyzed Suzuki cross-coupling of 2,9-Cl_2phen and arylboronic acids.[4] 3,8-Ar_2phens were synthesized through the Pd-catalyzed Negishi coupling of 3,8-Br_2phen and arylzincs.[8,9]

Scheme 1. Common synthetic methods for bipyridine and phenanthroline derivatives. a) annulation, b) Pd/Ni catalyzed homo/cross-coupling, c) second functionalization.

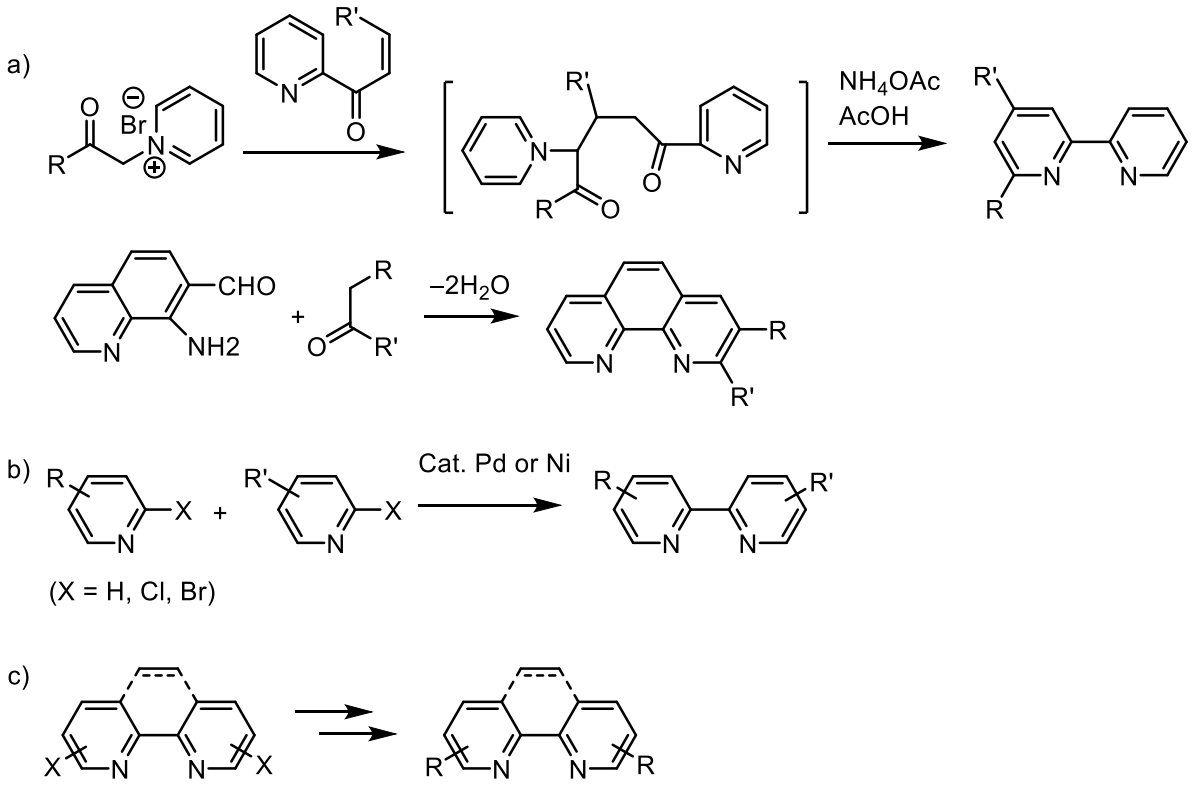

2. Bpy and phen ligands in transition metal catalysis

Bpy and phen ligands have been widely employed in numerous transition metal catalysis due to their strong chelation and interesting properties. Cu, Pd, Fe, Ni, and Ir catalyzed reactions have been well explored while many other transition metals such as Ag, Co, and etc. have also been reported. The selected examples will be briefly introduced herein.

2.1. Cu-catalyzed reactions

In 1999, Goodbrand and coworker reported ligand-accelerated catalysis of Ullmann condensation for triarylamine synthesis (Scheme 2).[17] The former method for the coupling of an aryl halide with a diphenylamine had used extremely harsh conditions in the presence of copper salt and added base.[18] The author tested phen, pyridine, bpy, racemic sparteine, 1,8-bis(dimethylamino)-naphthalene, 8-hydroxyquinoline, and *N*,*N*,*N*′,*N*′-tetramethylethylene-diamine. Among the seven ligands, phen greatly accelerated the reaction. The reaction finished in 3h at 125 ℃, which is shorter in time and significantly lower in temperature than normally

had required (6 h, 160 °C).

Scheme 2. Cu-phen catalyzed Ullmann coupling

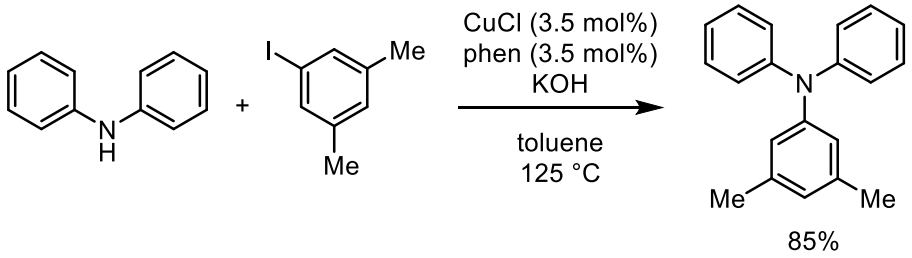

N-Arylimidazoles are important compounds for pharmaceutical research because of their significant biological activity. Ullmann-type coupling of aryl halides and imidazoles had been most commonly used for constructing C–N bonds, but usually required high temperatures and polar solvents such as DMF and NMP.[19] Hartwig and coworkers found that the use of dba (dibenzalacetone) and stoichiometric phen ligand allowed this reaction to occur in xylene at 110–125 ℃ (Scheme 3).[20]

Scheme 3. Cu-catalyzed coupling of aryl halides and imidazoles

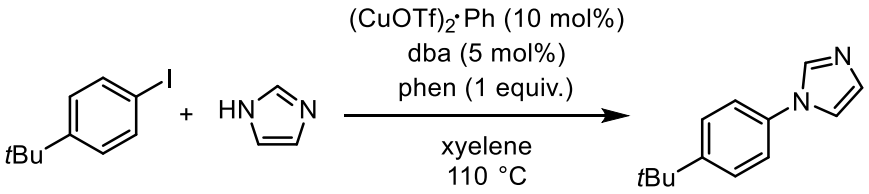

Bpy and phen type ligands have been often used in Cu-catalyzed C–O bond couplings as well. For example, Buchwald and coworkers reported O-arylation of amino alcohols using 3,4,7,8-tetramethylphenanthroline ligand (Scheme 4).[21] In this reaction, the use of the phenanthroline ligand gave O-arylated product while the use of a diketone ligand gave N-arylated product selectively.

Scheme 4. Cu-catalyzed O-arylation of amino alcohols

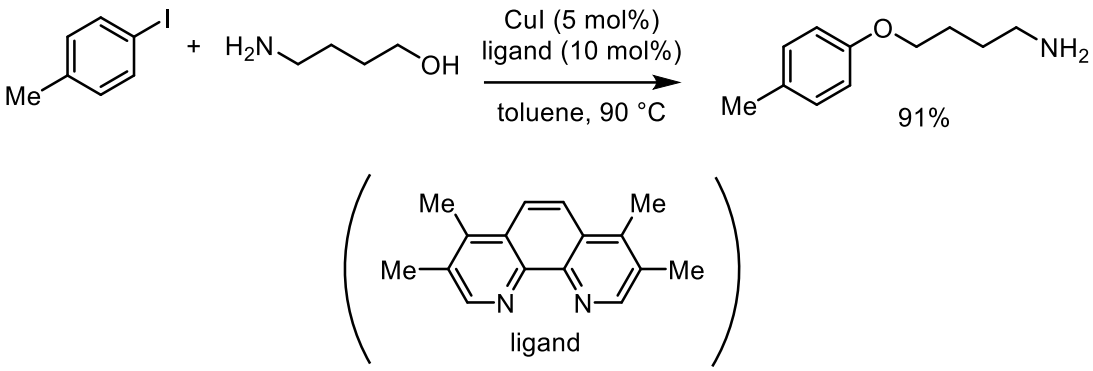

Taillefer and coworkers reported the copper-catalyzed α-arylation of benzyl phenyl ketones.[22] The author tested nine phenanthroline, dialkylamine, and diketone type ligands in the reaction development. Among them the bathophenanthroline ligand gave the best result (Scheme 5).

Scheme 5. Cu-catalyzed α-arylation of benzyl phenyl ketones with aryl iodides

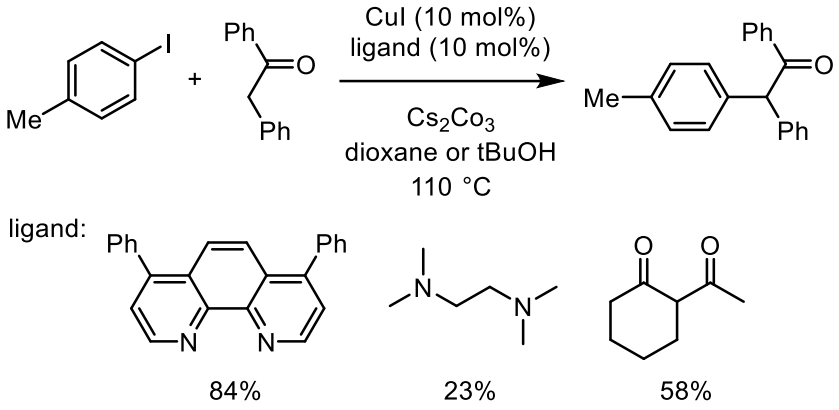

Selective introduction of trifluoromethyl groups into aromatic compounds is of great importance in the medicinal, agricultural, and material chemistry. Among aromatic trifluoromethylation reactions, copper mediated reactions were the most promising methods, but fluoroalkyl cross-coupling reactions had been much slower than ordinary cross-coupling reactions, and needed stoichiometric copper salts. In 2009, Amii and coworkers found that Cu^{I}-diamine complex can catalyze trifluoromethylation of aryl iodides (Scheme 6).[23] Among the

several ligands tested such as *N*,*N*,*N'*,*N'*,-tetramethylethylenediamine (TMEDA), bpy, and phen, the author found that the phen ligand significantly increased the product yield.

Scheme 6. Cu-catalyzed trifluoromethylation of aryl iodides

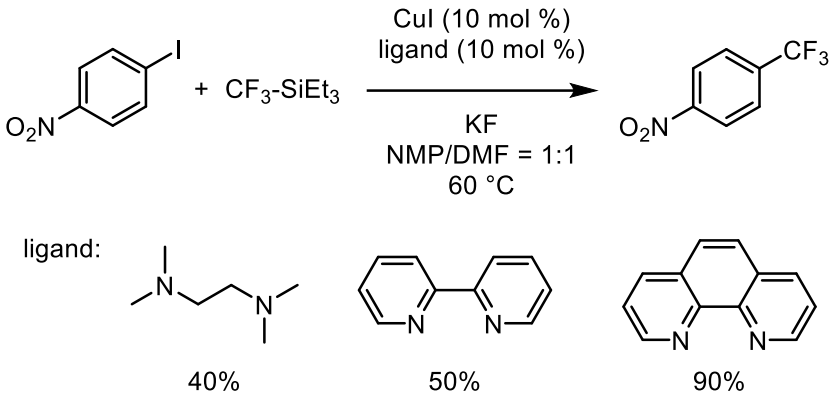

2.2 Pd-catalyzed reactions

Pd-catalyzed oxidative coupling reactions often employ the bipyridine and phenanthroline based ligands because of their stability under aerobic conditions unlike phosphine ligands.

Pd-catalyzed aerobic oxidative coupling reaction of alkenyl- and arylboron compounds with various olefins was reported by Jung and coworkers in 2006 (Scheme 7, 8).[24] This reaction works well in the absence of bases. Among many other ligands tested, bipyridine and phenanthroline type ligands were found to be greatly effective in this reaction. Specifically, the simple phen was most effective for the coupling of alkenyl boron compounds while 2,9-Me_2phen was very effective for the coupling of aryl boron compounds.

Scheme 7. Pd-catalyzed oxidative cross-coupling of an alkenylboronic acid ester with tert-butyl acrylate

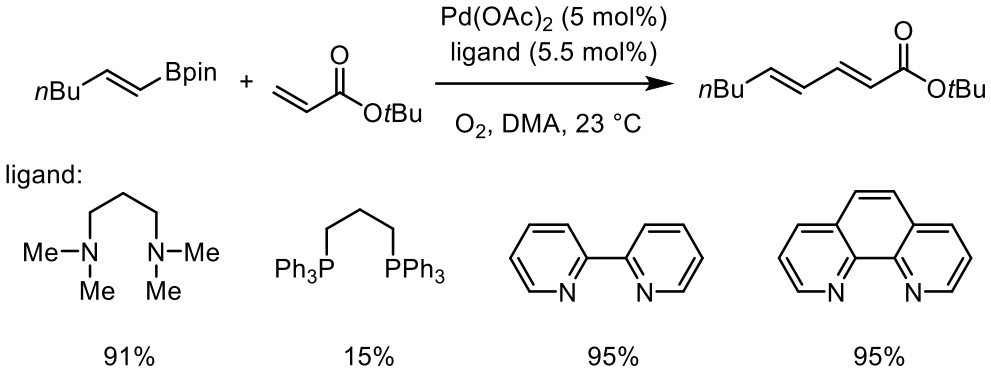

Scheme 8. Pd-catalyzed oxidative cross-coupling of arylboronic acid with tert-butyl acrylate

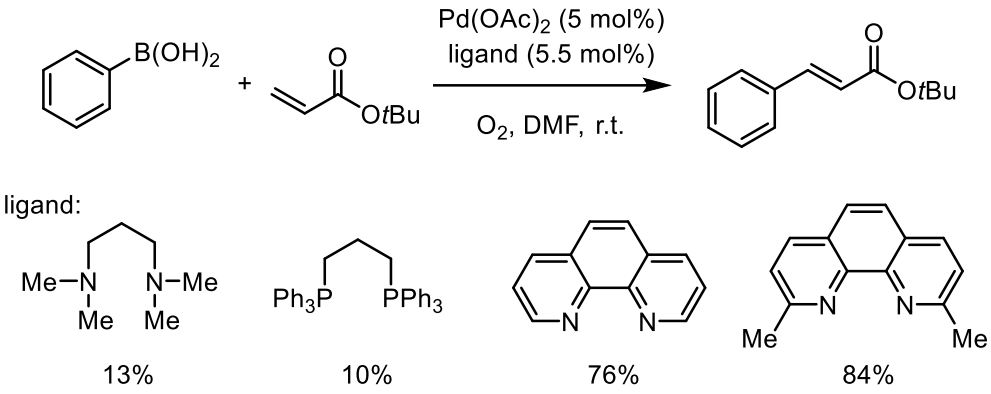

The aerobic oxidation of organic molecules which avoids the use of stoichiometric oxidants is a fundamental and important transformation in terms of green synthesis. Tsuji and coworkers achieved efficient Pd-catalyzed method for the aerobic oxidation of cyclohexanones into the corresponding conjugated enones (Scheme 9).[25] 5,5-Me_2bpy was found as the optimal ligand in this reaction.

Scheme 9. Pd-catalyzed aerobic oxidation of cyclohexanones

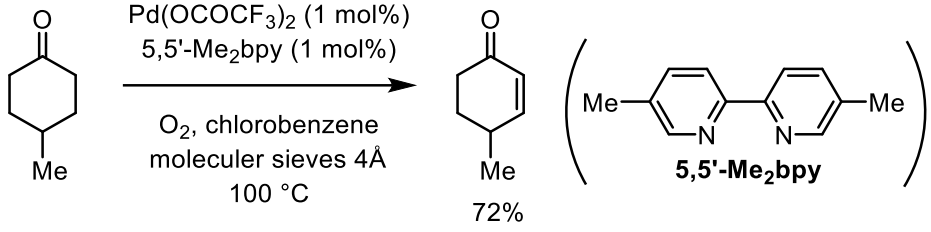

Pd-catalyzed oxidative C-H/C-H coupling of (hetero)arenes provides efficient access to valuable biaryl compounds. Stahl and coworkers recently developed Pd-catalyzed aerobic oxidative coupling of thiophens with phenanthroline dione ligands (phd) (Scheme 10).[26] The author claimed that Cu^{II} cocatalyst promotes this reaction by interacting with the diketone of the phd ligands.

Scheme 10. Pd/phd catalyzed aerobic oxidative coupling of thiophens

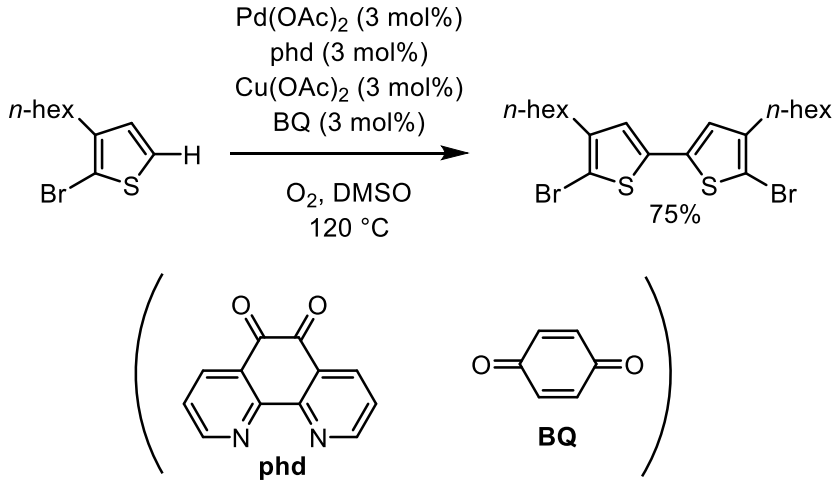

In 2008, Sawamura and coworkers reported Pd-catalzyed g-E-selective coupling reaction of aryl boronic acids and vinyl acetates (Scheme 11).[27] In this reaction, only bipyridine and phenanthroline type ligands were effective, while other types of ligands such as phosphines were ineffective.

Scheme 11. Pd-catalzyed g-E-selective coupling reaction of aryl boronic acids and vinyl acetates

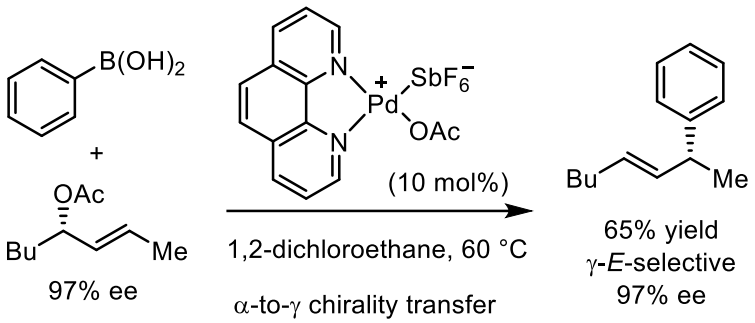

2.3. Fe-catalyzed reactions

Iron is one of the most cheapest atoms in the earth, and has interesting properties. Iron can adopt various oxidation states form -2 to +5. There have been increasing number of publications upon iron catalyzed reactions, and bipyridines and phenanthrolines have been often employed as ligands.[28]

Iron catalyzed direct arylation of unactivated C-H bonds was reported by Charette and coworkers (Scheme 12).[29] The optimized condition employed 5 mol% $Fe(OAc)_2$ and 10 mol % bathophenanthroline ligands.

Scheme 12. Iron-Catalyzed Direct Arylation of Benzene with aryl halides

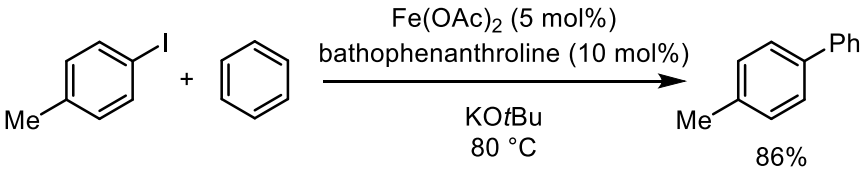

Transition metal catalyzed alkene hydrosilylation has been widely used for industrial production of organosilicons. Precious metal catalysts, especially platinum, are predominantly used for this transformation currently. Therefore, the development of base metal catalysis for this transformation, especially iron, is a growing research area. Peng, Zhu and coworkers first employed phenanthroline ligands in the iron catalyzed alkene hydrosilylation. 2,9-Diaryl-1,10-phenanthroline (2,9-Ar_2phen) ligands exhibited unexpected reactivity and selectivity in this

reaction (Scheme 13).[4] Among the series of 2,9-Ar_2phens, the *i*Pr-substituted ligand (Ar = 2,4,6-$(iPr)_3C_6H_2$) showed the best performance. π-π interaction between substrates and phenanthroline was beneficial for the selectivity according to the proposed mechanistic studies.

Scheme 13. Fe-catalyzed alkene hydrosilylation

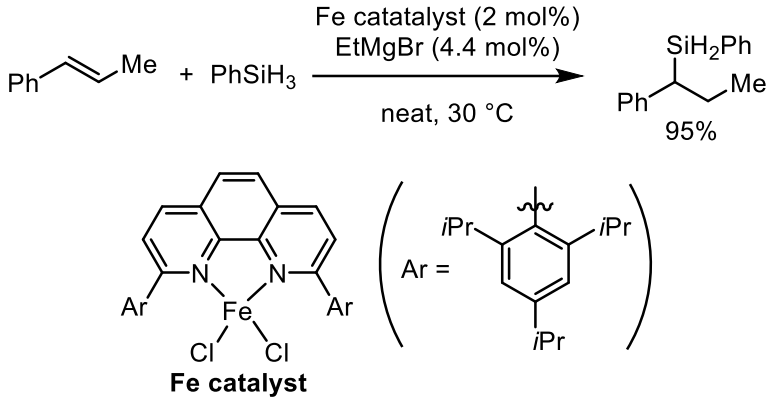

Ollevier el al. reported an Fe-catalyzed asymmetric ring opening reaction of 1,2-diaryl-*meso*-epoxides with indoles (Scheme 14).[30] The chiral bipyridine ligand gave high yield with excellent enantioselectivities.

Scheme 14. Fe-catalyzed asymmetric ring opening reaction of 1,2-diaryl-*meso*-epoxides and indoles

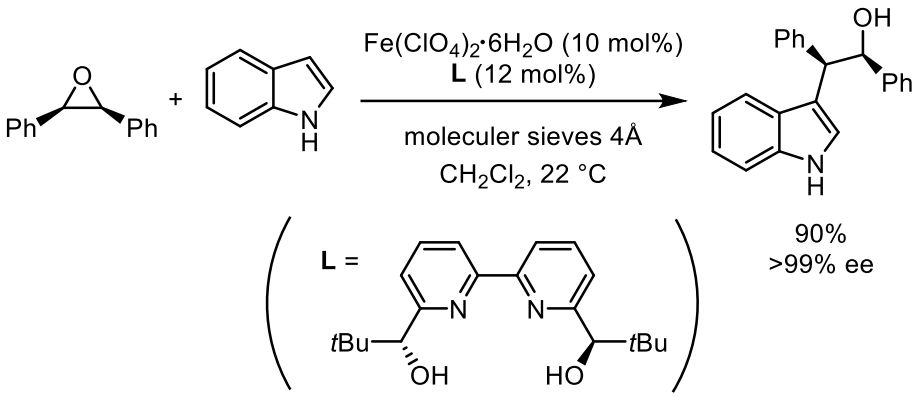

2.4. Ir-catalyzed borylations

Ir-catalyzed borylation reactions directly convert a C–H bond into a C–B bond. The pioneering work described by Hartwig, Ishiyama, Miyaura and coworkers converted aromatic C–H bonds with B_2pin_2 reagents in a mild condition catalyzed by $[IrCl(COD)]_2$ and bpy ligands (Scheme 15).[31] Ir complexes with bpy and phen ligands both exhibited high catalytic activities while pyridine, TMEDA, PPh_3, and dppe ligands were ineffective. The authors also characterized the potential active catalytic species [Ir(4,4-*t*Bu$_2$bpy)(Bpin)$_3$].

Scheme 15. Ishiyama-Miyaura-Hartwig borylation

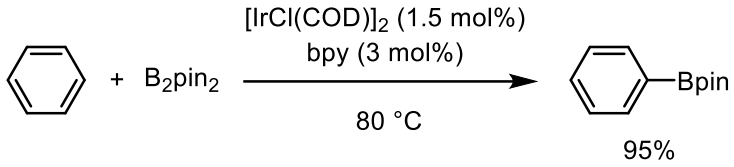

The regioselectivity of Ishiyama-Miyaura-Hartwig borylation was typically governed by steric factors, and functionalization occurs at the least hindered aryl C–H bond. Recently, Hartwig and coworkers disclosed a silyl-directed method that selectively functionalize an *ortho*-position. 4,4'-*t*Bu$_2$bpy ligand was used in this reaction (Scheme 16).[32]

Scheme 16. Silyl-directed Ir-catalyzed ortho-borylation

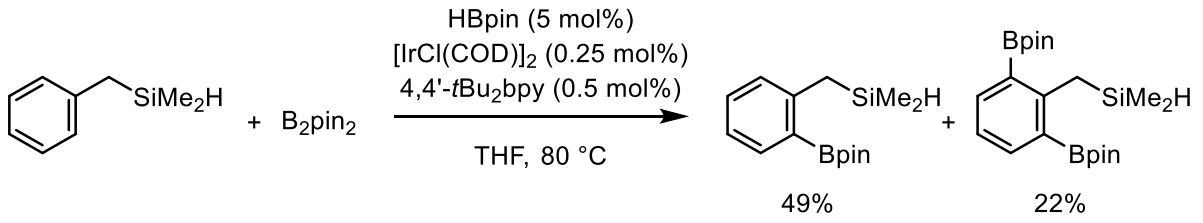

Hartwig and coworkers also developed silyl-directed borylation of alkyl C–H bonds. One of the keys to success was the use of the 3,8-disubstitued phenanthroline ligand (3,8-Mes$_2$phen, Scheme 17).[8] The ligand gave much better result compare to 4,4'-*t*Bu$_2$bpy.

Scheme 17. Silyl-directed Ir-catalyzed borylation of alkyl C-H bonds

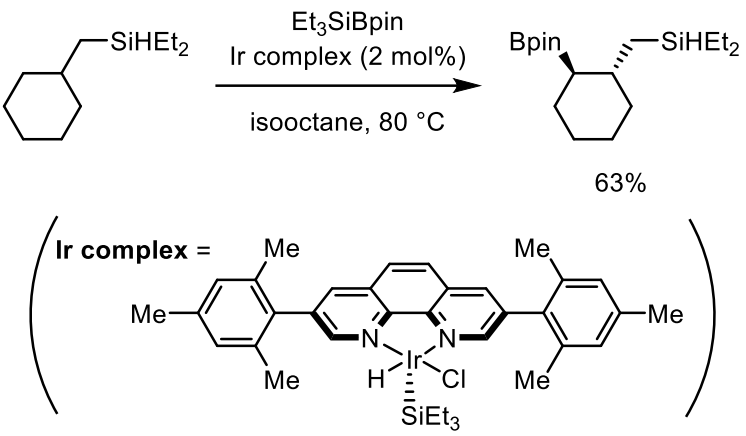

2.5. Ni-catalyzed cross-couplings

Recent Ni catalysis has enabled many interesting novel molecular transformations. The recent Ni-catalyzed reactions differ from conventional transtion metal catalysis in that they utilze single-electron processes in the reaction. The bpy ligands have been most frequently used for those reactions.

Weix and his coworkers reported Ni/4,4‘-$(OMe)_2$bpy catalyzed cross-electrophile coupling between aryl and alkyl halides using Zn or Mn reductant in 2012 (Scheme 18).[33] This cross-electrophlie coupling reaction obviate the use of conventional nucleophilic carbon reagents such as oragnic boronic acids and organic zincs, which have limited commercial availability.

Scheme 18. Cross-electrophile coupling of aryl and alkyl bromides using zinc reductant

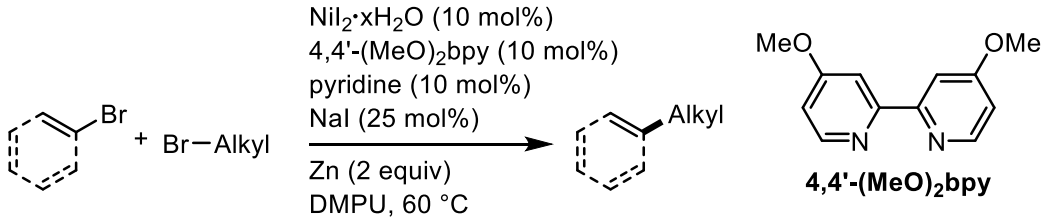

In 2014, Doyle, MacMillan and Molander groups’s pioneering works on nickel/photoredox dual catalysis using 4,4‘-*t*Bu_2bpy were reported. Since then, these metal/photoredox dual

catalysis, named metallaphotoredox catalysis, has gained much attention among many researchers. Doyle, MacMillan and coworkers disclosed Ni/photoredox dual catalytic decarboxylative coupling between aryl bromides and alkyl carboxylic acids (Scheme 19).[34]

Scheme 19. Ni/photoredox dual catalytic cross coupling of aryl bromides and N-α alkyl carboxylic acids

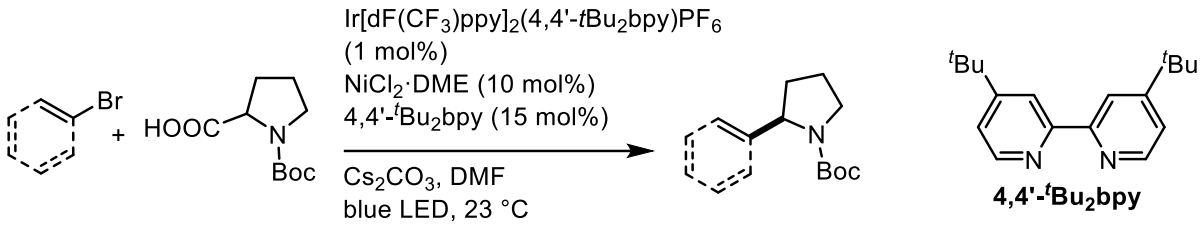

Ni/photoredox dual catalytic cross-coupling reaction that utilize single-electron transmetalation of alkyltrifluoroborates was reported by Molander and coworkers (Scheme 20).[35] 4,4'-*t*Bu$_2$bpy was used as ligand.

Scheme 20. Single-electron transmetalation in organoboron cross-coupling by photoredox/nickel dual catalysis

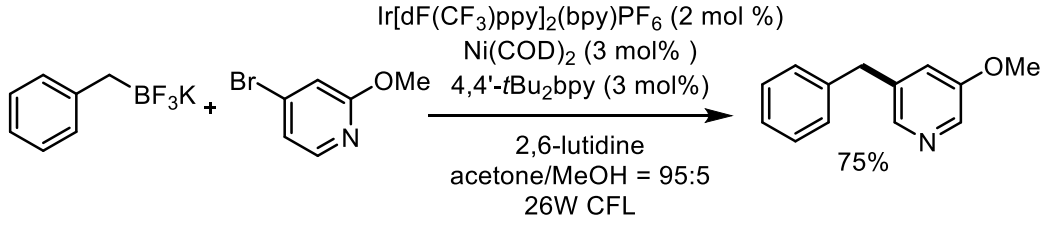

The Ni/photoredox dual catalytic system was further applied to many reactions such as C–O bond formation[36] and the triple catalytic cross-coupling reaction combined with a hydrgen atom trasfer catalyst to functionalize α-amino and α-oxy C(sp^3)-H bonds.[37] 4,4'-*t*Bu$_2$bpy again used as ligand for those reactions.

Baran and coworkers reported Ni-catalyzed decarboxylative cross-coulpling reations

utilzing redox active esteres (RAE) with 4,4‘-*t*Bu$_2$bpy ligand (Scheme 21).[38] In this catalysis, Ni^I(bpy) intermediate undergoes single-elctron transfer with RAE.

Scheme 21. Decarboxylative cross-coupling reaction using redox active esters

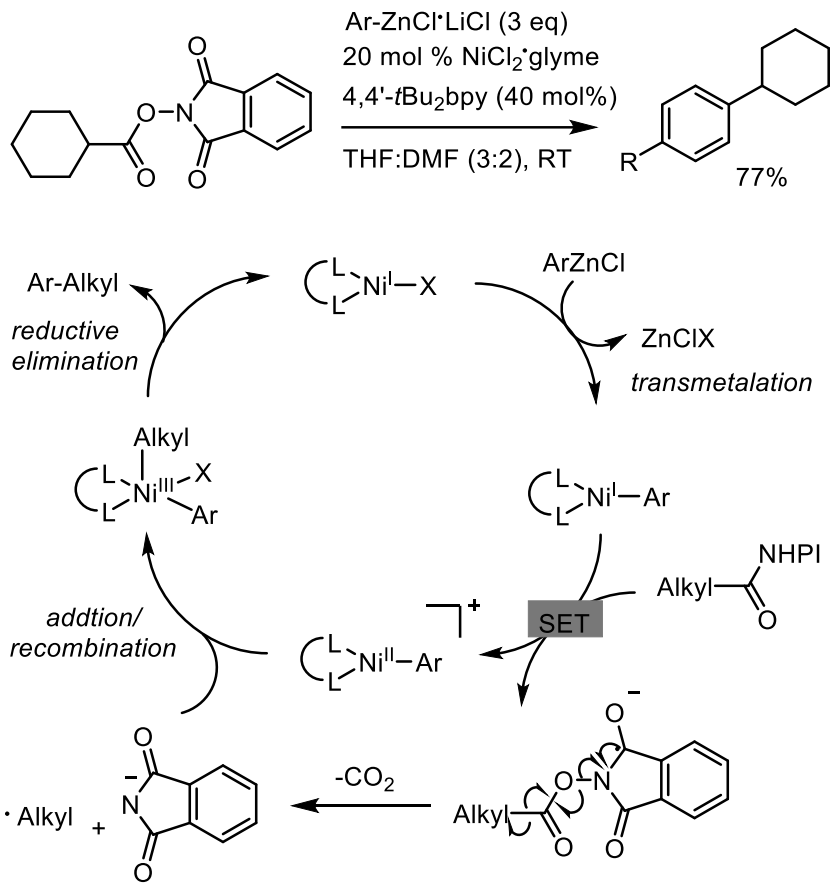

Baran and coworkers further showed that this RAE and Ni/4,4‘-*t*Bu$_2$bpy system can be applied to many interesting novel decarboxylative transformations such as decarboxylative borylation [39], decarboxylative alkenylation[40], and decarboxylative alkylation[41].

Baran also pioneered nickel/electrocataysis in which nickel catalysts are reduced and oxidized at electrodes (Scheme 22).[42] The excess amount of bpy ligand was optimal for this reaction.

Scheme 22. Aryl amination reaction using Nickel/electrocatalysis

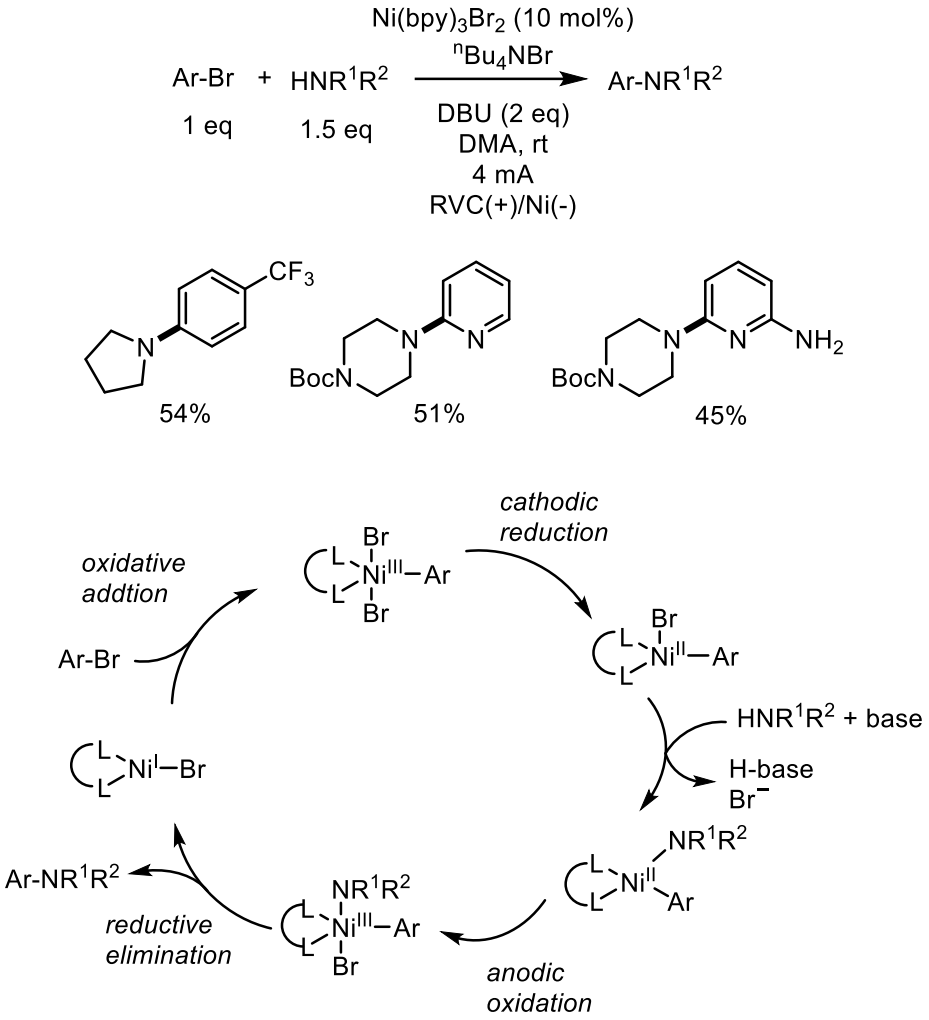

2.6. Photoredox catalysis

Photoredox catalysis is a type of catalysis that utilizes light energy to accelerate a chemical reaction via single-electron transfers (SET). Ru and Ir transition metal complexes are most commonly used as photocatalysts. Bpy and phenanthroline ligands are very important ligand in photoredox catalysis, as $Ru(bpy)_3^{2+}$ and $Ru(phen)_3^{2+}$ are widely used and one of the most studied photocatalysts. $Ir[dF(CF_3)ppy]_2(4,4'\text{-}t\text{Bu}_2\text{bpy})$ is also frequently used in organic synthesis. These photocatalysts absorb light energy via metal to ligand charge transfer (MLCT).

3. Problems of traditional bipyridine ligands

3.1. Formation of ML_2 and ML_3 species

Despite their broad use in many transiton metal catalysis, traditional bipyridine and phenanthroline ligands have two major problems: formation of [ML_2] and [ML_3] species and deleteriuos bimolecular pathways. In the most catalyses, catalytically active species are likely to be in the form of bpy-monochelated metal complexes [ML], but the formation of undesirable [ML_2] and [ML_3] species is facile with common bpy and phen ligands (Figure 3). These coordination behavior may lead to a decrease in catalytic efficiency. For example, Baran and his coworkers recently adressed this problem in his report on Ni/electrochemical catalysis.[42] They found that [Ni], [Ni(bpy)], [Ni(bpy)$_2$], and [Ni(bpy)$_3$] speices are in dynamic equilibria in the solution, and all the speices coexisted in significant amount when nickel and bpy ligand were added in 1:1 ratio.

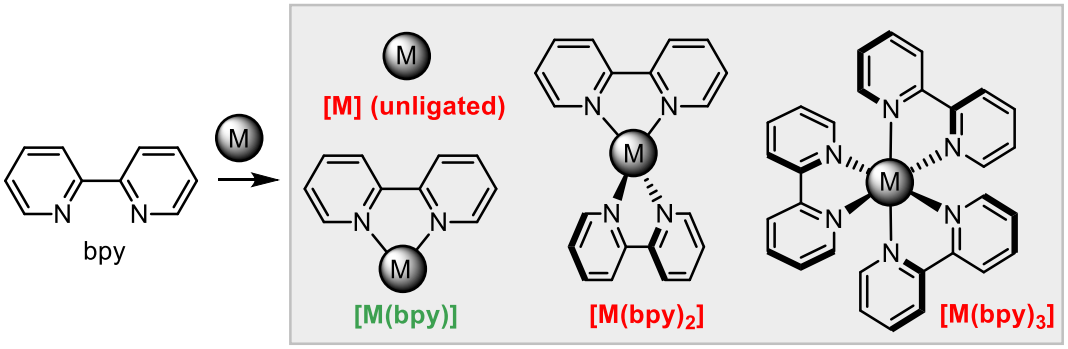

Figure 3. Dynamic coordination equilibrium of M-bpy complexes

3.2. Deleterious bimolecular pathways

The second major problem of using bpy and phen ligands is the deleterious bimolecular pathways. Since common bipyridines and phenanthrolines are very compact, there is little steric hinderance between [ML] species for bimolecular comproportionation or disproportionation reactions. These off-cycle reactions may decrease reaction selectivity and shorten catalyst life-time. Previous mechanistic studies have confirmed that many bimolecular reactions between nickel catalysts are facile. For example, Osakada and coworkers found that (bpy)Ni^{II}(Ph)Br complex can easily undergo bimolecular disproportionation reaction at room temperature in DMF solution, and following reductive elimination to give biphenyl homocoupling product (Scheme 23).[43]

Scheme 23. Disproportionation of (bpy)Ni^{II}(Ph)Br

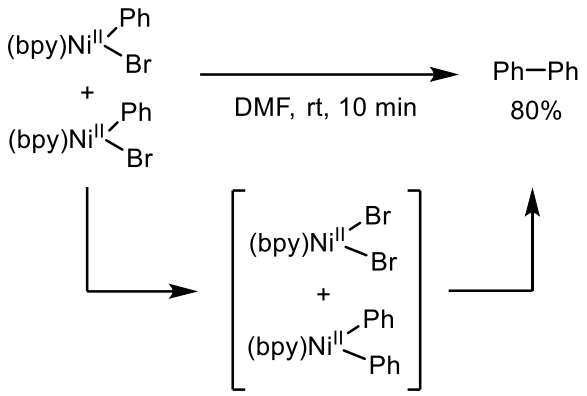

In 2019, Nocera and his coworkers thoroughly investigated the mechanism of Ni/photoredox dual catalyzed C-O bond forming reaction reported by MacMillan and coworkers.[44] They found that this reaction actually can proceed using only (bpy)Ni^{I} species, without Ir photocatalyst and light (Scheme 24). The author found that the turn over number (TON) decreases in high Ni concentration. Therefore, the author insisted that the reaction likely proceed via Ni^{I}/Ni^{III} catalytic cycle (Figure 4), but comproportionation between Ni^{I} and Ni^{III} species produce unreactive Ni^{II} species. The author claimed that the role of photoredox catalysis in the Ni-catalyzed C-O bond forming reaction is likely just regenerating the reactive Ni^{I} or Ni^{III} species from the unreactive Ni^{II} species (Figure 5).

Scheme 24. C-O bond forming reaction using Ni^{I} complex without photocatalysis

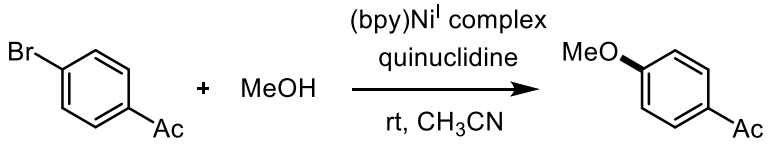

3.3 mol % (bpy)Ni^{I} complex	0.33 mol % (bpy)Ni^{I} complex
8.3 mM	0.83 mM
TON = 2.1	TON = 13.4

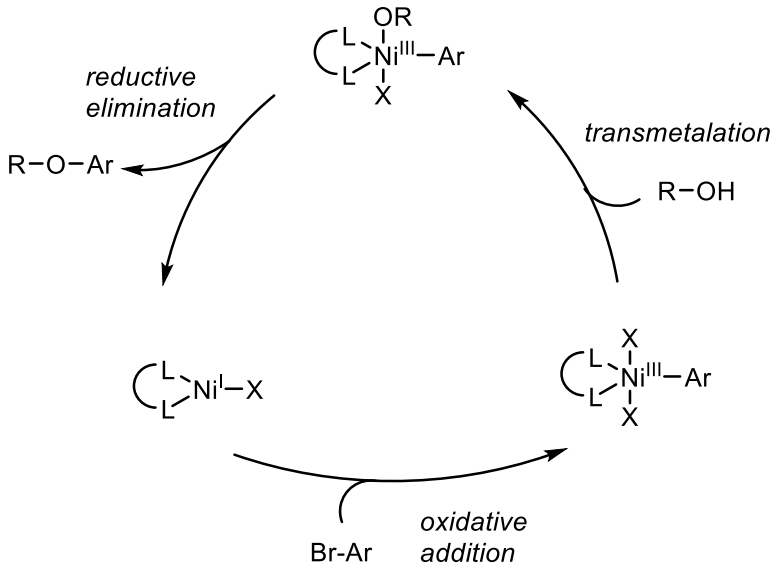

Figure 4. The revised mechanism for Ni-catalyzed C-O bond forming reaction

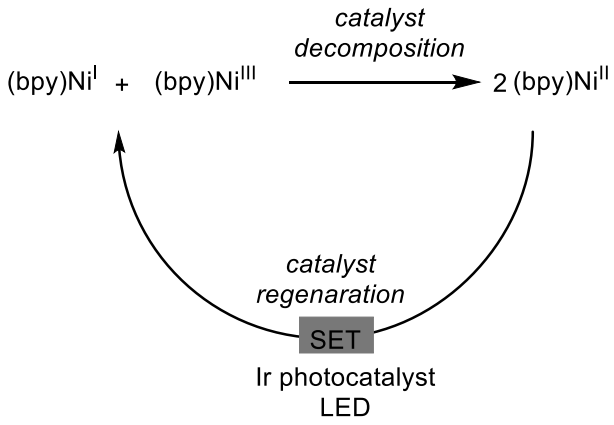

Figure 5. The revised role of the photocatalysis in Ni catalyzed C-O bond forming reaction

4. Overview of this thesis

2,2'-Bipyridine (bpy), 1,10-phenanthroline (phen) and their ring-substituted derivatives have been widely used in transition-metal catalysis as N,N'-bidentate ligands. Despite its broad use in many important transiton metal catalysis, traditional bipyridine and phenanthroline ligands have two major problems: formation of [ML_2] and [ML_3] species and deleteriuos bimolecular pathways.[42,43] The author aimed to address those problems by developing

dumbbell-shaped bipyridine and phenanthroline ligands. In this thesis, the author details the design and the synthesis of dumbbell-shaped bipyridine (dsbpy) and phenanthroline (dsphen) ligands which have bulky substituents at the N-β-positions. The applications of the ligands to the recently emerged synthetically interesting Ni-catalyzed reactions are also described.

References

[1] C. Kaes, A. Katz, M. W. Hosseini *Chemical Reviews* **2000,** *100,* 3553−3590.

[2] A. Bencini, V. Lippolis, *Coordination Chemistry Reviews* **2010,** *254*, 2096−2180.

[3] K. Kalyanasundaram, *Coordination Chemistry Reviews* **1982**, *46*, 159−244.

[4] M. Hu, Q. He, S. Fan, Z. Wang, L. Liu, Y. Mu, Q. Peng, S. Zhu *Nature Communications* **2018**, *9*, 221.

[5] G. Chelucci, R. P. Thummel, *Chem. Rev.* **2002**, *102*, 3129−3170.

[6] N. C. Fletcher, *J. Chem. Soc., Perkin Trans. 1,* **2002**, 1831–1842.

[7] C. Bolm, M. Zehnder, D. Bur, *Angew. Chem. Int. Ed. Engl.* **1990**, *29*, 205–207.

[8] M. A. Larsen, S. Cho, J. F. Hartwig, *J. Am. Chem. Soc.* **2016**, *138*, 762−765.

[9] M. A. Larsen, C. V. Wilson, J. F. Hartwig, *J. Am. Chem. Soc.* **2015**, *137*, 8633−8643.

[10] G. R. Newkome, A. K. Patri, E. Holder, U. S. Schubert *Eur. J. Org. Chem.* **2004**, 235−254.

[11] Y. Cheng, X. Han, H. Ouyang, Y. Rao *Chem. Commun.* **2012**, *48*, 2906–2908.

[12] S. Achar, J. D. Scott, J. J. Vittal, R. J. Puddephatt *Organometallics.* **1993**, *12*, 4592–4598.

[13] A. J. Buonomo, D. A. Everson, D. J. Weix *Synthesis* **2013**, *45*, 3099−3102.

[14] H. Nishiyama, S. Yamaguchi, S. Park, K. Itoh *Tetrahedron Asymmetry* **1993**, *4*, 143−150.

[15] R. P. Thummel *Synlett* **1992**, 1.

[16] A. R. Mackenzie, C. J. Moody, C. W. Rees *Tetrahedron*, **1986**, *42*, 3259−3268.

[17] H. B. Goodbrand, N. Hu *J. Org. Chem.* **1999**, *64*, 670−674.

[18] Lindley, J. *Tetrahedron* **1984**, *40*, 1433−1456.

[19] P. Lopez-Alvarado, C. Avendano, J. C. Menendez *J. Org. Chem.* **1995**, *60*, 5678−5682.

[20] A. Kiyomori, J. F. Marcoux, S. L. Buchwald *Tetrahedron Letters* **1999**, *40*, 2657−2660.

[21] A. Shafir, P. A. Lichtor, S. L. Buchwald *J. Am. Chem. Soc.* **2007**, *129*, 3490−3491.

[22] G. Danoun, A. Tlili, F. Monnier, M. Taillefer *Angew. Chem. Int. Ed.* **2012**, *51*, 12815−12819.

[23] M. Oishi, H. Kondo, H. Amii, *Chem. Commun.* **2009**, 1909–1911.

[24] K. Yoo, C. Yoon, K. Jung, *J. Am. Chem. Soc.* **2006**, *128*, 16384−16393.

[25] M. Tokunaga, S. Harada, T. Iwasawa, Y. Obora, Y. Tusji *Tetrahedron Letters* **2007**, *48*, 6860−6862.

[26] Stahl, JACS 2020 /10.1021/jacs.0c09962

[27] Sawamura et. al., *J. Am. Chem. Soc.*, **2008**, *130*, 17276−17277.

[28] I. Bauer, H.-J. Knölker *Chem. Rev.* **2015**, *115*, 3170−3387.

[29] F. Vallee, J. J. Mousseau, A. B. Charette *J. Am. Chem. Soc.* **2010**, *132*, 1514−1516.

[30] B. Plancq, M. Lafantaisie, S. Companys, C. Maroun, T. Ollevie *Org. Biomol. Chem.* **2013**, *11*, 7463–7466.

[31] T. Ishiyama, J. Takagi, K. Ishida, N. Miyaura, N. R. Anastasi, J. F. Hartwig *J. Am. Chem. Soc.* **2002**, *124*, 390−391.

[32] T. A. Boebel, J. F. Hartwig *J. Am. Chem. Soc.* **2008**, *130*, 7534−7535.

[33] D. A. Everson, B. A. Jones, D. J. Weix *J. Am. Chem. Soc.* **2012**, *134*, 6146−6159.

[34] Z. Zuo, D. T. Ahneman, L. Chu, J. A. Terrett, A. G. Doyle, D. W. C. MacMillan *Science* **2014**, *345*, 437–440.

[35] J. C. Tellis, D. N. Primer, G. A. Molander *Science*, **2014**, *345*, 433−436.

[36] J. A. Terrett, J. D. Cuthbertson, V. W. Shurtleff, D. W. C. MacMillan *Nature* **2015**, *524*, 330−334.

[37] M. H. Shaw, V. W. Shurtleff, J. A. Terrett, J. D. Cuthbertson, D. W. C. MacMillan *Science* **2016**, *352*, 1304–1308.

[38] J. Cornella, J. T. Edwards, T. Qin, S. Kawamura, J. Wang, C. Pan, R. Gianatassio, M. Schmidt, M. D. Eastgate, P. S. Baran *J. Am. Chem. Soc.* **2016**, *138*, 2174−2177.

[39] C. Li, J. Wang, L. M. Barton, S. Yu, M. Tian, D. S. Peters, M. Kumar, A. W. Yu, K. A. Johnson, A. K. Chatterjee, M. Yan, P. S. Baran *Science* **2017**, *356*, eaam7355.

[40] J. T. Edwards, R. R Merchant, K. S. McClymont, K. W. Knouse, T. Qin, L. R. Malins, B. Vokits, S. A. Shaw, D. Bao, F. Wei, T. Zhou, M. D. Eastgate, P. S. Baran *Nature* **2017**, *545*, 213−218.

[41] T. Qin, J. Cornella, C. Li, L. R. Malins, J. T. Edwards, S. Kawamura, B. D. Maxwell, M. D. Eastgate, P. S. Baran *Science* **2016**, *352*, 801−805.

[42] Y. Kawamata, J. C. Vantourout, D. P. Hickey, P. Bai, L. Chen, Q. Hou, W. Qiao, K. Barman, M. A. Edwards, A. F. Garrido-Castro, J. N. deGruyter, H. Nakamura, K. Knouse, C. Qin, K. J. Clay, D. Bao, C. Li, J. T. Starr, C. Garcia-Irizarry, N. Sach, H. S. White, M. Neurock, S. D. Minteer, P. S. Baran, *J. Am. Chem. Soc.* **2019**, *141*, 6392–6402.

[43] T, Yamanoto, S. Wakabayashi, K. Osakada *Journal of Organometallic Chemistry* **1992**, 428, 223−237.

[44] R. Sun, Y. Qin, S. Ruccolo, C. Schendermann, C. Costentin, D. G. Nocera *J. Am. Chem. Soc.* **2019**, *141*, 89−93.

Chapter 1

Design and Synthesis of Dumbbell-Shaped Bipyridine and Phenanthroline Ligands

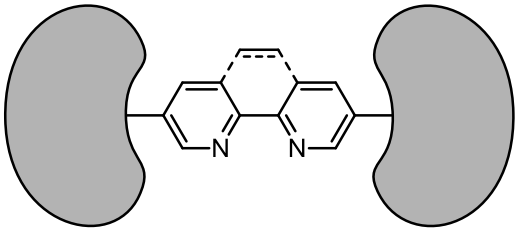

The synthesis of a new class of 2,2'-bipyridine ligands (dsbpys) and 1,10-phenanthroline (dsphen) having dumbbell-like shapes with differently substituted triarylmethyl groups and 2,6-dibenzhydryl-4-methylphenyl group at the N-β-positions are described. Analysis of metal coordination behaviors of the bpy ligands by UV-vis absorption spectroscopy indicated the apparent monochelating nature of the dumbbell-shaped bpy/phen ligands.

Introduction

2,2'-Bipyridine (bpy), 1,10-phenanthroline (phen) and their ring-substituted derivatives have been widely used in transition-metal catalysis as N,N'-bidentate ligands. Pursuing better catalytic properties of the metal complexes the bpy and phen ligands have been modified by introducing various substituents with different steric and electronic properties. For these purpose, the N-α-positions (C6, C6' in bpy and C2, C9 in phen) and the N-γ-positions (C4, C4' in bpy and C4, C7 in phen) have been the common sites of modification. The ligand modifications at the N-β-positions (C5, C5' in bpy and C3, C8 in phen), however, have attracted less attention in the research of homogeneous catalysis because both the steric and electronic effects at those positions are not significant in general.

Despite its broad use in many transiton metal catalysis, traditional bipyridine and phenanthroline ligands have two major problems: formation of $[ML_2]$ and $[ML_3]$ species and deleteriuos bimolecular pathways. The author aimed to address those problems by developing dumbbell-shaped bipyridine and phenanthroline ligands (Figure 1). I envisioned that distal steric effects of the substituents at the N-β-positions, which do not hamper the catalytic reactions by steric hindrance in the vicinity of the metal but develop outside the boundary of the catalytic space, can allow the selective monochelation to the metal center and effectively suppress the bimetallic pathways while sustaining catalytic activity.

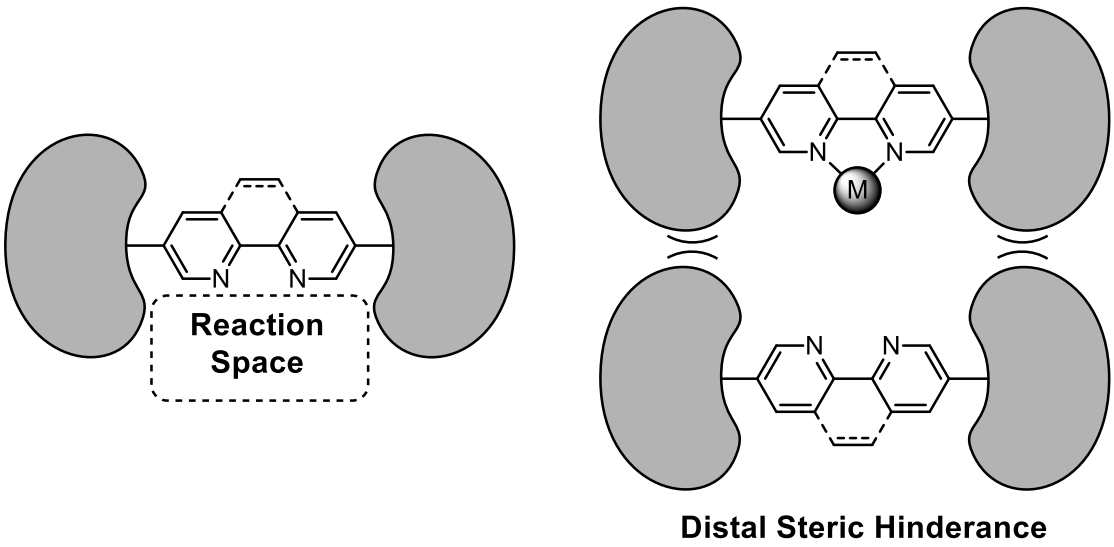

Figure 1. The design of the dumbbell-shaped bipyridine and phenanthroline

Result and Discussion

Thus, I designed the ligands to have dumbbell like structures by introducing bulky substituents such as triarylmethyl (Scheme 1) and 2,6-dibenzhydryl-4-methylphenyl groups at the N-β-positions (Scheme 2). The dsbpy ligands with triarylmethyl groups were synthesized in one step by applying the Pd-catalyzed deprotonative C(sp^3)–H arylation of heteroarylmethanes, which was recently reported by Walsh and co-workers.[1] Thus, six-fold C(sp^3)–H arylation of commercially available 5,5'-dimethyl-2,2'-bipyridine (5,5'-Me_2bpy) with aryl bromides (**1**) in the presence of a Pd catalyst afforded the corresponding dsbpys in reasonable yields (Scheme 1; **L1**–**L5** from **1a**–**e**, respectively).[2,3] The molecular structure of the dsbpy (**L5**) with the most pronounced steric demand was determined by X-ray diffraction analysis. Some of the meta-isopropyl groups form the side walls at the ends of the bipyridyl center axis, leaving a substantial accessible space around the bipyridyl scaffold (Figure 2, top). As shown in the top view (Figure 2, bottom), the depth of the distal steric barrier formed by side walls was about 0.34 nm.

Scheme 1. Synthesis of dsbpys through the Pd-catalyzed six-fold deprotonative C(sp^3)–H arylation of 5,5'-Mebpy.

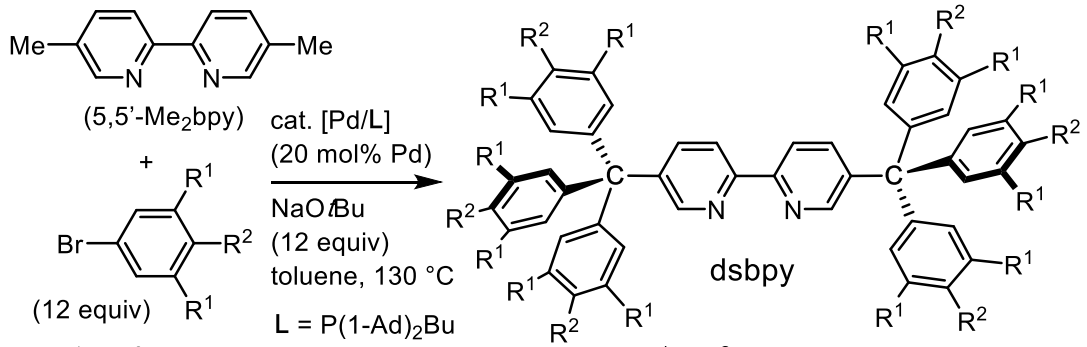

1a (R^1 = R^2 = H)	**L1** (R^1 = R^2 = H)	29%
1b (R^1 = H, R^2 = *t*Bu)	**L2** (R^1 = H, R^2 = *t*Bu)	39%
1c (R^1 = Me, R^2 = H)	**L3** (R^1 = Me, R^2 = H)	30%
1d (R^1 = Et, R^2 = H)	**L4** (R^1 = Et, R^2 = H)	42%
1e (R^1 = *i*Pr, R^2 = H)	**L5** (R^1 = *i*Pr, R^2 = H)	52%

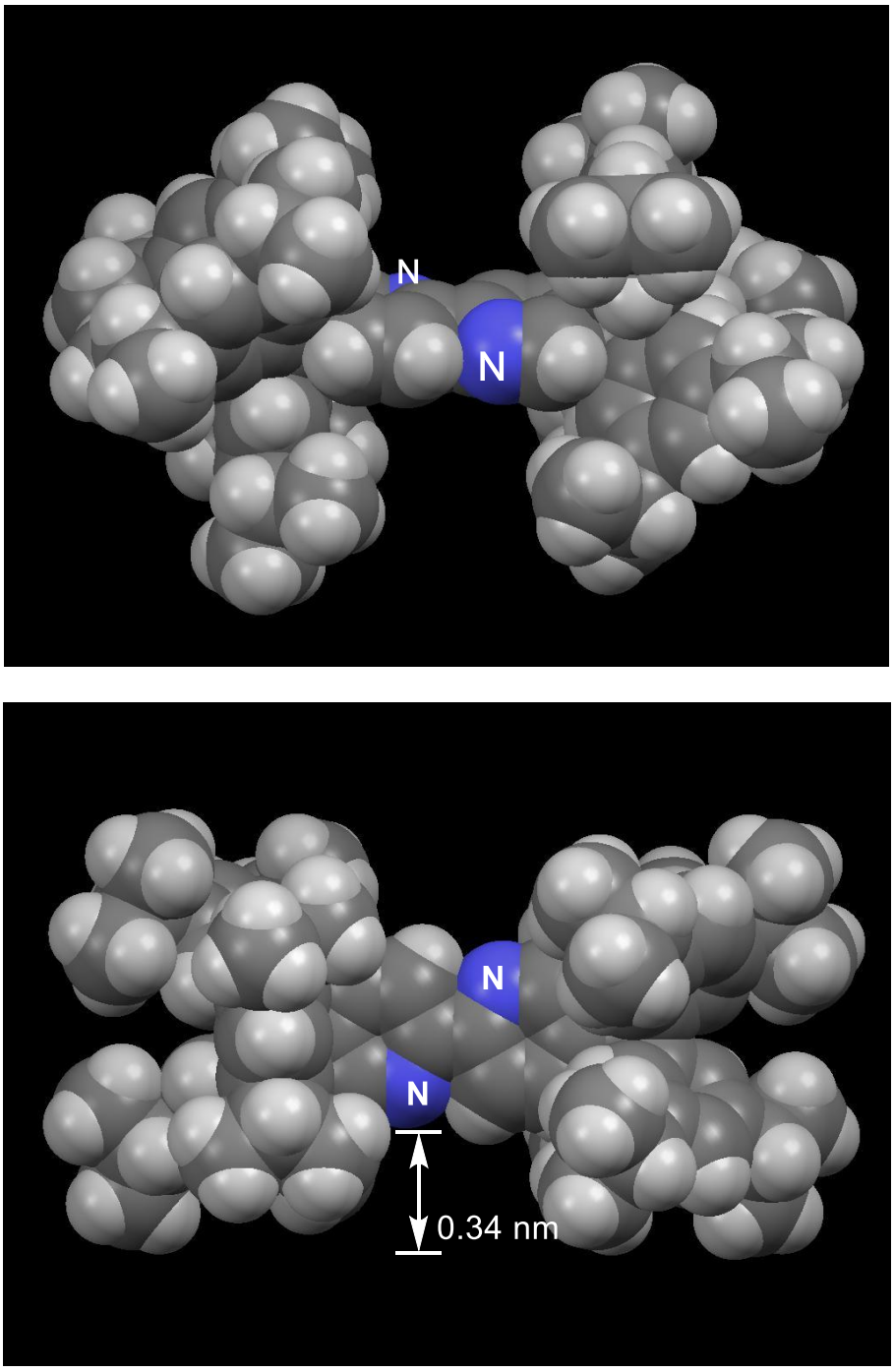

Figure 2. The space-filling models of **L5** determined by X-ray diffraction analysis (solvents are omitted for clarity. top: front view; bottom: top view).

Furthermore, another bulky substituent, 2,6-dibenzhydryl-4-methylphenyl (bhp) was introduced into bipyridine and phenanthroline structures via Pd-catalyzed Negishi cross-coupling reaction (Scheme 2).[4,5] The reaction between 5,5'-dibromo-2,2'-bipyridine and the prepared aryl zinc gave bhp-type dsbpy **L6** in 12%. Unfortunately, **L6** had very low solubility, and was barely soluble to CH_2Cl_2. Thus, I decided not to use **L6** in the further research. The reaction with 3,8-dibromo-1,10-phenanthroline gave the bhp-type dumbbell-shaped phenanthroline (**L7**, dsphen) in 50% yield. The solubility of this ligand was moderate, and recrystallization with CH_2Cl_2 and hexane gave cubic crystal. The space-filling models of **L7** determined by X-ray diffraction analysis are shown in Figure 3. As shown in the front view (Figure 3, top), two bhp substituents are successfully introduced to N-β sites and form steric environment around phenanthroline. As shown in the top view (Figure 3, bottom), the introduced bulky bhp substituents lean to the phenanthroline backbone and surround open reaction site around coordination site.

Scheme 2. Synthesis of dsbpy and dsphen through Pd-catalyzed Negishi cross-coupling

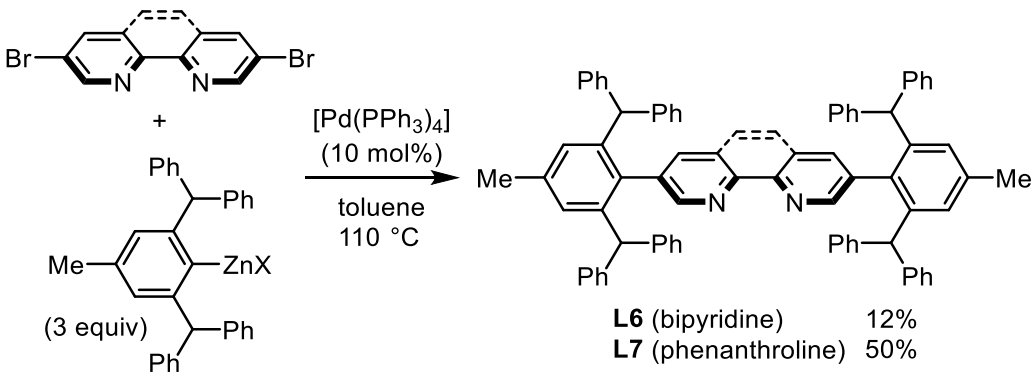

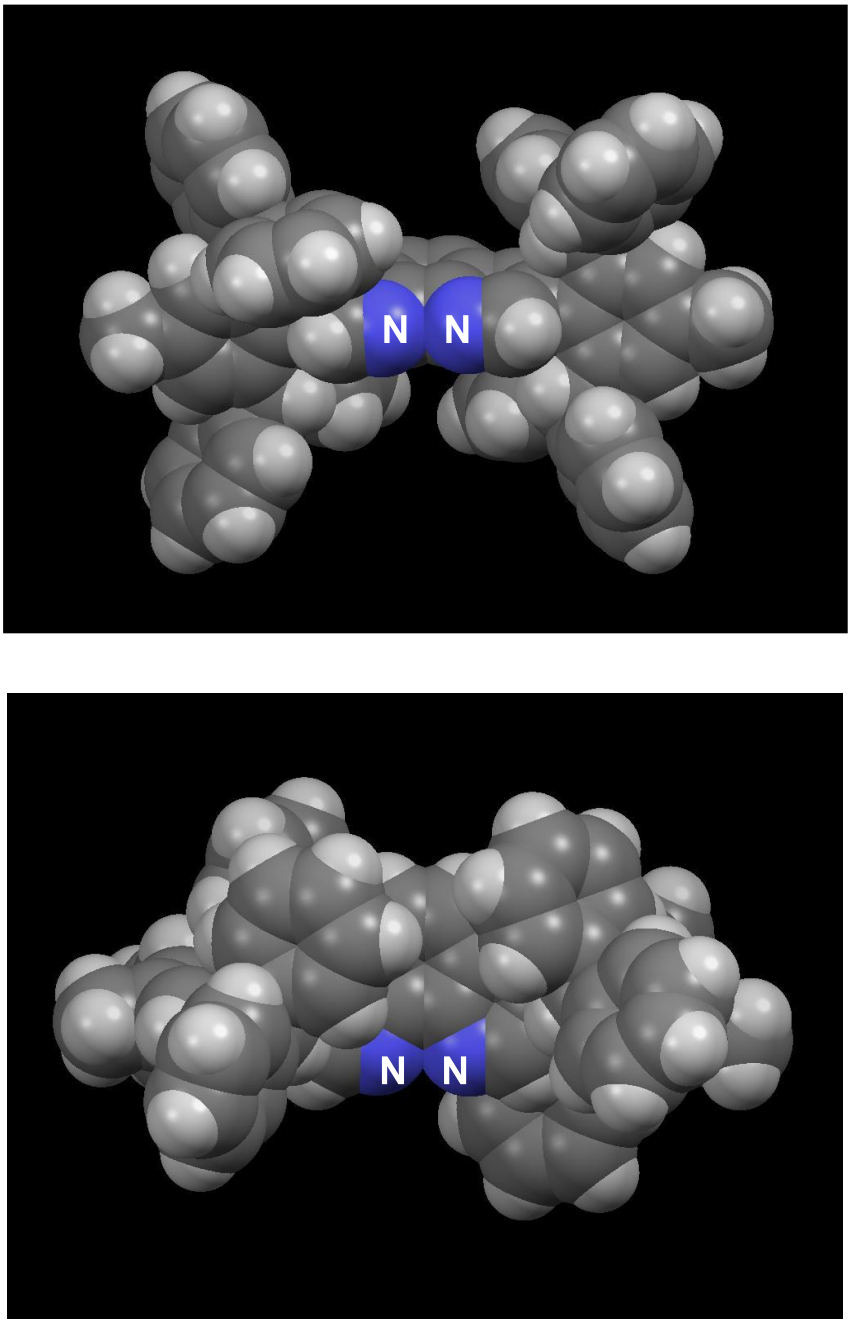

Figure 3. The space-filling models of **L7** determined by X-ray diffraction analysis (solvents are omitted for clarity. top: front view; bottom: top view.).

2. Coordination behavior of nickel(II) and dsbpy/dsphen ligands

To evaluate the substituent effects at the N-β-positions on the metal-ligand coordination

equilibria, titrations between $NiBr_2$·DME (DME: 1,2-dimethoxyethane) and bpy/phen ligands (5,5'-Me_2bpy, **L1**–**L5**, and **L7**) were conducted in *N,N*-dimethylacetamide (DMA) at room temperature while monitored by UV-vis absorption spectroscopy (270–350 nm). To quantify the coordination equilibria, the concentration profiles for each Ni species and the Gibbs free energies were constructed with the equilibrium restricted factor analysis aided by the *Sivvu* program (See the experimental section for the details).[6] The results are summarized in Figure 4–10.

As shown in Figure 4, with 5,5'-Me_2bpy, continuous addition of the Ni salt until a 1:2 Ni/L ratio was reached led to the exclusive formation of a bischelated complex [Ni(5,5'-Me_2bpy)$_2$].[7] The reaction at a 1:1 Ni/L ratio afforded a mixture of a monochelated complex [Ni(5,5'-Me_2bpy)], the bischelated complex [Ni(5,5'Me_2bpy)$_2$], and an unligated Ni species. Even with excess Ni (Ni/ligand 1.5:1), the bischelated complex [Ni(5,5'-Me_2bpy)$_2$] still remained in the solution, indicating a strong tendency of 5,5'Me_2bpy to cause a second chelation as demonstrated in the literature for the parent bpy ligand and 4,4'-dimethyl-2,2'-bipyridine.[6,8]

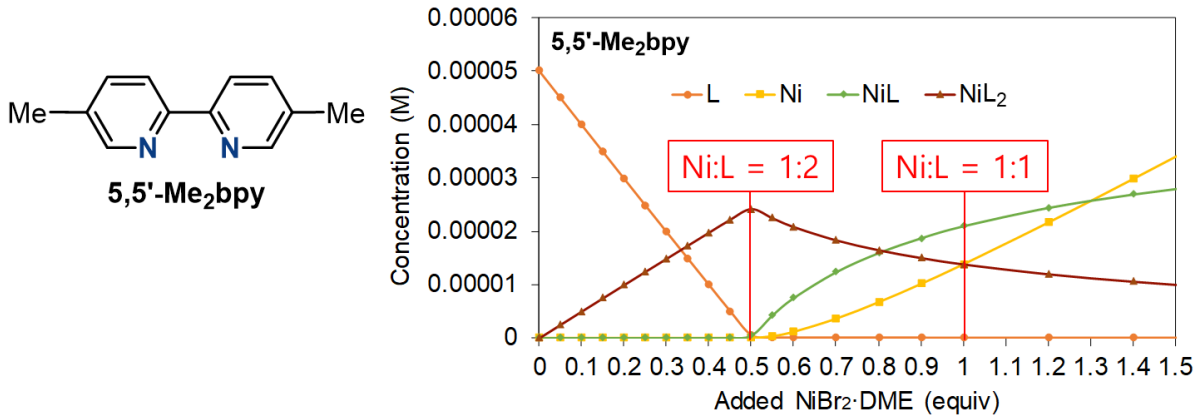

Figure 4. The concentration profile for Ni species with 5,5'-Me_2bpy

In the case of simplest dsbpy **L1**, which is substituted with trityl groups, provided a coordination profile similar to that of 5,5'-Me_2bpy (Figure 5). The formation of undesired NiL_2 species were not suppressed at a Ni to ligand 1:1 ratio.

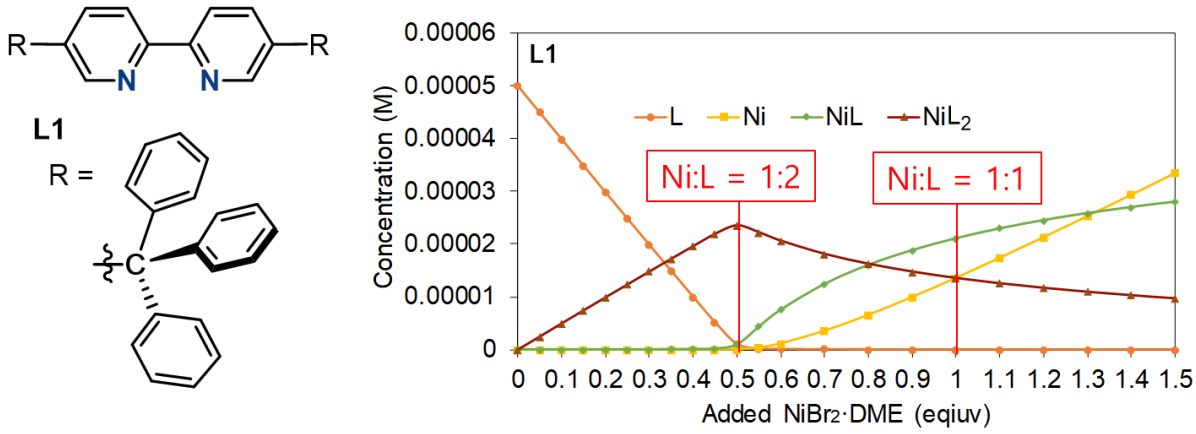

Figure 5. The concentration profile for Ni species with **L1**

In the case of **L2**, which has *t*Bu-substituents at the para-positions, it quite significantly suppressed bis-ligated nickel species. The ligand gave a higher distribution for monochelated Ni complex [Ni(**L2**)] at nickel to ligand 1:1 ratio, albeit with the substantial coexistence of a Ni species [Ni(**L2**)$_2$] with participation of the second **L2** molecule (Figure 6).

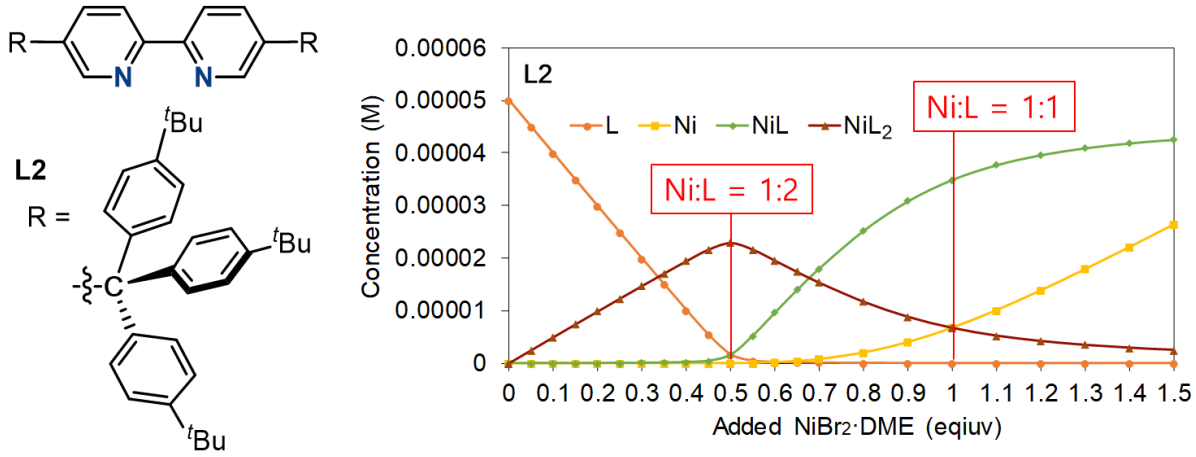

Figure 6. The concentration profile for Ni species with **L2**

Encouragingly, more selective monochelation was achieved by **L3**, which has methyl substituents at the meta-positions. The formation of undesired NiL$_2$ was nearly suppressed in the Ni to L 1:1 ratio, and gave a lot of catalytically active species NiL.

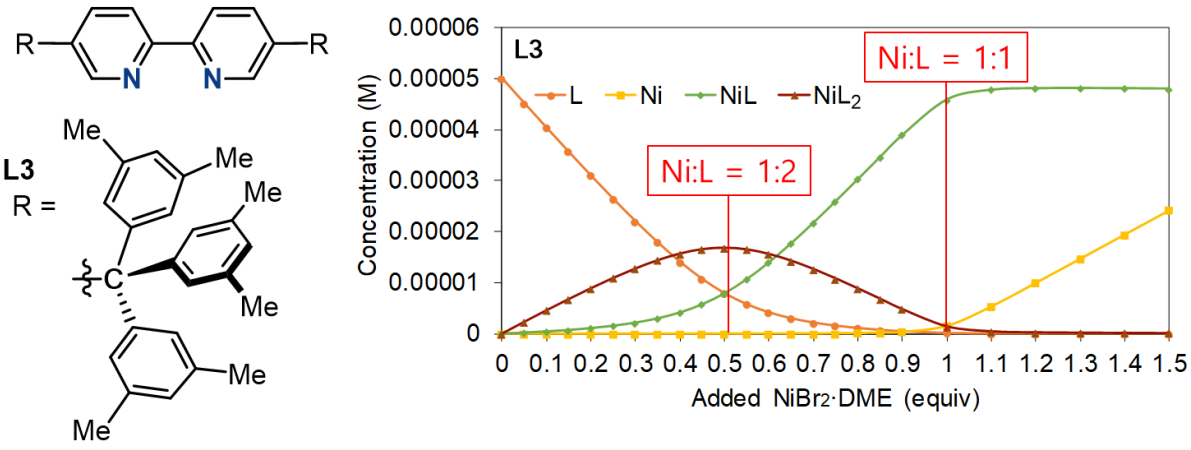

Figure 7. The concentration profile for Ni species with **L3**

Bulkier ligands such as **L4** with ethyl substituents and **L5** with isopropyl substituents, were more effective and almost completely suppressed the undesired species at a nickel to ligand 1:1 ratio (Figure 8 and 9). Notably in the case of **L5**, the formation of NiL_2 was quite suppressed even in the nickel to ligand 1:2 ratio.

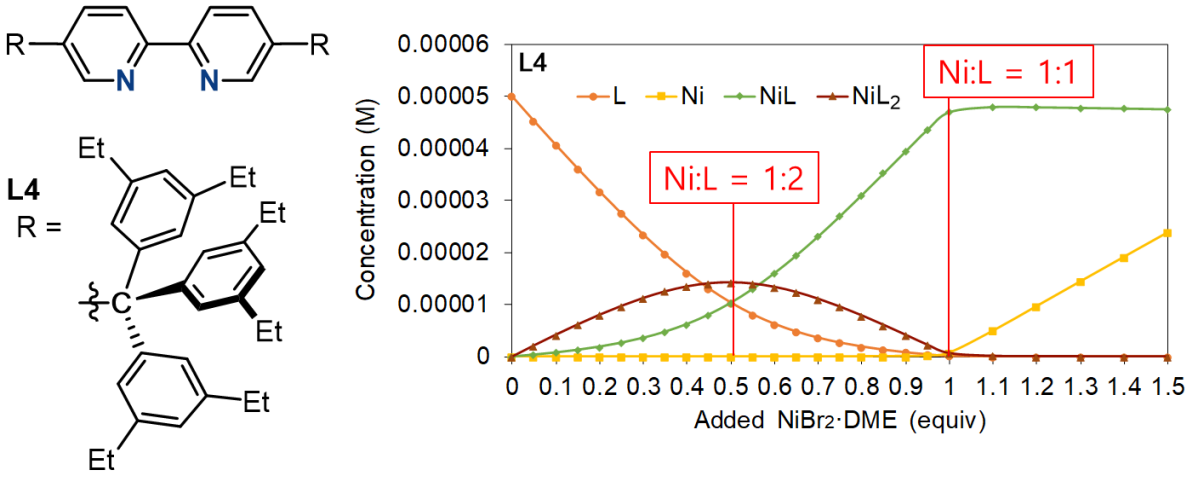

Figure 8. The concentration profile for Ni species with **L4**

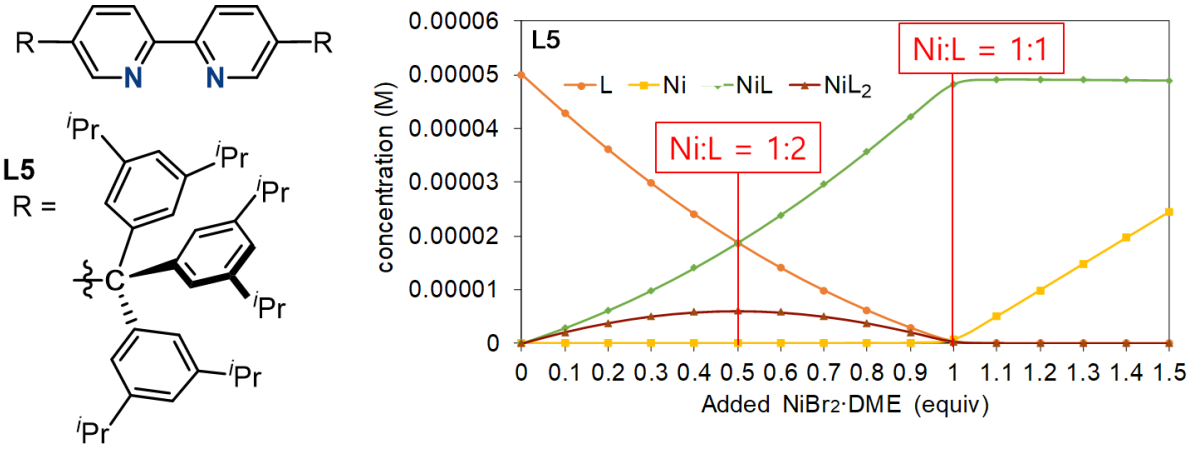

Figure 9. The concentration profile for Ni species with **L5**

The dumbbell-shaped phenanthroline ligand, 2,6-dibenzhydryl-4-methylphenyl (bhp) substituted phenanthroline ligand **L7,** also effectively suppressed the formation of [Ni(**L7**)$_2$] species throughout the solution (Figure 10).

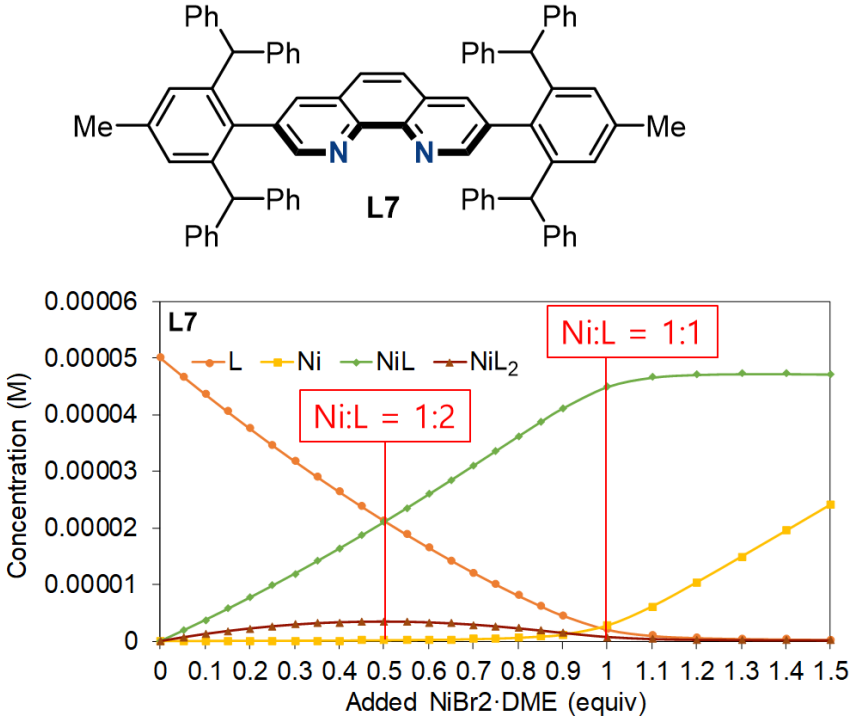

Figure 10. The concentration profile for Ni species with **L7**

Finally, the Gibbs free energy differences between the first ([Ni] to [NiL], ΔG_1) and second ([NiL] to [NiL$_2$], ΔG_2) ligand bindings (L = 5,5'-Me$_2$bpy, **L1**–**L5**, and **L7**) are summarized in Figure 11 (calculated from the above ERFA analysis).[6] It clearly shows the trend that the bulkier substituents at the N-β-position makes the second ligand coordination more difficult. 5,5-Me$_2$bpy ligand has almost no barrier for the second ligand coordination, as the ΔG_2 - ΔG_1 value was 2.05 kJ/mol. 5,5-triphenylmethyl$_2$bpy, **L1**, also barely hinders second ligand coordination (ΔG_2 - ΔG_1 = 2.19 kJ/mol). The para-*t*Bu-substituted dsbpy (**L2**) moderately inhibited second coordination (G_2 - ΔG_1 = 8.15 kJ/mol). 3,5-disubstituted dsbpys (**L3-L5**) had much higher barrier for the second ligand coordination, and bulkier substituent showed better inhibition (**L3**, methyl, ΔG_2 - ΔG_1 = 17.10 kJ/mol; **L4**, ethyl, ΔG_2 - ΔG_1 = 20.98 kJ/mol; **L5**, isopropyl, ΔG_2 - ΔG_1 = 22.78 kJ/mol). The bhp-substituted phenanthroline ligand **L7**, showed similar inhibitory effect comparable to **L3** (ΔG_2 - ΔG_1 for **L7** = 17.26 kJ/mol).

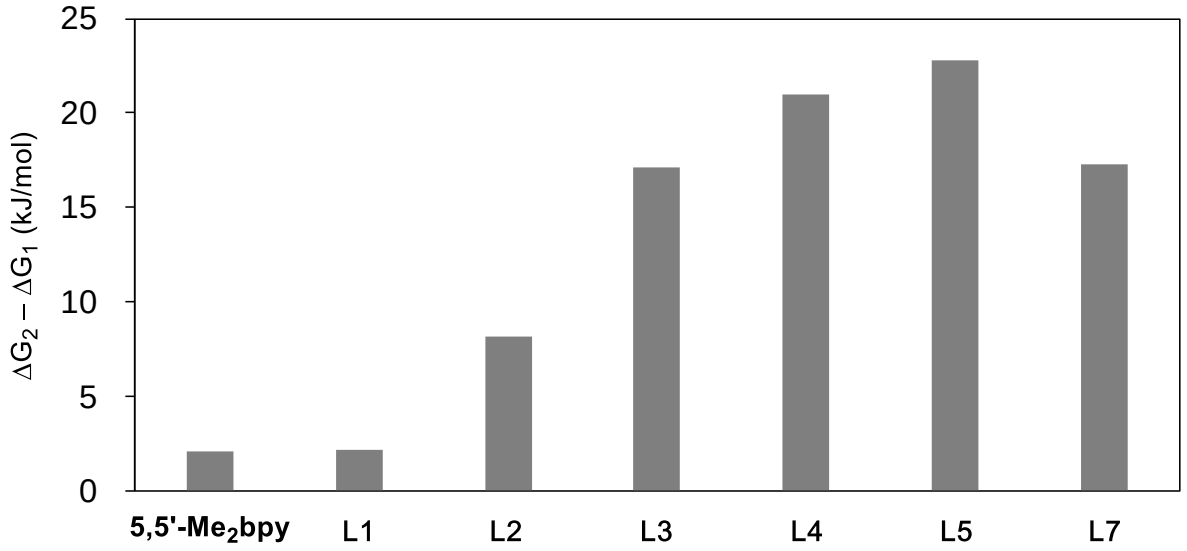

Figure 11. Gibbs free energy differences between the first ([Ni] to [Ni**L**], ΔG_1) and second ([Ni**L**] to [Ni**L**$_2$], ΔG_2) ligand binding (**L** = 5,5'-Me$_2$bpy, **L1–L5**, and **L7**).

Cyclic voltammetry analysis

Cyclic voltammetry (CV) analysis was carried out to examine the electrochemical characteristics of [Ni-(5,5'-Me$_2$bpy)] and [Ni-(**L5**)] systems. CV experiments were performed with a CH instruments 760D electrochemical workstation and CHI version 660E software

using a three-electrode cell with a glassy carbon electrode (diameter : 3 mm), a Pt wire counter electrode, and a $Ag/AgNO_3$ reference electrode. The studied compounds were dissolved in an electrolyte solution containing 0.1 M $^{n}Bu_4NBr$ in DMA solution. The electrode potential was calibrated with a ferrocene/ferrocenium (Fc/Fc^{+}) redox couple in the solution. A half-wave potential ($E_{1/2}$) was the middle potential between the anodic and cathodic peak potentials (E_{pa} and E_{pc}): $E_{1/2} = (E_{pa} + E_{pc}) / 2$.

A cyclic voltammogram of 5,5'-Me_2bpy is shown in Figure 12. The irreversible wave, showing anodic peak potential at −2.82 V, was observed. An addition of an equivalent of $NiBr_2$·DME to the DMA solution provided three reversible waves (Figure 13) at −1.45, −1.78, and −2.52 V ($E_{1/2}$) indicating formation of Ni complexes.

The CV curves of **L5** ligand, not completely dissolved due to low solubility, show an irreversible wave at −2.41 V (peak potential) and a reversible wave at $E_{1/2}$ = −2.59 V (Figure 14). In contrast, the addition of $NiBr_2$·DME dissolved **L5** ligand in the DMA solution. A quasi reversible wave at $E_{1/2}$ = −1.51 V and an irreversible wave at −2.02 V (peak potential) were observed (Figure 15).

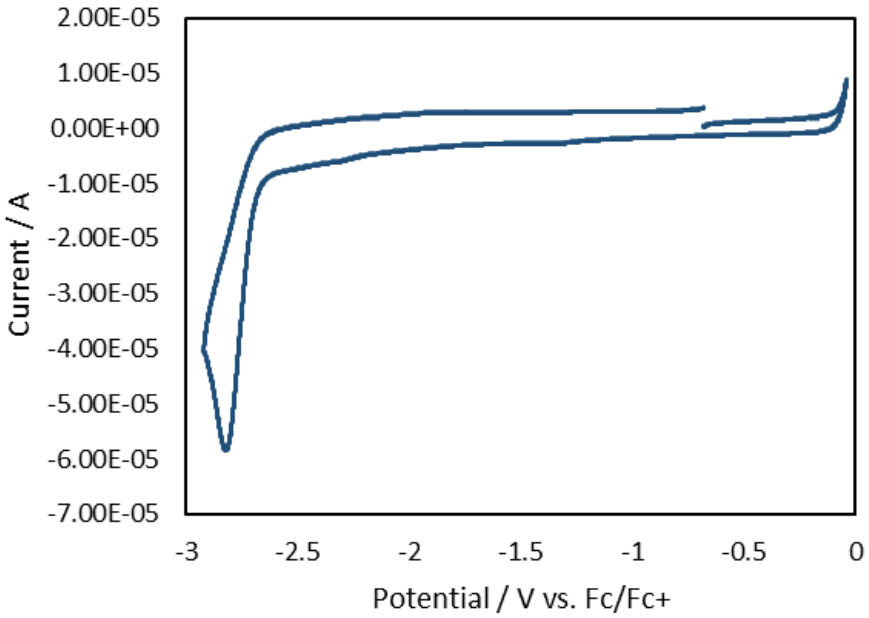

Figure 12. CV of a 100 mM $^{n}Bu_4NBr$ in DMA solution containing 1.0 mM 5,5'-Mebpy ligand. The scan rate was v = 0.1 V s^{-1}.

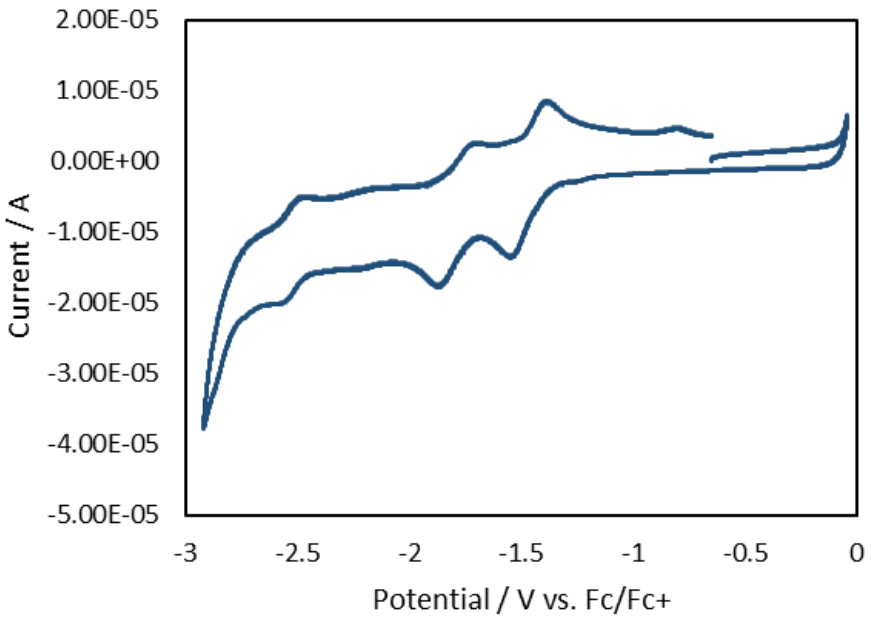

Figure 13. CV of a 100 mM nBu_4NBr in DMA solution containing 1.0 mM $NiBr_2 \cdot DME$ and 1.0 mM 5,5'Me_2bpy. The scan rate was v = 0.1 V s-1.

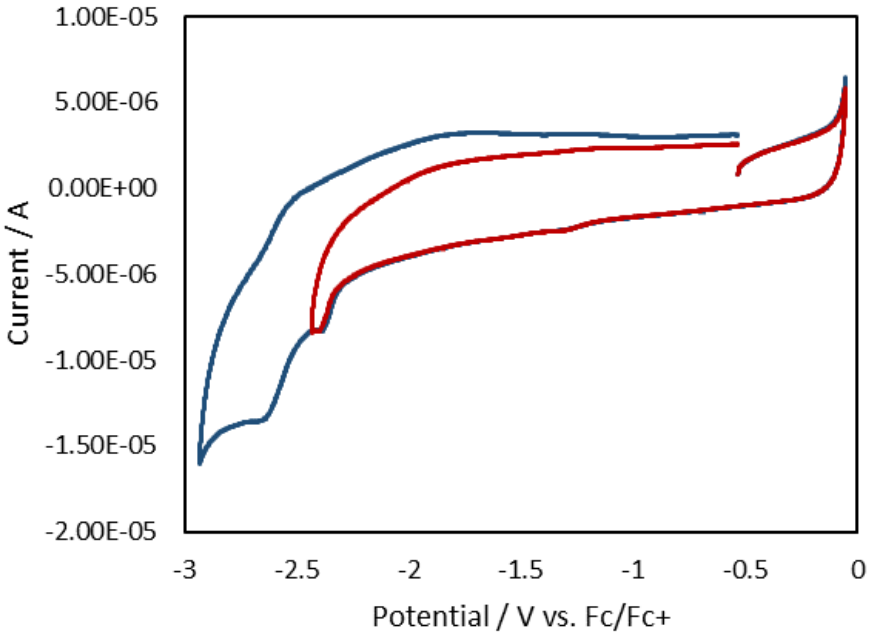

Figure 14. CV of a 100 mM $^{n}Bu_4NBr$ in DMA solution containing 1.0 mM **L5** (not completely dissolved due to low solubility). The scan rate was v = 0.1 V s^{-1}.

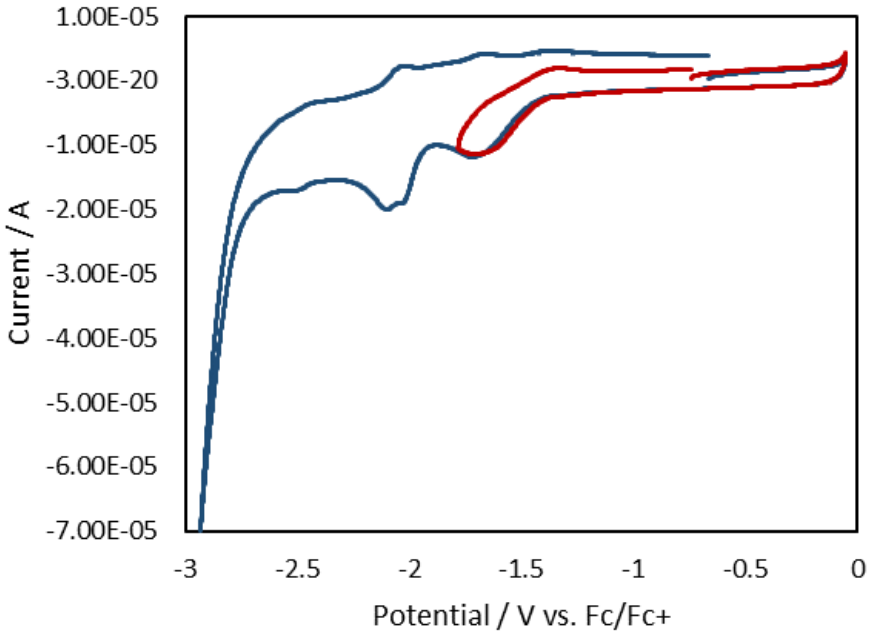

Figure 15. CV of a 100 mM nBu_4NBr in DMA solution containing 1.0 mM $NiBr_2$·DME and 1.0 mM **L5** (completely dissolved). The scan rate was v = 0.1 V s-1.

Conclusion

In summary, the author has synthesized and characterized dumbbell-shaped bipyridine (dsbpy, **L1**–**L6**) and phenanthroline (dsphen, **L7**) ligands bearing bulky substituents (triarylmethly groups for **L1**–**L5**, and 2,6-dibenzhydryl-4-methylphenyl groups for **L6**–**L7**) at the N-β-positions. The dsbpy/dsphen-Ni^{II} titration monitored by UV absorption spectroscopy showed strong monochelation properties of dsbpys (**L3**–**L5**) and dsphen (**L7**). The crystal structures of dsbpy (**L5**) and dsphen (**L7**) were determined by X-ray diffraction analysis, while the electrochemical characteristic of [Ni-(**L5**)] was examined by CV analysis.

Experimental Section

General. NMR spectra were recorded on a JEOL ECX-II (400 MHz for ^1H NMR, 100.5 MHz for ^{13}C NMR). Chemical shift values are referenced to Me_4Si (^1H; 0 ppm), $CDCl_3$ (^{13}C; 77.16

ppm), C_6D_6 (^{1}H; 7.16 ppm, ^{13}C; 128.0 ppm). IR spectra were measured with a PerkinElmer Frontier instrument. TLC analyses were performed on commercial glass plates bearing a 0.25-mm layer of Merck Silica gel 60F_{254}. Silica gel (Kanto Chemical Co., Ltd., Silica gel 60 N, spherical, neutral) was used for column chromatography. All reactions were carried out under nitrogen or argon atmosphere. Materials were obtained from commercial suppliers or prepared according to standard procedures unless otherwise noted.

5,5'-Dimesityl-2,2'-bipyridine (5,5'-Mes$_2$bpy)

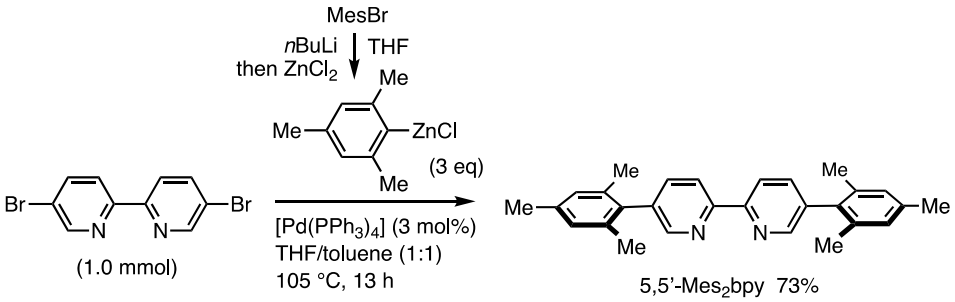

2-Bromomesitylene (0.449 mL, 3.0 mmol) and THF (3 mL) were placed in Schlenk tube with a stirring bar. The Schlenk tube was cooled to –40 °C, and *n*-butyllithium (1.57 M in hexane, 1.91 mL, 3 mmol) was added dropwise. The solution was stirred at –40 °C for 30 min, and then $ZnCl_2$ (409 mg, 3.0 mmol) in THF (3 mL) was added. The mixture was warmed to room temperature, and then 5,5'-dibromo-2,2'-bipyridine (314 mg, 1.0 mmol), [$Pd(PPh_3)_4$] (34.7 mg, 0.03 mmol, 3 mol%) and toluene (6 mL) were added. The mixture was heated at 105 °C for 13 h. After cooling to room temperature, 15% NaOH aq was added, and the mixture was extracted with $CHCl_3$ (20 mL x 3). The organic layer was dried with Na_2SO_4, filtered, and evaporated under vacuum. CH_3CN (40 mL) was added to the residue, and the resulting suspension was vigorously stirred at 60 °C for 1 h. The remained solid was collected by filtration, and then passed through SiO_2 with eluent (EtOAc/$CHCl_3$ = 1:1). The solvent was removed under vacuum to give 5,5'-Mes$_2$bpy as white solids (287 mg, 73% yield).

M.p.: 298.7–299.5 °C. **^{1}H NMR** (400 MHz, $CDCl_3$): δ 8.57–8.47 (m, 4H), 7.67 (dd, J = 7.8, 2.3 Hz, 2H), 7.00 (s, 4H), 2.36 (s, 6H), 2.07 (s, 12H). **^{13}C NMR** (100.5 MHz, $CDCl_3$): δ 154.4, 149.8, 138.1, 137.5, 136.7, 136.2, 134.9, 128.4, 120.6, 21.0, 20.8. **IR** (ATR): 2919, 2853, 1609, 1592, 1541, 1459, 1380, 1356, 1228, 1123, 1062, 1034, 999, 848, 754, 742 cm^{-1}. **HR-FDMS** (*m/z*): $[M]^+$ Calcd for $C_{28}H_{28}N_2$ 392.2252; found, 392.2247. 5,5'-Mes$_2$bpy has been reported in

the patent literature,[9] but its spectroscopic characterization has not been demonstrated.

5,5'-Dityrityl-2,2'-bipyridine (L1)

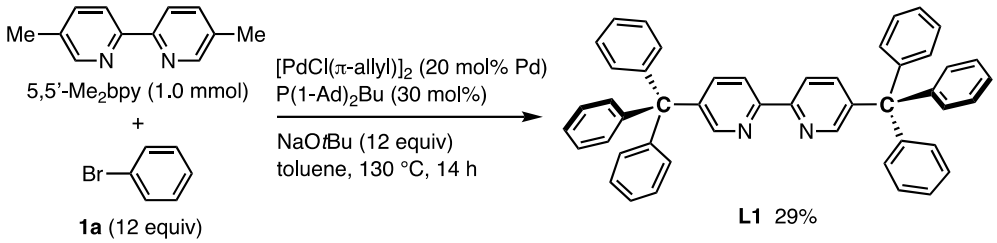

In a nitrogen-filled glove box, [PdCl(π-allyl)]$_2$ (36.6 mg, 0.1 mmol, 20 mol% Pd), P(1-Ad)$_2$Bu (108 mg, 0.3 mmol, 30 mol%) and toluene (10 mL) were placed in an oven-dried vial tube. After stirring at room temperature for 5 min, 5,5'-dimethyl-2,2'-bipyridine (5,5'-Me$_2$bpy, 184 mg, 1.0 mmol, 1.0 eq), bromobenzene (**1a**, 1.88 g, 12 mmol, 12 eq), and NaO*t*Bu (1.15 g, 12 mmol, 12 eq) were added. The tube was sealed with screw cap, and it was brought out of the glove box. The reaction mixture was stirred at 130 °C for 14 h. After cooling to room temperature, 2N NaOH aq (20 mL) was added, and then the mixture was extracted with $CHCl_3$ (40 mL x 3). The organic layer was washed with brine, dried with $MgSO_4$, filtered and evaporated under reduced pressure. The residue was purified by silica gel column chromatography (EtOAc/$CHCl_3$ = 20:80) to give orange solids. CH_3CN (50 mL) was added to the residue, and the resulting suspension was vigorously stirred at 60 ℃ for 2 h. The remained solid was collected by filtration to give **L1** as white solids (188 mg, 29% yield).

M.p.: > 300 ℃. **^{1}H NMR** (400 MHz, $CDCl_3$): δ 8.54 (d, J = 1.8 Hz, 2H), 8.25 (d, J = 8.2 Hz, 2H), 7.67 (dd, J = 8.7, 2.3 Hz, 2H), 7.32–7.18 (m, 30H). **^{13}C NMR** (100.5 MHz, $CDCl_3$): δ 153.1, 151.9, 145.7, 142.5, 139.1, 130.9, 127.8, 126.3, 119.6, 63.3. **IR** (ATR): 3055, 1594, 1543, 1492, 1459, 1442, 1243, 1184, 1083, 1022, 892, 837, 762, 747, 699 cm^{-1}. **HR-FDMS** (*m/z*): $[M]^+$ Calcd for $C_{48}H_{36}N_2$ 640.2878; found, 640.2863.

5,5'-Bis(tris(4-(*tert*-butyl)phenyl)methyl)-2,2'-bipyridine (L2)

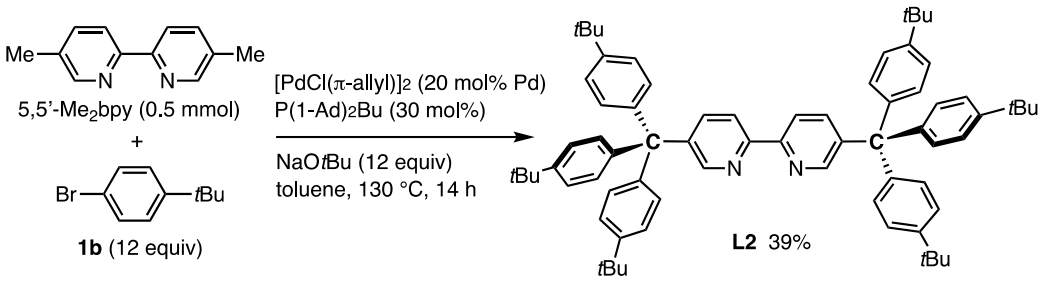

In a nitrogen-filled glove box, $[PdCl(\pi\text{-allyl})]_2$ (18.2 mg, 0.05 mmol, 20 mol% Pd), P(1-Ad)$_2$Bu (53.7 mg, 0.15 mmol, 30 mol%) and toluene (5 mL) were placed in an oven-dried vial tube. After stirring at room temperature for 5 min, 5,5'-dimethyl-2,2'-bipyridine (5,5'-Me$_2$bpy, 92.1 mg, 0.50 mmol, 1.0 eq), 1-bromo-4-*tert*-butylbenzene (**1b**, 1.28 g, 6.0 mmol, 12 eq), and NaO*t*Bu (577 mg, 6.0 mmol, 12 eq) were added. The tube was sealed with screw cap, and it was brought out of the glove box. The reaction mixture was stirred at 130 °C for 14 h. After cooling to room temperature, NH_4Cl aq (20 mL) was added, and then the mixture was extracted with $CHCl_3$ (10 mL x 3). The organic layer was washed with brine, dried with $MgSO_4$, filtered and evaporated under reduced pressure. The residue was purified by silica gel column chromatography ($CHCl_3$) to give yellow solids. CH_3CN (50 mL) was added to the residue, and the resulting suspension was vigorously stirred at 60 ℃ for 1 h. The remained solid was collected by filtration to give **L2** contaminated with impurities as pale-yellow solids (294 mg, ~90% purity). Next, $CHCl_3$ (5 mL) and CH_3CN (30 mL) were added to the residue, and the resulting suspension was vigorously stirred at 90 ℃ for 15 min. The remained solid was collected by filtration to give **L2** as white solids (190 mg, 39% yield).

M.p.: > 300 ℃. **^{1}H NMR** (400 MHz, $CDCl_3$): δ 8.49 (d, J = 1.8 Hz, 2H), 8.22 (d, J = 8.2 Hz, 2H), 7.65 (dd, J = 8.3, 2.3 Hz, 2H), 7.28–7.21 (m, 12H), 7.14–7.07 (m, 12H), 1.30 (s, 54H). **^{13}C NMR** (100.5 MHz, $CDCl_3$): δ 153.0, 151.9, 148.7, 143.1, 142.8, 139.3, 130.5, 124.4, 119.3, 62.0, 34.3, 31.3. **IR** (ATR): 2960, 1507, 1469, 1397, 1363, 1268, 1109, 1023, 842, 823, 753, 677 cm^{-1} **HR-FDMS** (*m/z*): $[M]^+$ Calcd for $C_{72}H_{84}N_2$ 976.6634; found, 976.6641.

5,5'-Bis(tris(3,5-dimethylphenyl)methyl)-2,2'-bipyridine (L3)

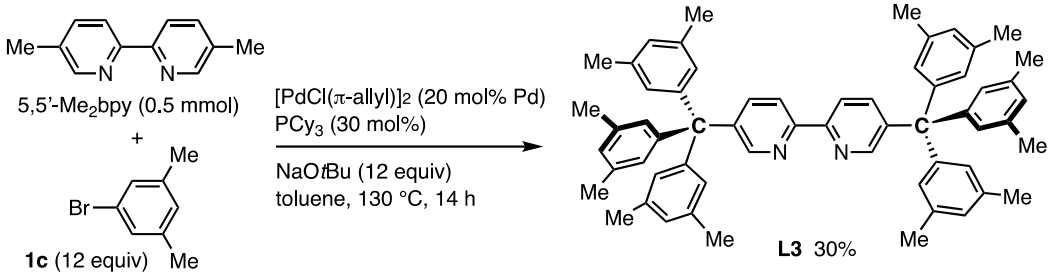

In a nitrogen-filled glove box, $[PdCl(\pi\text{-allyl})]_2$ (18.3 mg, 0.05 mmol, 20 mol% Pd), PCy_3 (42.1 mg, 0.3 mmol, 30 mol%) and toluene (5 mL) were placed in an oven-dried vial tube. After stirring at room temperature for 5 min, 5,5'-dimethyl-2,2'-bipyridine (5,5'-Me_2bpy, 92.1 mg, 0.5 mmol, 1.0 eq), 1-bromo-3,5-dimethylbenzene (**1c**, 1.11 g, 6.0 mmol, 12 eq), and NaO*t*Bu (577 mg, 6.0 mmol, 12 eq) was added. The tube was sealed with screw cap, and it was brought out of the glove box. The reaction mixture was stirred at 130 °C for 14 h. After cooling to room temperature, saturated NH_4Cl aq (20 mL) was added, and then the mixture was extracted with toluene (40 mL x 3). The organic phase was washed with brine, dried with $MgSO_4$, filtered and evaporated under reduced pressure. The residue was purified by silica gel column chromatography (EtOAc/Hexane = 5:95) to give yellow solid. CH_3CN (30 mL) was added to the residue, and the resulting suspension was vigorously stirred at 60 °C for 2 h. The remained solid was collected by filtration to give **L3** as pale yellow solid (120 mg, 30% yield).

M.p.: > 300 °C. **^{1}H NMR** (400 MHz, $CDCl_3$): δ 8.57 (d, J = 1.8 Hz, 2H), 8.19 (d, J = 9.2 Hz, 2H), 7.68 (dd, J = 8.7, 2.8 Hz, 2H), 6.84 (s, 12H), 6.82 (s, 6H), 2.21 (s, 36H). **^{13}C NMR** (100.5 MHz, $CDCl_3$): δ 152.8, 151.8, 145.9, 143.2, 139.4, 136.8, 128.7, 127.7, 119.5, 63.0, 21.6. **IR** (ATR): 2917, 1594, 1466, 1374, 1025, 846, 819, 762, 711 cm^{-1}. **HR-FDMS** (*m/z*): $[M]^+$ Calcd for $C_{60}H_{60}N_2$ 808.4756; found, 808.4744.

5,5'-Bis(tris(3,5-diethylphenyl)methyl)-2,2'-bipyridine (L4)

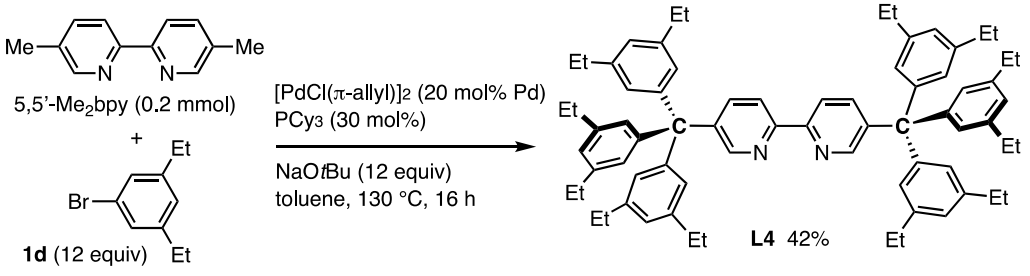

In a nitrogen-filled glove box, [PdCl(π-allyl)]$_2$ (7.3 mg, 0.02 mmol, 20 mol% Pd), PCy_3 (16.8 mg, 0.06 mmol, 30 mol%) and toluene (2 mL) were placed in an oven-dried vial tube. After stirring at room temperature for 5 min, 5,5'-dimethyl-2,2'-bipyridine (5,5'-Me$_2$bpy, 36.8 mg, 0.2 mmol, 1.0 eq), 1-bromo-3,5-diethylbenzene (**1d**, 511 mg, 2.4 mmol, 12 eq), and NaO*t*Bu (231 mg, 2.4 mmol, 12 eq) was added. The tube was sealed with screw cap, and it was brought out of the glove box. The reaction mixture was stirred at 130 °C for 16 h. After cooling to room temperature, saturated NH_4Cl aq (20 mL) was added, and then the mixture was extracted with Et_2O (20 mL x 3). The organic phase was washed with brine, dried with $MgSO_4$, filtered and evaporated under reduced pressure. The residue was purified by silica gel column chromatography (EtOAc/Hexane = 5:95) to give yellow solid. CH_3CN (25 mL) was added to the residue, and the resulting suspension was vigorously stirred at 60 ℃ for 2 h. The remained solid was collected by filtration to give **L4** as off-white solid (81.3 mg, 42% yield).

M.p.: 231.7–232.3 ℃. **^{1}H NMR** (400 MHz, $CDCl_3$): δ 8.60 (d, J = 1.8 Hz, 2H), 8.19 (d, J = 7.8 Hz, 2H), 7.74 (dd, J = 8.2, 2.3 Hz, 2H), 6.94 (s, 12H), 6.83 (s, 6H), 2.51 (q, J = 7.8 Hz, 24H), 1.13 (t, J = 7.8 Hz, 36H). **^{13}C NMR** (100.5 MHz, $CDCl_3$): δ 152.8, 151.8, 146.2, 143.5, 143.3, 139.2, 127.9, 125.0, 119.5, 63.5, 29.0, 15.8. **IR** (ATR): 2961, 2929, 2868, 1593, 1542, 1457, 1414, 1370, 1219, 1062, 1025, 868, 772, 741 cm^{-1}. **HR-FDMS** (*m/z*): $[M]^+$ Calcd for $C_{72}H_{84}N_2$ 976.6634; found, 976.6622.

5,5'-Bis(tris(3,5-diisopropylphenyl)methyl)-2,2'-bipyridine (L5)

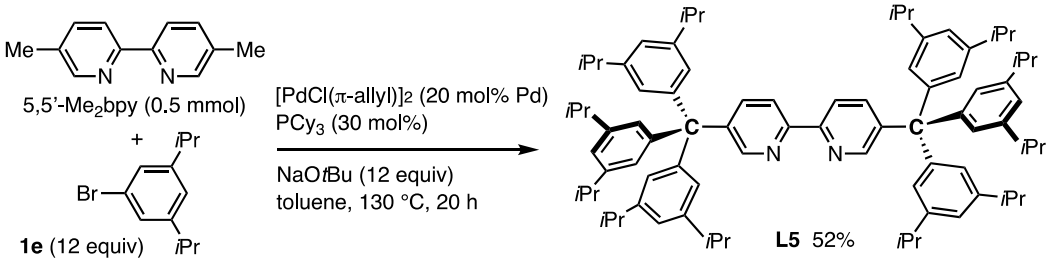

In a nitrogen-filled glove box, [PdCl(π-allyl)]$_2$ (18.3 mg, 0.05 mmol, 20 mol% Pd), PCy_3 (42.1 mg, 0.3 mmol, 30 mol%) and toluene (5 mL) were placed in an oven-dried vial tube. After stirring at room temperature for 5 min, 5,5'-dimethyl-2,2'-bipyridine (5,5'-Me$_2$bpy, 92.1 mg, 0.5 mmol, 1.0 eq), 1-bromo-3,5-diisipropylbenzene (**1e**, 1.45 g, 6.0 mmol, 12 eq), and NaO*t*Bu (577 mg, 6.0 mmol, 12 eq) was added. The tube was sealed with screw cap, and it was brought out of the glove box. The reaction mixture was stirred at 130 °C for 20 h. After cooling to room

temperature, saturated NH_4Cl aq (20 mL) was added, and then the mixture was extracted with Et_2O (30 mL x 3). The organic phase was washed with brine, dried with $MgSO_4$, filtered and evaporated under reduced pressure. The residue was purified by silica gel column chromatography (EtOAc/Hexane = 5:95) to give yellow solid. $CHCl_3$ (10 mL) and CH_3CN (40 mL) were added to the residue, and the resulting suspension was vigorously stirred at 60 ℃ for 2 h. The remained solid was collected by filtration to give **L5** as off-white solid (297 mg, 52% yield).

M.p.: 256.7–258.0 ℃. **^{1}H NMR** (400 MHz, $CDCl_3$): δ 8.64 (d, J = 1.8 Hz, 2H), 8.20 (d, J = 8.7 Hz, 2H), 7.80 (dd, J = 8.7, 2.8 Hz, 2H), 6.97 (s, 12H), 6.83 (s, 6H), 2.76 (septet, J = 6.9 Hz, 12H), 1.12 (d, J = 6.9 Hz, 72H). **^{13}C NMR** (100.5 MHz, $CDCl_3$): δ 152.7, 151.8, 147.7, 146.3, 143.7, 139.1, 126.4, 121.9, 119.5, 64.1, 34.2, 24.0. **IR** (ATR): 2958, 2868, 1592, 1464, 1361, 1190, 1024, 866, 843, 758, 738, 719 cm^{-1}. **HR-FDMS** (*m*/z): $[M]^+$ Calcd for $C_{84}H_{108}N_2$ 1144.8512; found, 1144.8496.

5,5'-bis(2,6-dibenzhydryl-4-methylphenyl)-2,2'-bipyridine (L6)

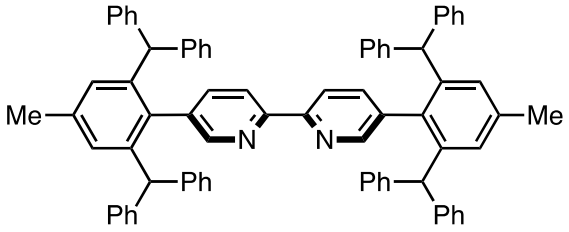

2-Bromo-1,3-bis(diphenylmethyl)-5-methylbenzene (2.11 g, 4.2 mmol) and THF (8.4 mL) were placed in Schlenk tube with a stirring bar. The Schlenk tube was cooled to -40 ℃, and *n*-butyllithium (1.57 M in hexane, 2.68 mL, 4.2 mmol) was added dropwise. The solution was stirred at -40 ℃ for 1 h and then $ZnCl_2$ (409 mg, 4.2 mmol) in THF (5 mL) was added at -25 ℃. The mixture was warmed to room temperature, and then 5,5'-dibromo-2,2'-bipyridine (440 mg, 1.4 mmol), $[Pd(PPh_3)_4]$ (161.8 mg, 0.14 mmol) and toluene (8.4 mL) were added. The mixture was heated at 110 ℃ for 37 h. After cooling to room temperature, saturated Na_2CO_3 aq was added, and the mixture was extracted with $CHCl_3$ (50 mL x 3). The organic layer was dried with Na_2SO_4, filtered, and evaporated under vacuum. The residue was purified by silica gel column chromatography (EtOAc/CH_2Cl_2 = 0:100 to 5:95) to give white solids. CH_3CN (50 mL) was added to the residue, and the resulting suspension was vigorously stirred at 60 ℃ for 2 h. The

remained solid was collected by filtration to give the desired compound as white solids (173 mg, 12% yield).

M.p.: > 300 °C. **^{1}H NMR** (400 MHz, $CDCl_3$): δ 8.18 (d, J = 2.0 Hz, 2H), 8.03 (d, J = 8.4 Hz, 2H), 7.27-7.11 (m, 24H), 6.98-6.83 (m, 18H), 6.80 (s, 4H), 5.22 (s, 4H), 2.23 (s, 6H). **^{13}C NMR** (100.5 MHz, $CDCl_3$): δ 154.3, 149.8, 143.7, 143.4, 142.8, 138.6, 137.4, 135.6, 129.5, 128.7, 128.2, 126.2, 119.8, 54.0, 21.7. **IR** (ATR): 3061, 3024, 2922, 1598, 1493, 1447, 1031, 846, 764, 752, 697 cm^{-1}. **HR-FDMS** (*m/z*): $[M]^+$ Calcd for $C_{76}H_{60}N_2$ 1000.4756; found, 1000.4765.

3,8-bis(2,6-dibenzhydryl-4-methylphenyl)-1,10-phenanthroline (L7)

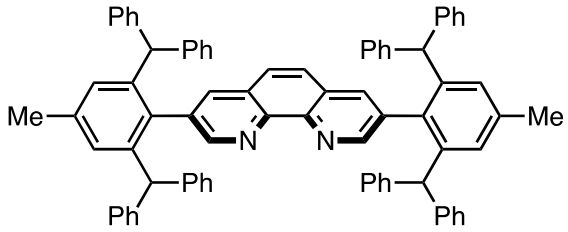

2-Bromo-1,3-bis(diphenylmethyl)-5-methylbenzene (2.11 g, 4.2 mmol) and THF (8.4 mL) were placed in Schlenk tube with a stirring bar. The Schlenk tube was cooled to -40 °C, and *n*-butyllithium (1.57 M in hexane, 2.68 mL, 4.2 mmol) was added dropwise. The solution was stirred at -40 °C for 1 h, and then $ZnCl_2$ (409 mg, 4.2 mmol) in THF (5 mL) was added. The mixture was warmed to room temperature, and then 3,8-dibromo-1,10-phenanthroline (473 mg, 1.4 mmol), $[Pd(PPh_3)_4]$ (161.8 mg, 0.14 mmol) and toluene (8.4 mL) were added. The mixture was heated at 110 °C for 44 h. After cooling to room temperature, saturated Na_2CO_3 aq was added, and the mixture was extracted with CH_2Cl_2 (50 mL x 3). The organic layer was dried with Na_2SO_4, filtered, and evaporated under vacuum. The residue was purified by silica gel column chromatography (EtOAc/hexane = 50:50) to give 1.38 g of yellow solid. The solid was recrystallized with CH_2Cl_2/MeOH and then washed with MeOH to give the desired compound as white solids (725 mg, 50% yield).

M.p.: > 300 °C. **^{1}H NMR** (400 MHz, $CDCl_3$): δ 8.93 (d, J = 1.6 Hz, 2H), 7.29-7.07 (m, 24H), 7.05, (s, 4H), 7.09-7.03 (m, 8H), 6.92 (d, J = 2.0 Hz, 2H), 6.84 (s, 4H), 6.80-6.72 (m, 8H), 5.17 (s, 4H), 2.25 (s, 6H). **^{13}C NMR** (100.5 MHz, $CDCl_3$): δ 151.2, 144.6, 143.7, 143.2, 143.0, 137.6, 135.4, 134.7, 129.5, 128.7, 128.3, 128.0, 127.5, 126.4, 126.3, 126.1, 54.3, 21.7 **IR** (ATR): 3024, 1598, 1562, 1493, 1447, 1421, 1275, 1061, 916, 763, 744, 697 cm^{-1}. **HR-FDMS** (*m/z*): $[M]^+$

Calcd for $C_{78}H_{60}N_2$ 1024.4756; found, 1024.4768.

Calculation details for equilibrium restricted factor analysis with *SIVVU*

In 2008, Griend and co-workers reported characterization of Ni(II)/2,2'-bipyridine and Ni(II)/1,10-phenanthroline complexes using equilibrium restricted factor analysis (ERFA), which is a technique for extracting spectral and thermodynamic information for component species involved in solution equilibria.[6] The authors wrote their own code in the form of *Matlab* protocols using a graphical user interface named *Sivvu*, and shared the program on their website (http://sivvu.org/). To quantify Ni(II)-bpy coordination equilibria in our research, the concentration profiles for each Ni species and the free ligand were constructed with ERFA aided by the *Sivvu* program. In Griend's report,[6] the UV-vis absorbance at 450–900 nm was used for quantification of Ni(II)-bpy coordination equilibria. However, due to low solubility of the dsbpy ligands, we adopted the strong absorbance at 270–350 nm for the analysis. Recently, Kitamura and co-workers used absorbance data at UV range (270 and 273 nm) for quantification of metal/1,10-phenanthroline-type ligand coordination equilibria (metal = Ba^{2+}, Ca^{2+}, Mg^{2+}, or Zn^{2+}).[10]

Titration with 5,5'-Me_2bpy

5,5'-Me_2bpy in DMA solution (3 mL, 0.05 mM, 0.15 mmol) was placed in a 1 cm pathlength quartz cell equipped with a stir bar, and then it was capped with a rubber septum. N iBr_2·DME in DMA solution (1.70 mM) was continuously added to the cell by micro syringe (0.05, 0.1, 0.15, 0.2, 0.25, 0.3, 0.35, 0.4, 0.45, 0.5, 0.55, 0.6, 0.7, 0.8, 0.9, 1.0, 1.2, 1.4, 1.6, 1.8, 2.0, 2.4, and 3.0 equiv. relative to 5,5'-Me_2bpy). The solution was stirred at room temperature for 2 min, and then the absorption (270–350 nm) was recorded for every 0.5 nm. The spectra are shown in Figure 16.

5,5'-Me_2bpy has a maximum absorption wavelength at 290 nm. When $NiBr_2$·DME was added up to 0.6 equiv., the absorbance at 290 nm was decreased and the new peaks were observed around 308 nm and 319 nm, indicating the ligation of 5,5'-Me_2bpy to nickel. When $NiBr_2$·DME was further added up to 3 equiv., the absorbances around 308 nm and 319 nm

changed slightly. These can be attributed to concentration changes for each Ni species due to dynamic coordination equilibrium.

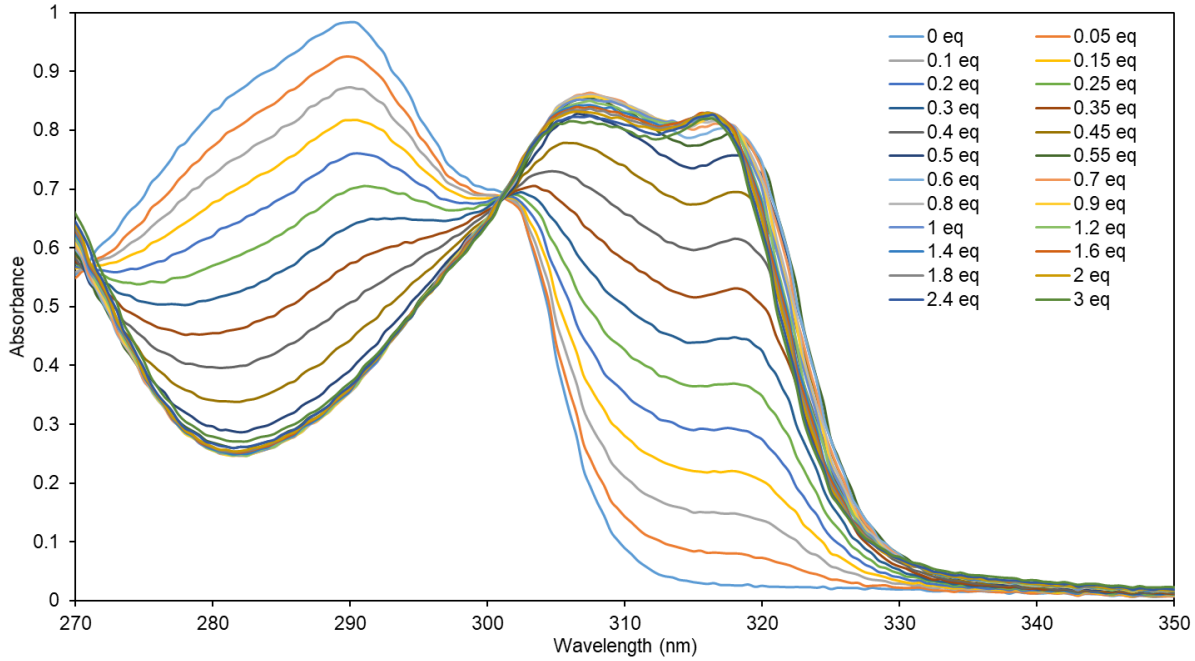

Figure 16. Absorption data for the titration test between 5,5'-Me_2bpy and $NiBr_2$·DME in DMA.

The chemical model for the calculation with EFRA aided by the *Sivvu* program is shown in Figure 17. The absorbing chemical species are set to L, NiL_1, NiL_2, and NiL_3. The ligand-free Ni species (NiL_0, $NiBr_2$·DME) has almost no absorption at 270–350 nm. The chemical species with known molar absorptivity curve (ligand) was set to be refined as "N", and those with the unknowns (NiL_1, NiL_2, and NiL_3) were set to be refined as "Y". Mass balance vectors define the number of each reagent (L and Ni) used to form the given chemical species. Chemical reaction vectors define the chemical reactions between all the chemical species. We set the initial ΔG_1 (binding of the first ligand), ΔG_2 (binding of the second ligand), ΔG_3 (binding of the third ligand) value as –50, –40, –30 kJ/mol, respectively. The initial values had no influence on the finally calculated ΔG_1, ΔG_2, and ΔG_3 values in most cases, unless they were set to extremely unreasonable values.

The estimated molar absorptivity curves and concentration profiles are shown in Figure 18, 19. The Gibbs free energy difference between chemical reactions are given as ΔG_1 = –36.29

kJ/mol, ΔG_2 = –38.39 kJ/mol, ΔG_3 = –20.76 kJ/mol. Although the determination coefficient for the estimation was good (R^2 = 0.99981), the estimated molar absorptivity curve of NiL_3 is noisy and unreasonable (close to unligated 5,5'-Me_2bpy). This is probably because the concentration of NiL_3 was very low in all the solutions as shown in Figure 19. Thus, we assumed that the concentration of NiL_3 was negligible throughout the titration.

CHEMICAL MODEL							
Chemical Species	L	Ni	NiL	NiL_2	NiL_3		
Absorbing(Y/N):	Y	N	Y	Y	Y		
Refined(Y/N):	N	N	Y	Y	Y		
Mass Balance Vectors (L):	1	0	1	2	3		
(Ni):	0	1	1	1	1	$\Delta G°_{initial}$	refined?
Chemical Reaction Vectors (First ligation, ΔG_1):	-1	-1	1	0	0	-50	Y
(Second ligation, ΔG_2)	-1	0	-1	1	0	-40	Y
(Third ligation, ΔG_3)	-1	0	0	-1	1	-30	Y

Figure 17. The chemical model calculation with 5,5'-Me_2bpy

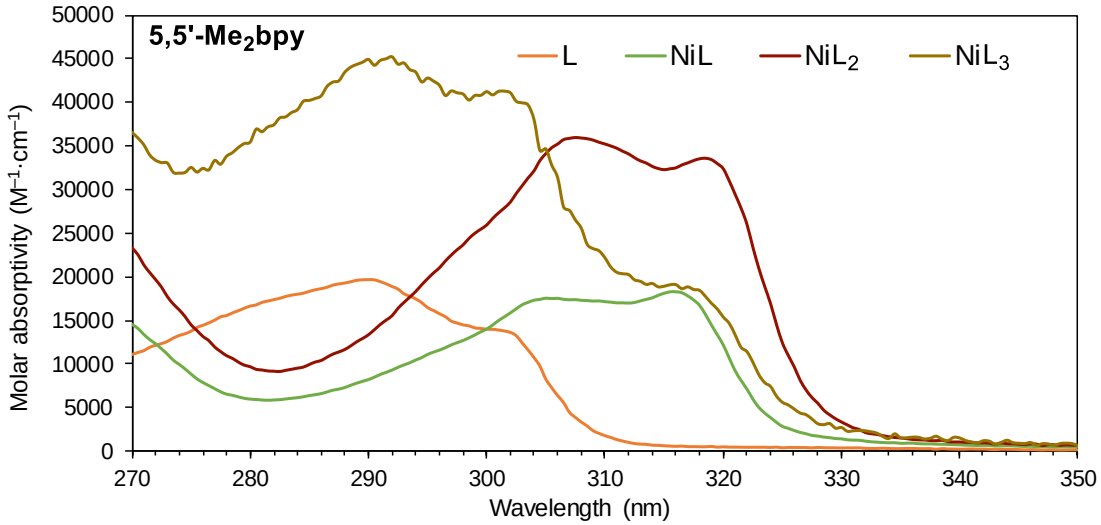

Figure 18. Calculated molar absorptivity curves with 5,5'-Me_2bpy

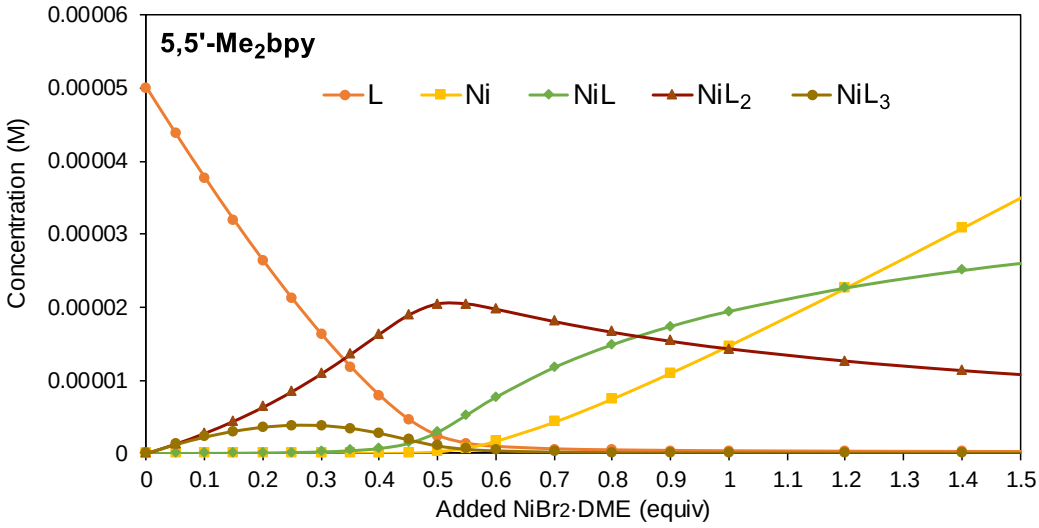

Figure 19. Concentration profiles with 5,5'-Me$_2$bpy. $\Delta G_1 = -36.29$ kJ/mol, $\Delta G_2 = -38.39$ kJ/mol, $\Delta G_3 = -20.76$ kJ/mol. $R^2 = 0.99981$.

Following the above result, we reconstructed a chemical model calculation without NiL_3, as shown in Figure 20. The estimated molar absorptivity curves and concentration profiles are shown in Figure 21, 22. The Gibbs free energy difference between chemical reactions are given as $\Delta G_1 = -47.88$ kJ/mol, $\Delta G_2 = -45.83$ kJ/mol with reasonable molar absorptivity curves and R^2 value (0.099874). Thus, we adopted this model for this research.

CHEMICAL MODEL						
Chemical Species	L	Ni	NiL	NiL2		
Absorbing(Y/N):	Y	N	Y	Y		
Refined(Y/N):	N	N	Y	Y		
Mass Balance Vectors (L):	1	0	1	2		
(Ni):	0	1	1	1	ΔG°initial	refined?
Chemical Reaction Vectors (First ligation, ΔG1):	-1	-1	1	0	-50	Y
(Second ligation, ΔG2)	-1	0	-1	1	-20	Y

Figure 20. The chemical model calculation with 5,5'-Me$_2$bpy (without NiL_3)

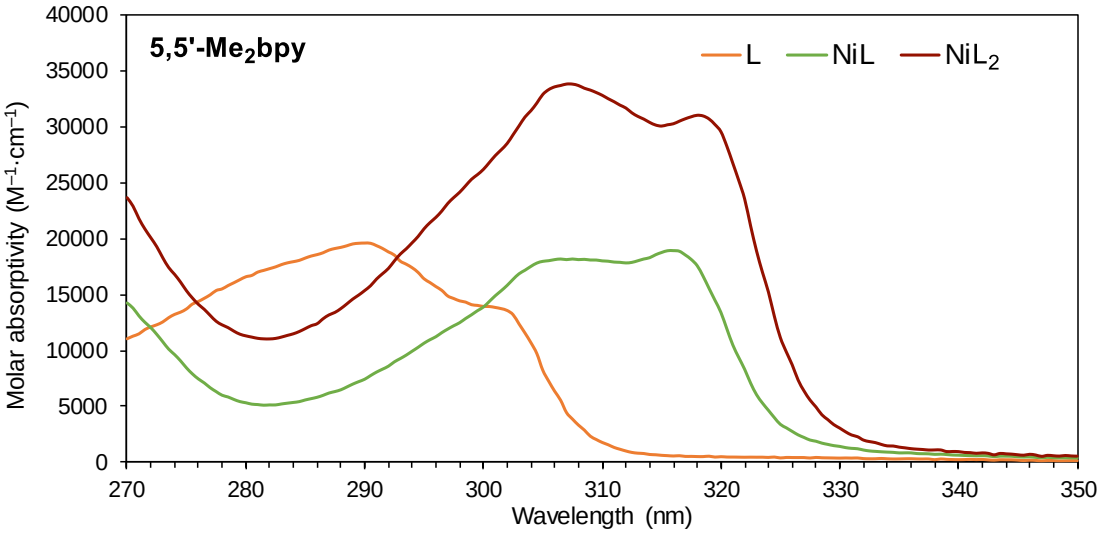

Figure 21. Calculated molar absorptivity curves with 5,5'-Me_2bpy (without NiL_3)

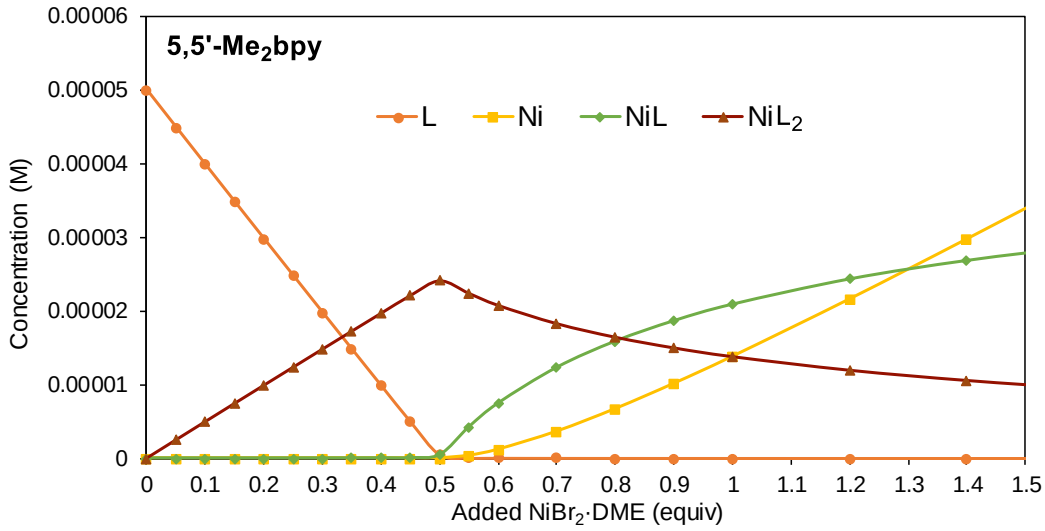

Figure 22. Concentration profiles with 5,5'-Me_2bpy (without NiL_3). ΔG_1 = –47.88 kJ/mol, ΔG_2 = –45.83 kJ/mol, R^2 = 0.99874.

Titration with L1

L1 in DMA solution (3 mL, 0.05 mM, 0.15 mmol) was placed in a 1 cm pathlength quartz cell equipped with a stir bar, and then it was capped with a rubber septum. $NiBr_2$·DME in DMA solution (1.95 mM) was continuously added to the cell by micro syringe (0.05, 0.1, 0.15, 0.2, 0.25, 0.3, 0.35, 0.4, 0.45, 0.5, 0.55, 0.6, 0.7, 0.8, 0.9, 1.0, 1.1, 1.2, 1.3, 1.4, 1.5, 1.7, 2.0, 2.4, and 3.0 equiv. relative to **L1**). The solution was stirred at room temperature for 2 min, and then the absorption (270–350 nm) was recorded for every 0.5 nm. The spectra are shown in Figure

23. The estimated molar absorptivity curves and concentration profiles are shown in Figure 24, 25. The chemical model shown in Figure 20 was used for the analysis.

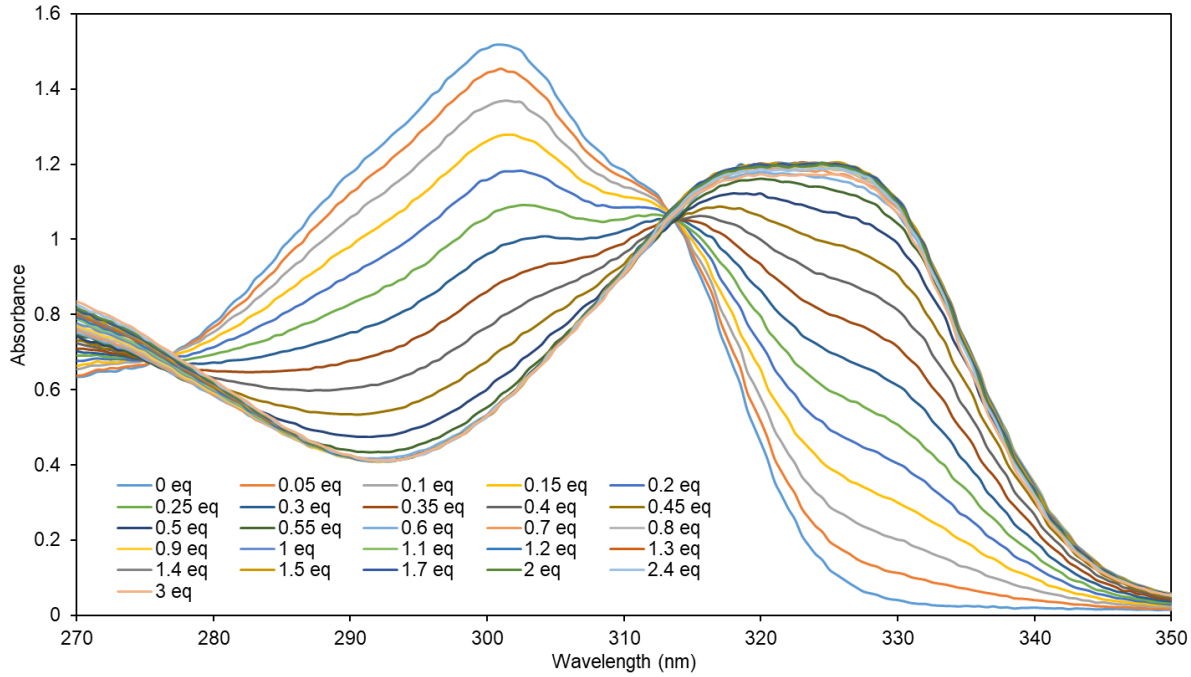

Figure 23. Absorption data for the titration test between **L1** and $NiBr_2$·DME in DMA

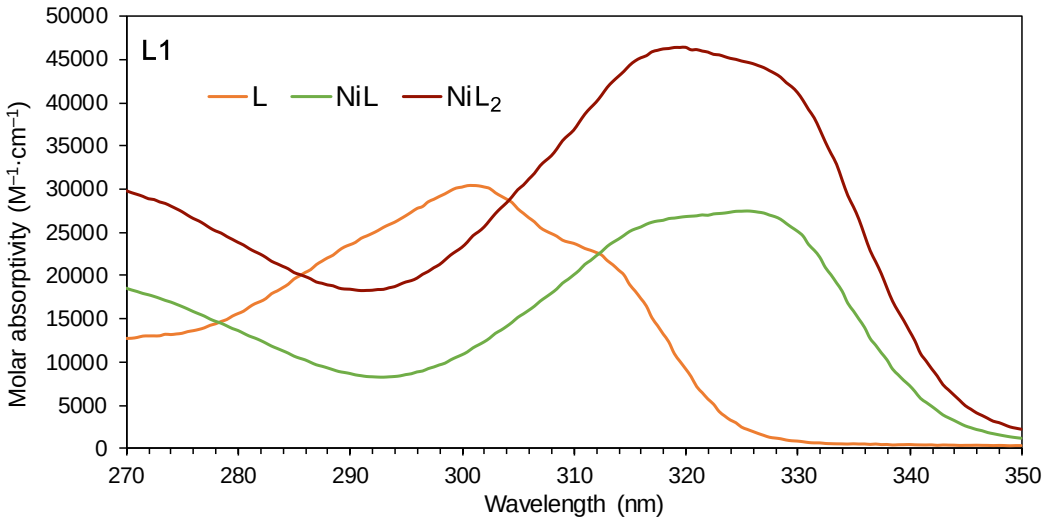

Figure 24. Calculated molar absorptivity curves with **L1**

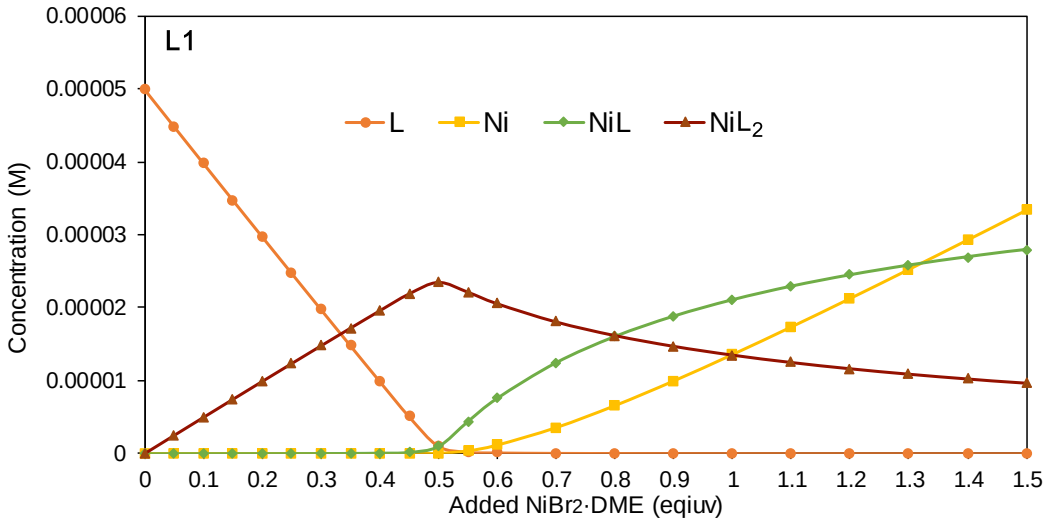

Figure 25. Concentration profiles with **L1**. $\Delta G_1 = -44.18$ kJ/mol, $\Delta G_2 = -41.99$ kJ/mol, $R^2 = 0.99849$.

Titration with L2

L2 in DMA solution (3 mL, 0.05 mM, 0.15 mmol) was placed in a 1 cm pathlength quartz cell equipped with a stir bar, and then it was capped with a rubber septum. $NiBr_2$·DME in DMA solution (1.55 mM) was continuously added to the cell by micro syringe (0.05, 0.1, 0.15, 0.2, 0.25, 0.3, 0.35, 0.4, 0.45, 0.5, 0.55, 0.6, 0.65, 0.7, 0.8, 0.9, 1.0, 1.1, 1.2, 1.3, 1.4, 1.5, 1.7, 2.0, 2.4, and 3.0 equiv. relative to **L2**). The solution was stirred at room temperature for 2 min, and then the absorption (270–350 nm) was recorded for every 0.5 nm. The spectra are shown in Figure 26. The estimated molar absorptivity curves and concentration profiles are shown in Figure 27, 28. The chemical model shown in Figure 20 was used for the analysis.

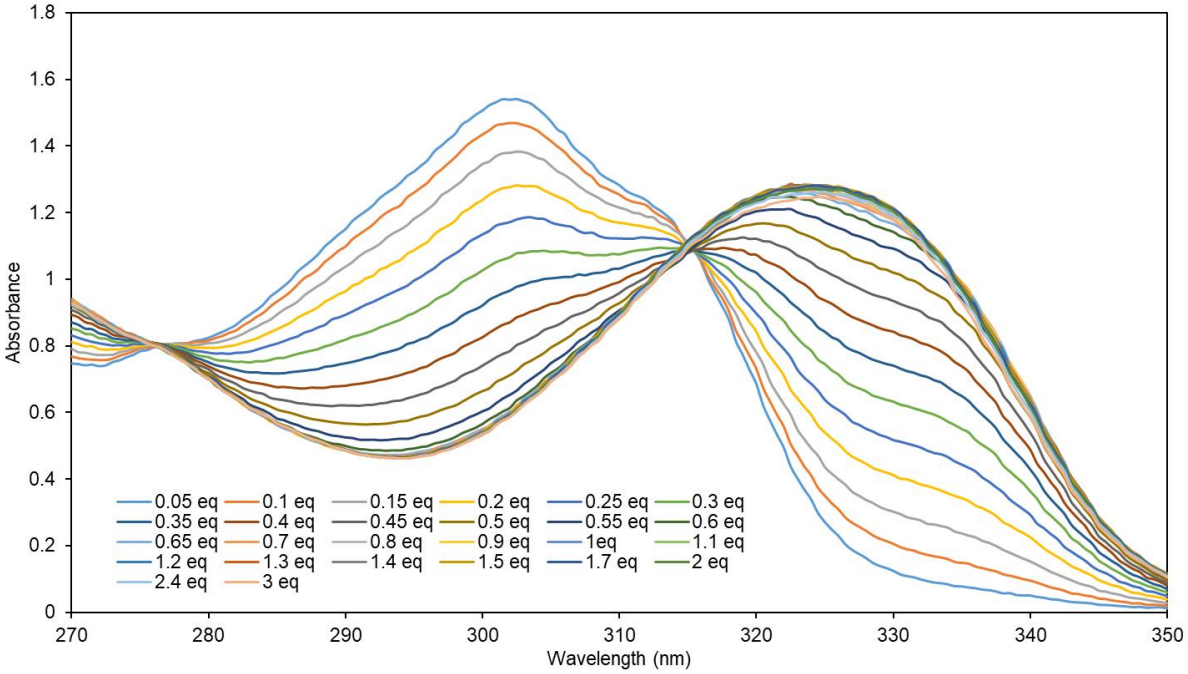

Figure 26. Absorption data for the titration test between **L2** and $NiBr_2$·DME in DMA

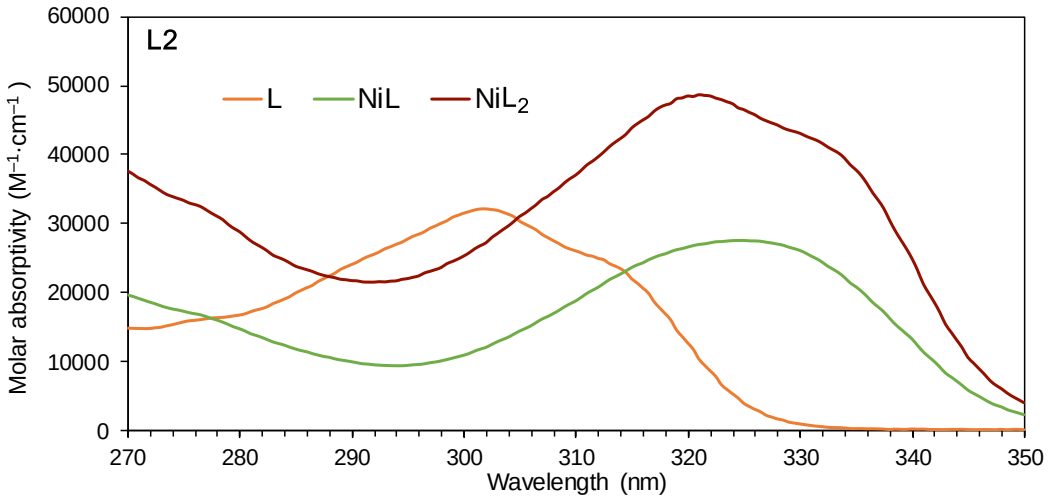

Figure 27. Calculated molar absorptivity curves with **L2**

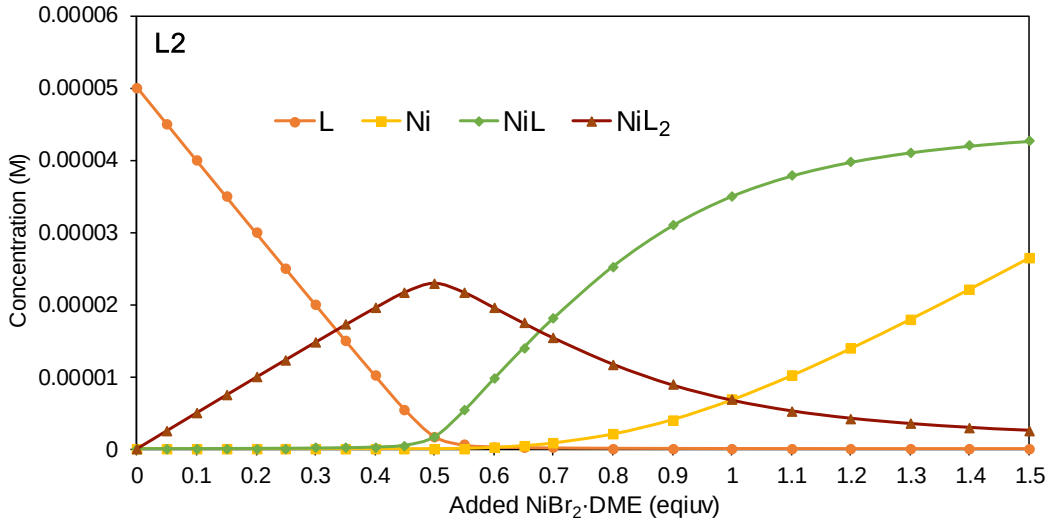

Figure 28. Concentration profiles with **L2**. $\Delta G_1 = -47.67$ kJ/mol, $\Delta G_2 = -39.52$ kJ/mol, $R^2 = 0.99714$.

Titration with L3

L3 in DMA solution (3 mL, 0.05 mM, 0.15 mmol) was placed in a 1 cm pathlength quartz cell equipped with a stir bar, and then it was capped with a rubber septum. $NiBr_2$·DME in DMA solution (1.95 mM) was continuously added to the cell by micro syringe (0.05, 0.1, 0.15, 0.2, 0.25, 0.3, 0.35, 0.4, 0.45, 0.5, 0.55, 0.6, 0.65, 0.7, 0.75, 0.8, 0.85, 0.9, 1.0, 1.1, 1.2, 1.3, 1.4, 1.5, 1.7, 2.0, 2.4, and 3.0 equiv. relative to **L3**). The solution was stirred at room temperature for 2 min, and then the absorption (270–350 nm) was recorded for every 0.5 nm. The spectra are shown in Figure 29. The estimated molar absorptivity curves and concentration profiles are shown in Figure 30, 31. The chemical model shown in Figure 20 was used for the analysis.

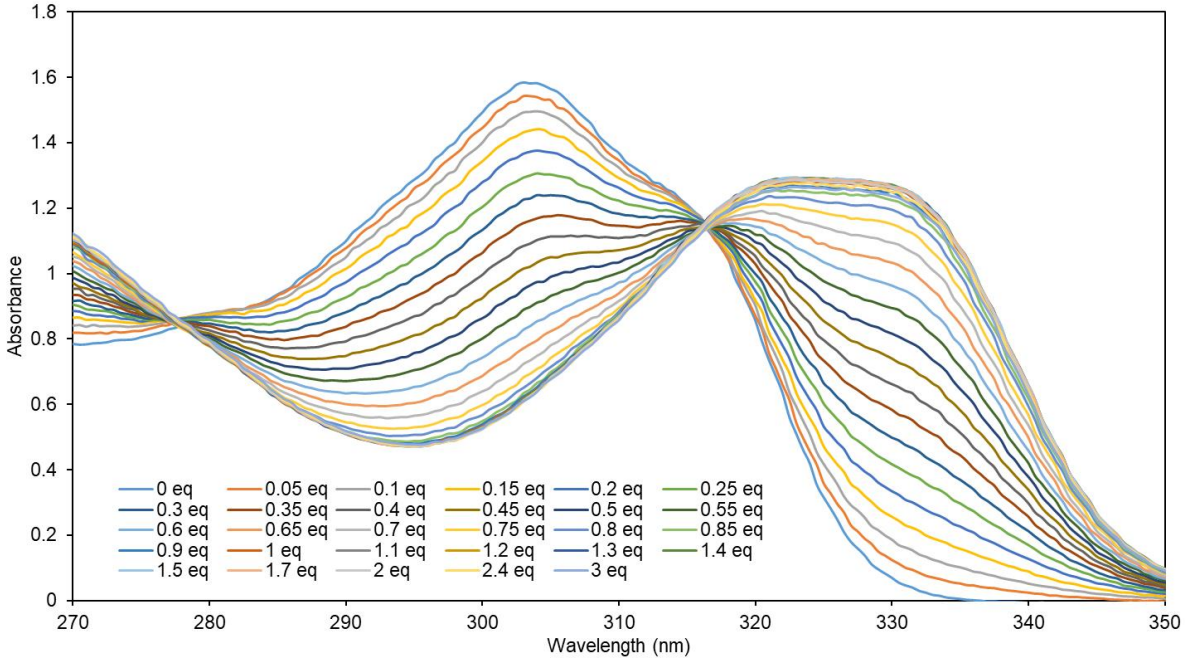

Figure 29. Absorption data for the titration test between **L3** and $NiBr_2 \cdot DME$ in DMA

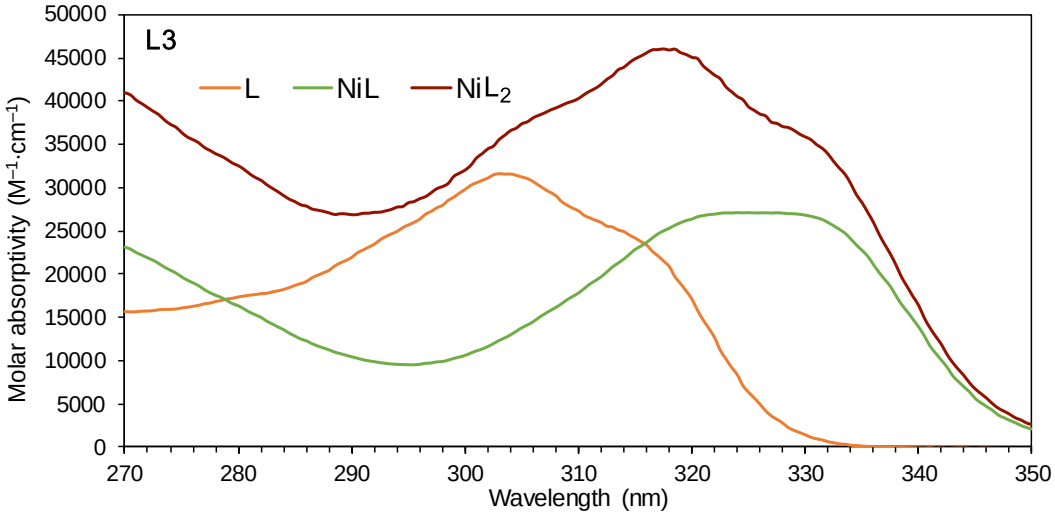

Figure 30. Calculated molar absorptivity curves with **L3**

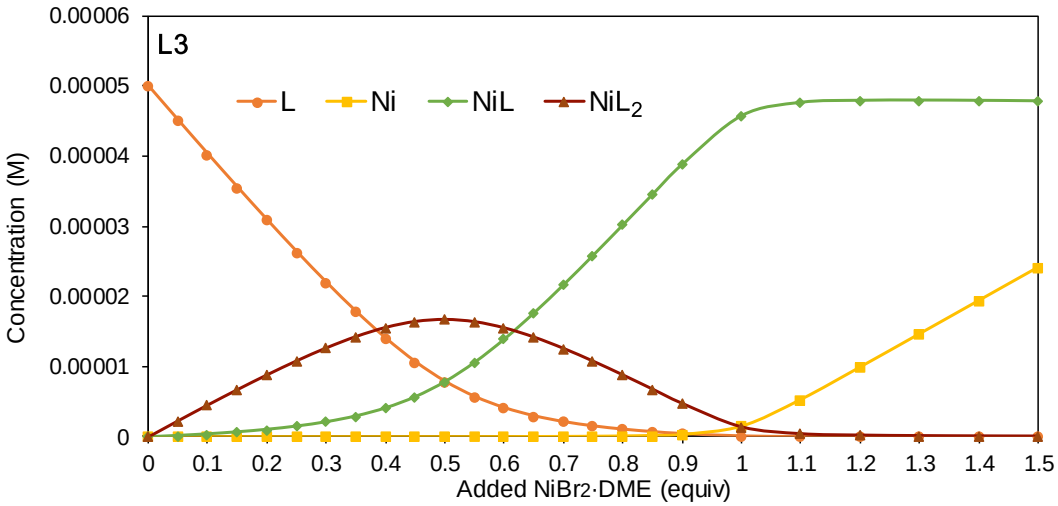

Figure 31. Concentration profiles with **L3**. $\Delta G_1 = -48.08$ kJ/mol, $\Delta G_2 = -30.98$ kJ/mol, $R^2 = 0.99514$.

Titration with L4

L4 in DMA solution (3 mL, 0.05 mM, 0.15 mmol) was placed in a 1 cm pathlength quartz cell equipped with a stir bar, and then it was capped with a rubber septum. $NiBr_2$·DME in DMA solution (1.53 mM) was continuously added to the cell by micro syringe (0.05, 0.1, 0.15, 0.2, 0.25, 0.3, 0.35, 0.4, 0.45, 0.5, 0.55, 0.6, 0.65, 0.7, 0.75, 0.8, 0.85, 0.9, 0.95, 1.0, 1.1, 1.2, 1.3, 1.4, 1.5, 1.7, 2.2, and 3.0 equiv. relative to **L4**). The solution was stirred at room temperature for 2 min, and then the absorption (270–350 nm) was recorded for every 0.5 nm. The spectra are shown in Figure 32. The estimated molar absorptivity curves and concentration profiles are shown in Figure 33, 34. The chemical model shown in Figure 20 was used for the analysis.

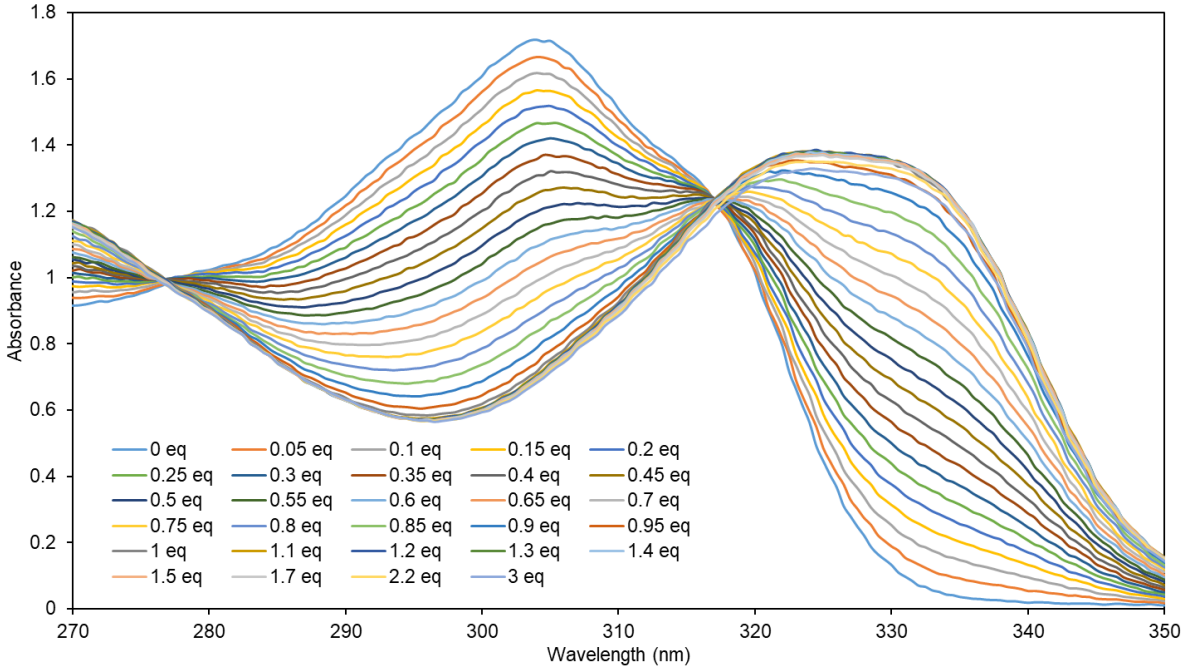

Figure 32. Absorption data for the titration test between **L4** and $NiBr_2$·DME in DMA

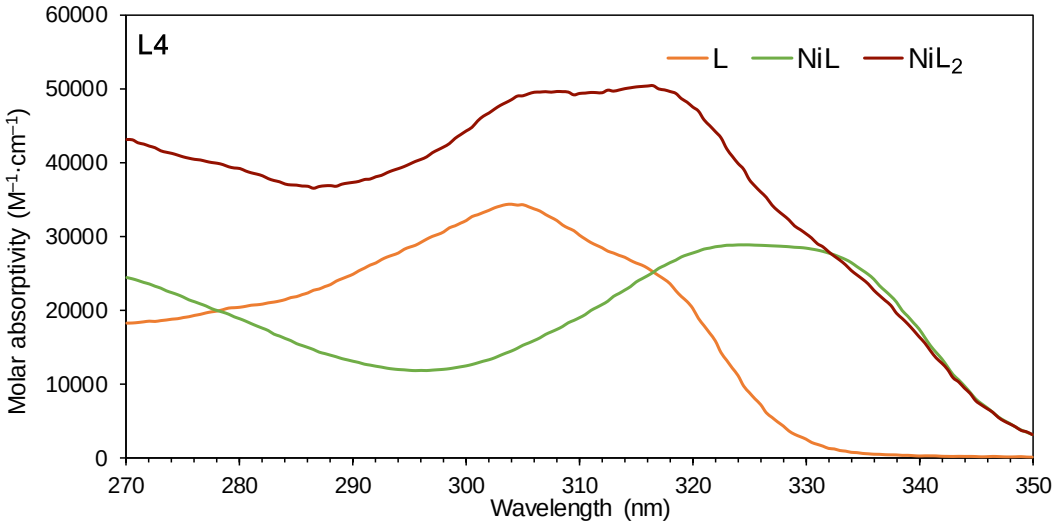

Figure 33. Calculated molar absorptivity curves with **L4**

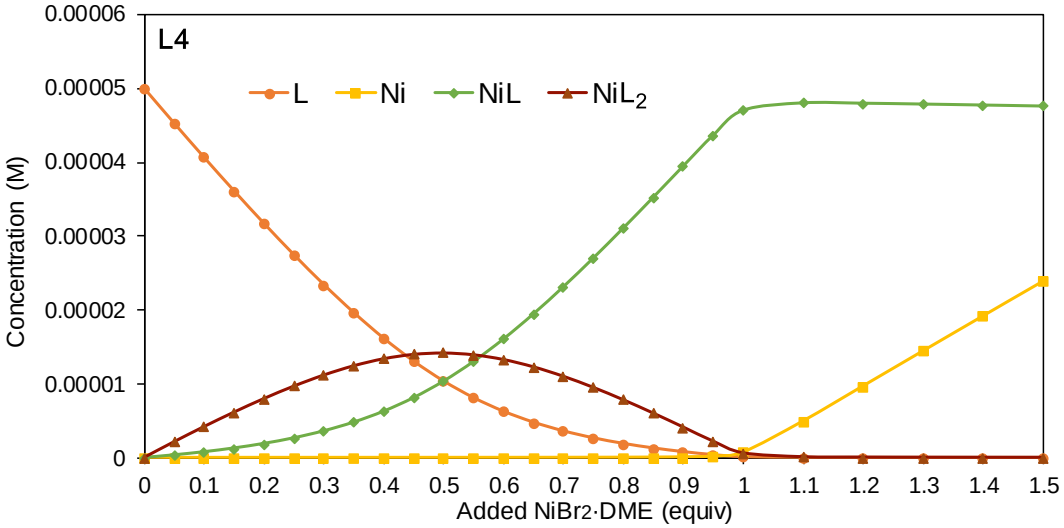

Figure 34. Concentration profiles with **L4**. $\Delta G_1 = -50.21$ kJ/mol, $\Delta G_2 = -29.19$ kJ/mol, $R^2 = 0.99953$.

Titration with L5

L5 in DMA solution (3 mL, 0.05 mM, 0.15 mmol) was placed in a 1 cm pathlength quartz cell equipped with a stir bar, and then it was capped with a rubber septum. $NiBr_2$·DME in DMA solution (3.52 mM) was continuously added to the cell by micro syringe (0.1, 0.2, 0.3, 0.4, 0.5, 0.6, 0.7, 0.8, 0.9, 1.0, 1.1, 1.2, 1.3, 1.4, 1.5 equiv. relative to **L5**). The solution was stirred at room temperature for 2 min, and then the absorption (270–350 nm) was recorded for every 0.5 nm. The spectra are shown in Figure 35. The estimated molar absorptivity curves and concentration profiles are shown in Figure 36, 37. The chemical model shown in Figure 20 was used for the analysis. The noisy curve of NiL_2 is due to its low concentration.

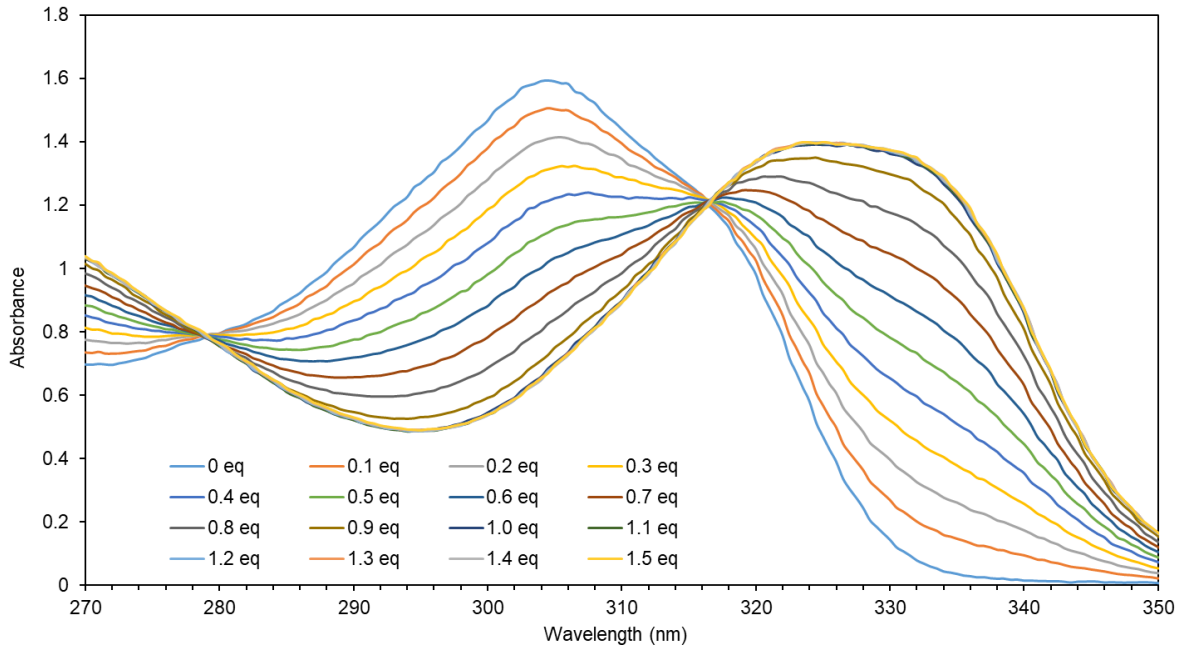

Figure 35. Absorption data for the titration test between **L5** and $NiBr_2 \cdot DME$ in DMA

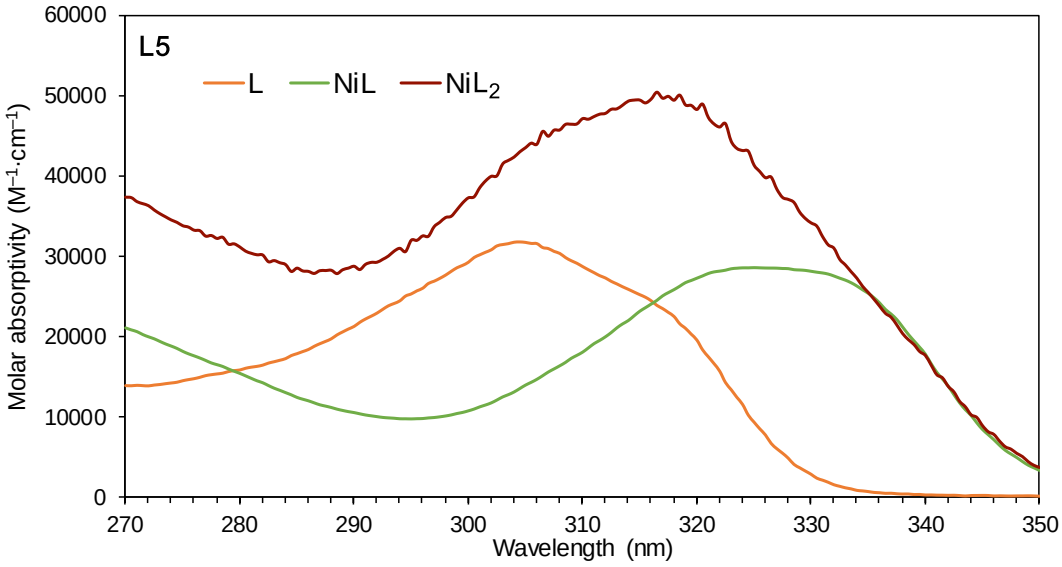

Figure 36. Calculated molar absorptivity curves with **L5**

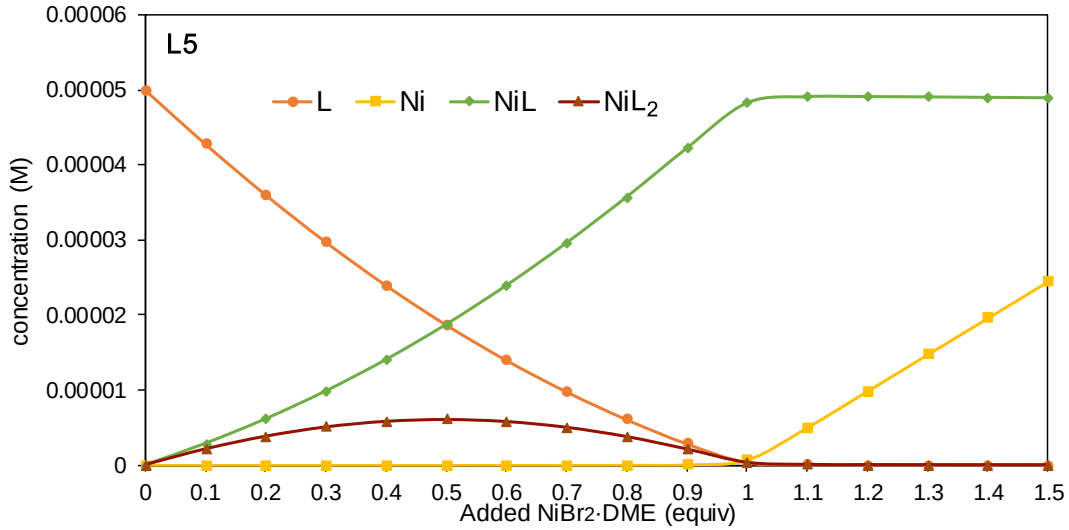

Figure 37. Concentration profiles with **L5**. ΔG_1 = –46.98 kJ/mol, ΔG_2 = –24.19 kJ/mol, R^2 = 0.99939.

Titration with L7

L7 in DMA solution (3 mL, 0.05 mM, 0.15 mmol) was placed in a 1 cm pathlength quartz cell equipped with a stir bar, and then it was capped with a rubber septum. $NiBr_2$·DME in DMA solution (1.47 mM) was continuously added to the cell by micro syringe (0.05, 0.1, 0.15, 0.2, 0.25, 0.3, 0.35, 0.4, 0.45, 0.5, 0.55, 0.6, 0.65, 0.7, 0.75, 0.8, 0.85, 0.9, 1.0, 1.1, 1.2, 1.3, 1.4, 1.5, 1.7, 2.0, 2.4, and 3.0 equiv. relative to **L7**). The solution was stirred at room temperature for 2 min, and then the absorption (270–350 nm) was recorded for every 0.5 nm. The spectra are shown in Figure 38. The estimated molar absorptivity curves and concentration profiles are shown in Figure 39, 40. The chemical model shown in Figure 20 was used for the analysis.

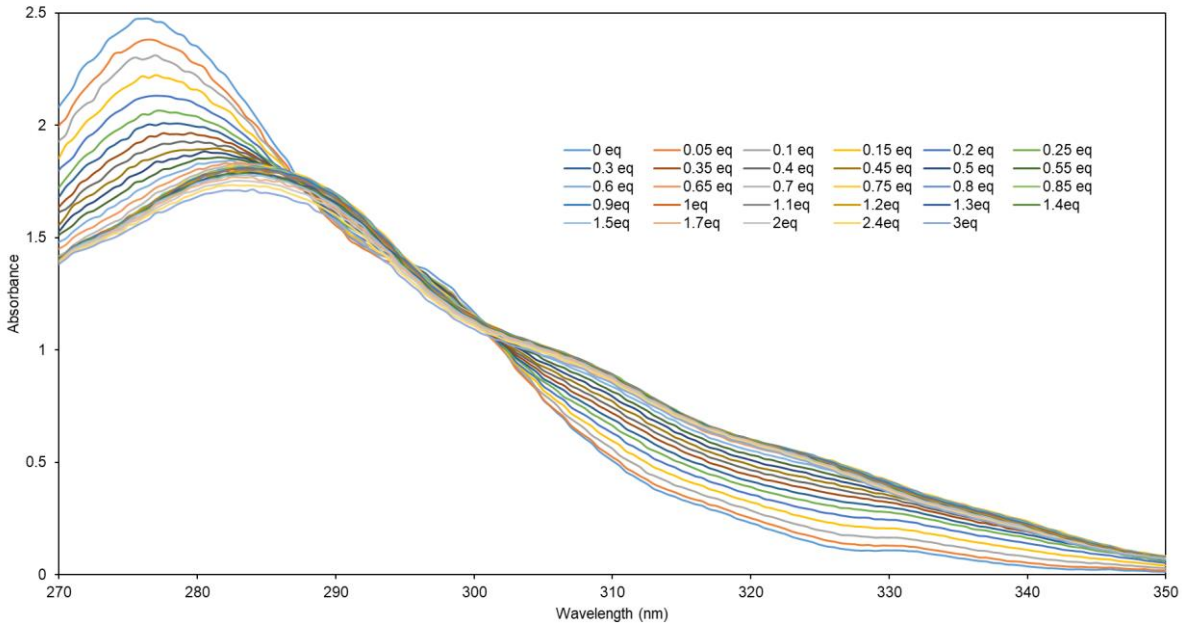

Figure 38. Absorption data for the titration test between **L7** and $NiBr_2$·DME in DMA

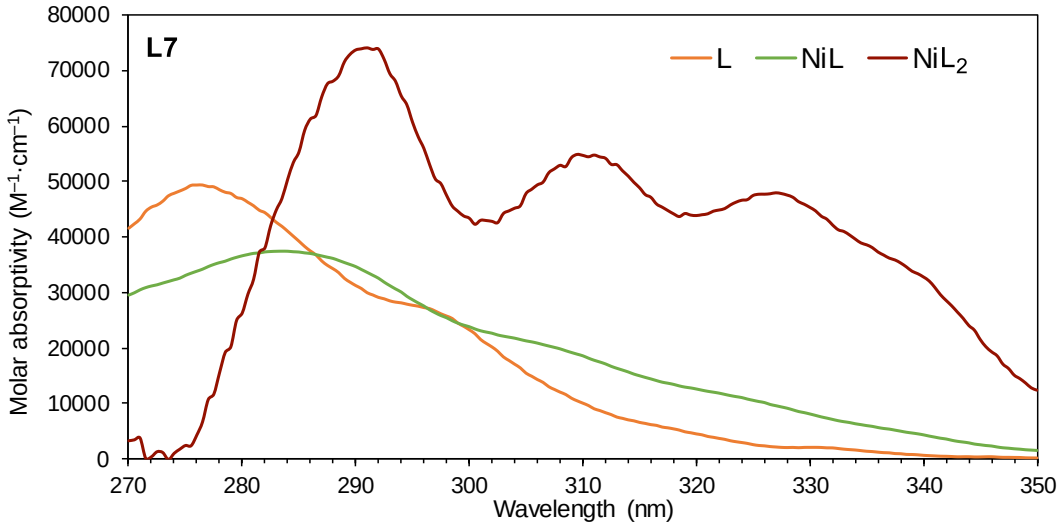

Figure 39. Calculated molar absorptivity curves with **L7**

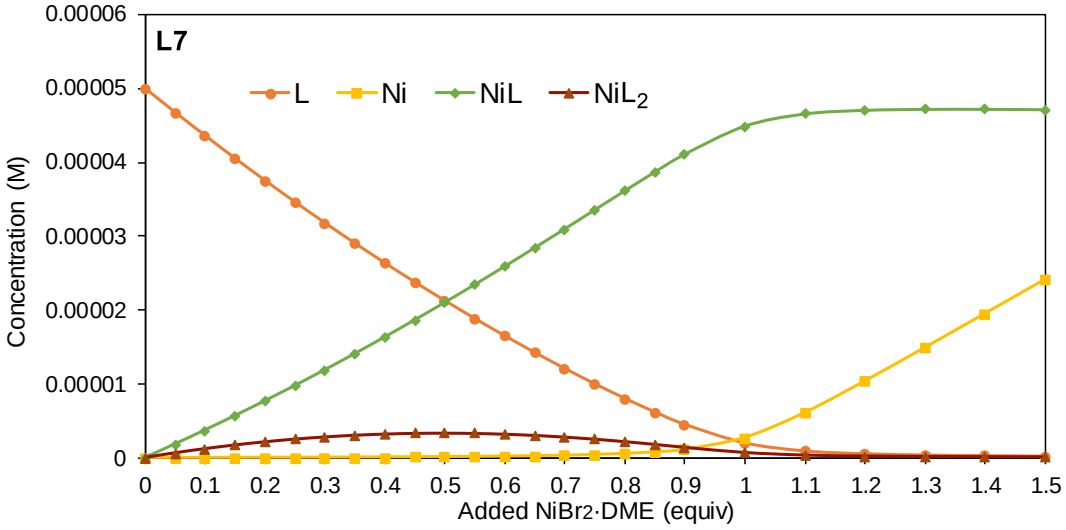

Figure 40. Concentration profiles with **L7**. $\Delta G_1 = -39.42$ kJ/mol, $\Delta G_2 = -22.16$ kJ/mol, $R^2 = 0.99978$.

References

[1] S. Zhang, B. Hu, Z. Zheng, P. J. Walsh, *Adv. Synth. Catal.* **2018**, *360*, 1493–1498.

[2] The synthesis of 5,5'-bis[tris(4-hydroxyphenyl)methyl]-2,2'-bipyridine and its derivatives from 2,2'-bipyridine-5,5'-dicarboxylic acid diethyl ester was reported by Kato group, but they have not been used as a ligand in transition-metal catalysis. T. Hatano, T. Kato, *Tetrahedron* **2008**, *64*, 8368–8380.

[3] The crude products of the six-fold C(sp^3)–H arylation of 5,5'-Me_2bpy contained the corresponding four-fold arylated compounds as detected by ^{1}H NMR analysis.

[4] G. Berthon-Gelloz, M. A. Siegler, A. L. Spek, B. Tinant, J. N. H. Reekc, I. E. Markó, *Dalton Trans.* **2010**, *39*, 1444−1446.

[5] M. A. Larsen, S. Cho, J. F. Hartwig, *J. Am. Chem. Soc.* **2016**, *138*, 762−765.

[6] D. A. V. Griend, D. K. Bediako, M. J. DeVries, N. A. DeJong, L. P. Heeringa, *Inorg. Chem.* **2008**, *47*, 656–662.

[7] The concentration of the corresponding trischelated Ni^{II} complexes ([Ni(5,5'-Me_2bpy)$_3$]) was low enough to be negligible for quantification of the coordination equilibria throughout the titration. See the experimental section for details.

[8] Y. Kawamata, J. C. Vantourout, D. P. Hickey, P. Bai, L. Chen, Q. Hou, W. Qiao, K. Barman, M. A. Edwards, A. F. Garrido-Castro, J. N. deGruyter, H. Nakamura, K. Knouse, C. Qin, K. J. Clay, D. Bao, C. Li, J. T. Starr, C. Garcia-Irizarry, N. Sach, H. S. White, M.

Neurock, S. D. Minteer, P. S. Baran, *J. Am. Chem. Soc.* **2019**, *141*, 6392–6402.

[9] Y. Chi, H.-H. Yeh, Luminescent platinum(II) complexes with biazolate chelates, US Patent 9040702, May 26, 2015.

[10] S. Fujii, R. Ishimura, A. Nakagawa, N. Kitamura, *Phys. Chem. Chem. Phys.* **2017**, *19*, 28943–28949.

Chapter 2

Application of the Dumbbell-Shaped Bipyridine and Phenanthroline Ligands in Transition Metal Catalysis: Ni-catalyzed Cross-Couplings

The application of the dsbpy and dsphen ligands to the representative Ni-catalyzed cross-coupling reactions are described. The ligands **L3**, **L4**, **L5**, and **L7** showed superior performances in the Ni-catalyzed cross-electrophile coupling and the Ni/photoredox synergistically catalyzed decarboxylative coupling reactions.

Introduction

Ni-catalyzed cross-coupling reactions

Traditional transition metal catalyzed cross-coupling reactions such as palladium catalyzed Suzuki coupling reactions (C-C) and Buchwald-Hartwig aminations (C-N) are largely based on two-electron redox processes such as oxidative additions and reductive eliminations. In these catalysis, palladium which mostly adopts even-number oxidation states, Pd^0 and Pd^{II}, has been most frequently used (Figure 1). However, chemical society has seen great potential of single-electron processes in transition metal catalyzed cross-coupling reactions during the last decade. In these catalysis, the another group 10 element, nickel, has gained much attention (Figure 2).[1] Due to the smaller d-orbitals, nickel has higher electron paring energies and thus readily forms paramagnetic open-shell intermediates, in contrast to palladium which usually forms diamagnetic closed-shell species. Moreover, nickel is relatively stable in odd-number oxidation states such as Ni^I and Ni^{III} as well as even-number oxidation states Ni^0 and Ni^{II}. These features allow nickel to readily undergo single electron pathways as well as traditional two-electron processes in the catalytic reaction.

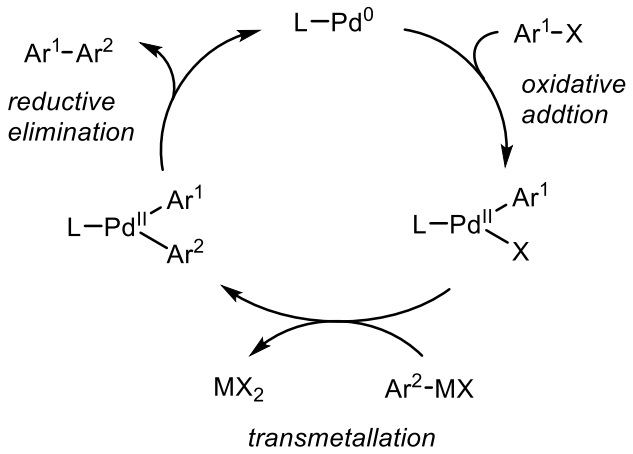

Figure 1. A classic mechanism of Pd-catalyzed cross-coupling reaction that utilize two-electron redox processes

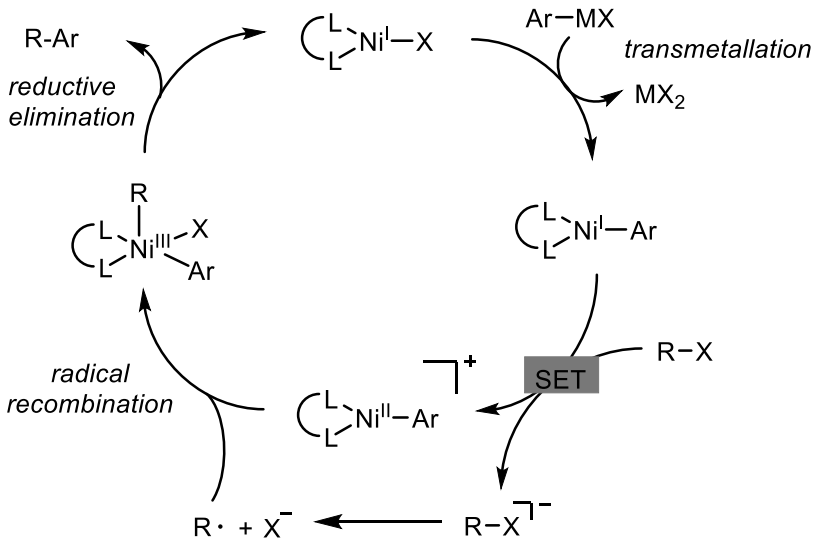

Figure 2. A mechanism of Ni-catalyzed cross-coupling reaction that utilize single electron transfer processes (SET)

The role of bpy ligands

In classic transition metal catalyzed cross-coupling reactions that utilize two electron redox pathways, phosphines and NHCs are usually employed as ligands. However, in the recent Ni-catalyzed reactions that utilizing single-electron redox processes, bipyridines have been most frequently employed.[1] Why bipyridine ligands have been effective in those novel Ni catalysis is yet unclear, but some hypothesis has been made. Frist, N-donor ligands are weak-field ligands relative to phosphines and NHCs, and hence prefer paramagnetic high-spin nickel species. Those high-spin nickel species may easily undergo single-electron processes. Second, bipyridines are redox non-innocent ligands, which can form $(bpy)^{+1}$ or $(bpy)^{-1}$ oxidation states. This redox activity of bpy ligand may assist single-electron processes in the catalytic cycle by stabilizing Ni intermediates. For example, the XPS analysis of a formal $(bpy)Ni^{I}$ speices, $[(4,4'\text{-}t\text{Bu}_2\text{bpy})\text{NiCl}]_2$, characterized that the real configuration is $[(4,4'\text{-}t\text{Bu}_2\text{bpy})^{-1}N^{II}Cl]_2$ (Figure 3).[2]

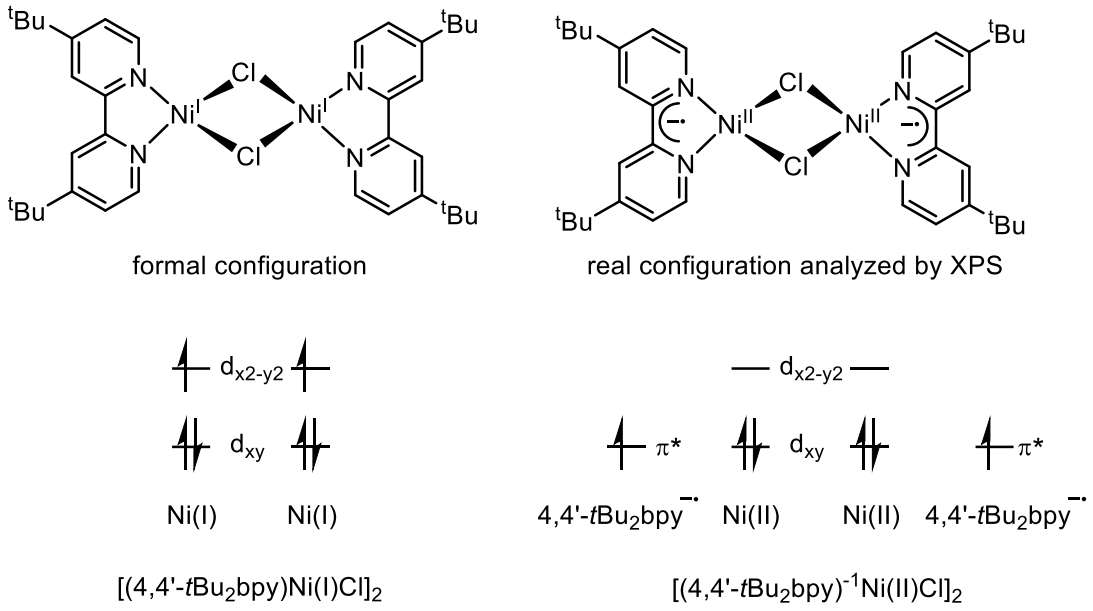

Figure 3. The electron configuration of [(4,4'-*t*Bu$_2$bpy)NiCl]$_2$

In addition, it is also noteworthy that nickel to bpy metal-to-ligand charge transfer (MLCT) can also play a great roll under visible light excitation conditions (Figure 4).[3,4]

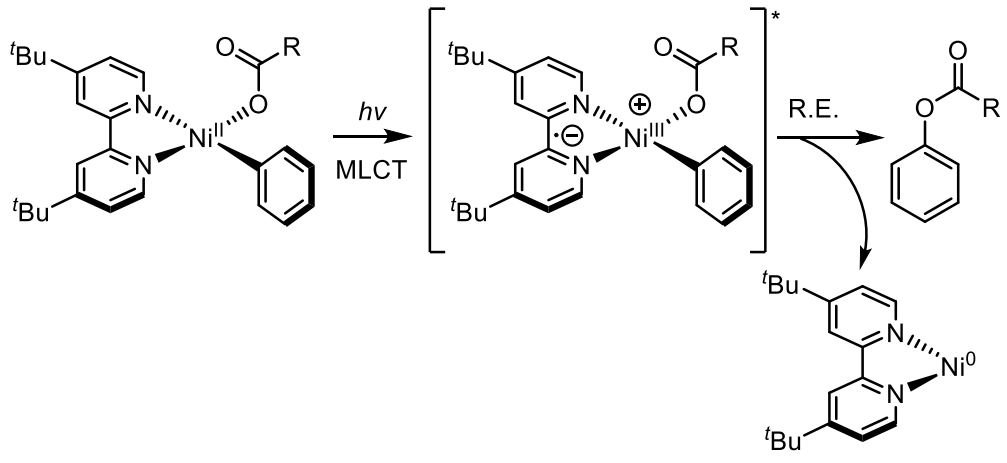

Figure 4. MLCT accelerated reductive elimination

Application of the dsbpy and dsphen ligands in Ni-catalyzed cross-couplings

To validate the potential usefulness of the newly developed dsbpy and dsphen ligands, I

tested these ligands in the representative Ni-catalyzed cross-coupling reactions. The author envisioned that those reactions can be improved by using dsbpy/dsphen ligands instead of conventional bpys previously employed.

1. C(sp^2)-C(sp^3) cross-electrophile coupling reaction

One selected reaction is Ni-catalyzed cross-electrophile coupling reaction developed by Weix and his coworkers (Scheme 1).[5] This reaction defers from conventional cross-couplings in which one electrophile and one nucleophile are coupled. Instead, this reaction cross-couples abundant aryl bromides and alkyl bromides electrophiles under Zn metal reductant. In the Weix's condition, 4,4'-$(OMe)_2$bpy and 1,10-phenanthroline were used as the optimal ligand. However, the reported protocol required substantial Ni loading (5~10 mol%) and the use of additives such as NaI and pyridine for attaining acceptable yields of the desired cross-coupling product.

Scheme 1. The cross-electrophile coupling reaction developed by Weix group

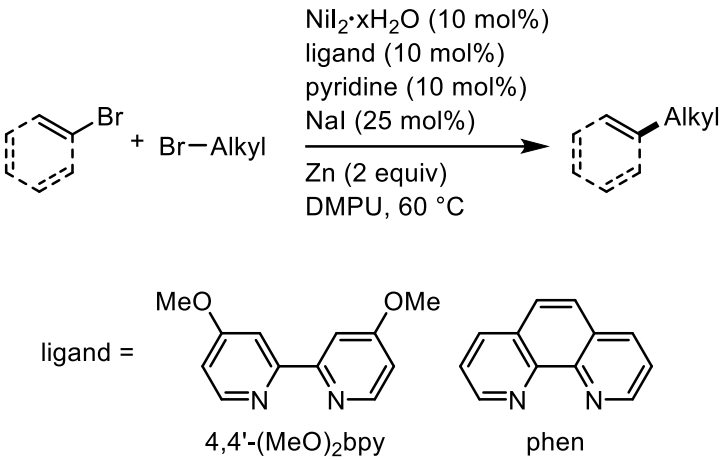

In the postulated reaction mechanism (Figure 5), Ni forms various oxidation states throughout the catalytic cycle, such as Ni^0, Ni^I, Ni^{II} and Ni^{III}. The reaction starts with the reduction of Ni^{II} to Ni^0 by Zn or Mn metal reductant. The Ni^0 undergoes oxidative addition with aryl halides to give (bpy)Ni^{II}(Ar)X. The (bpy)Ni^I species undergoes halogen atom abstraction with alkyl halide to give an alkyl radical, and this alkyl radical recombinates with the

(bpy)Ni^{II}(Ar)X to give (bpy)Ni^{III}(Ar)(Alkyl)X and follwing reductive elmination give the product.

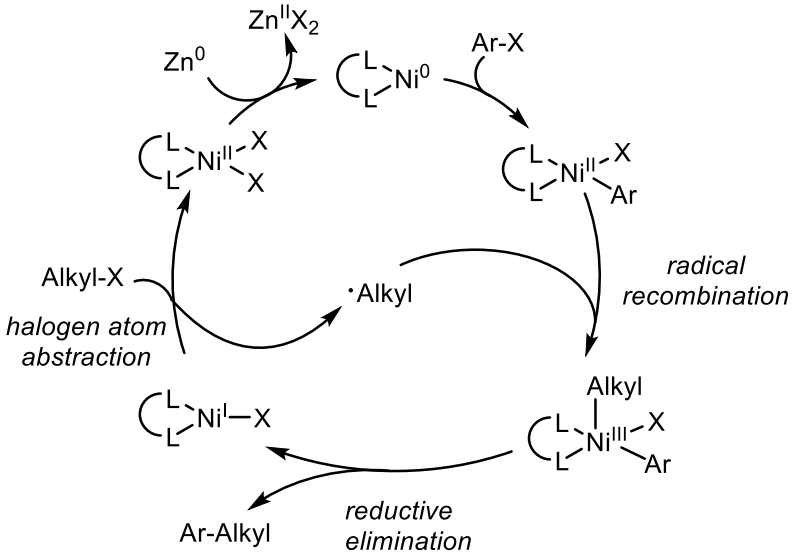

Figure 5. The proposed mechanism of the cross-electrophile coupling reaction

However, the reaction can be disturbed by the plausible undesired pathways. First, as discussed in the general introduction and the chapter 1, conventional bpy ligand easily undergo undesired multi-ligation and forms inactive nickel species (Figure 6). Moreover, control of the homocoupling reaction can be difficult, because of the undesired bimetallic pathways (Figure 7). I envisioned that the use of dsbpy ligands can prevent those undesired pathways by the distal steric effects, and increase the effectivity and selectivity of the reaction.

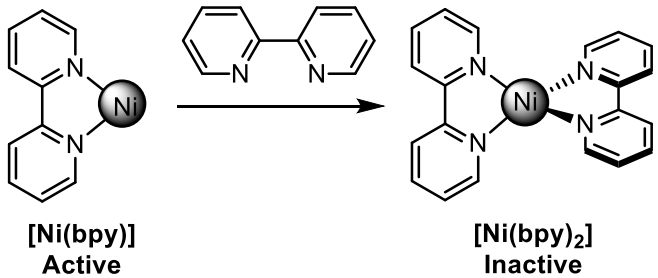

Figure 6. Undesired multi-ligation

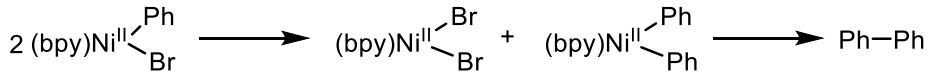

Figure 7. Undesired bimetallic pathways

Indeed, I observed that the reaction between bromobenzene (**1a**, 0.5 mmol) and bromododecane (**2a**, 0.6 mmol) in DMA (0.25 M) at 60 °C for 14 h in the presence of Zn as a reductant (2 equiv) and a Ni catalyst (1 mol%) prepared in situ from $NiBr_2$·DME (1 mol%) and 2,2'-bipyridine (bpy) (1.1 mol%) resulted in only 34% yield of dodecylbenzene (**3a**) with the formation of homocoupling product biphenyl (**4**) as the major product (57%; Table 1, entry 1).[6] However, under the same conditions, the simplest dsbpy ligand (**L1**) substantially suppressed the formation of **4** with a slightly improved yield of the cross-coupling product (49% of 3a, entry 2). Encouragingly, while the para-*t*Bu-substituted dsbpy (**L2**) showed a similar but less favorable ligand performance (entry 3), much improved cross-coupling efficiencies were observed with the bulkier series of dsbpy ligands (**L3–L5**), giving 3a in 83–86% yields, respectively (entries 4–6). Reported substituted bpy ligands such as 4,4'-tBu_2bpy, 4,4'$(MeO)_2$bpy, and 5,5'-Me_2bpy (structures shown in Table 1) gave unfavorable product distributions similar to that with the parent bpy ligand (Table 1, entries 7–9). Slightly bulky ligand 5,5'-Mes_2bpy gave similar result with 5,5'-Me_2bpy (entry 10). The 6,6'-disubstituted ligand (6,6'-Me_2bpy) induced no conversion of the substrates (entry 11), which supports the importance of distal steric effect by substitution of the 5,5'-positions. Interestingly, functionalization of 5,5'-position with another bulky substituent, 2,6-bis(benzhyryl)-4-methyl-phenyl (bhp), also showed better performance compare to the conventional ligands (**L6**, 59% yield, entry 13). However, due to the extremely low solubility of **L6** in DMA, direct comparison of the substituent effect was difficult. The unsubstituted phen ligand showed bad selectivity as unsubstituted bpy (28%, entry 12). Interestingly, the bhp-type dumbbell-shaped phenanthroline ligand **L7** also showed similar performance comparable to **L3**–**L5** (81% yield, entry 14). This further supports the ligand design principle in this research.

Table 1. Ni-catalyzed cross-electrophile coupling between **1a** and **2a**[a]

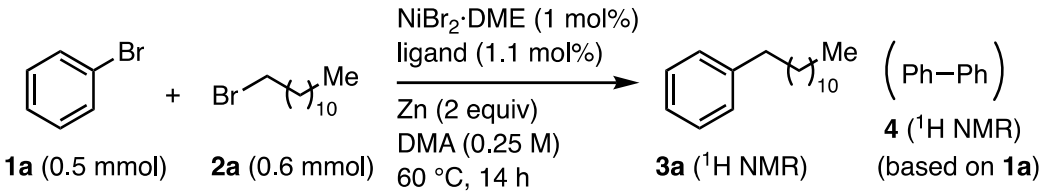

1a (0.5 mmol) **2a** (0.6 mmol) **3a** (^{1}H NMR) **4** (^{1}H NMR) (based on **1a**)

Entry	Ligand	**3a** [%][b]	**4** [%][b]
1	bpy	34	57
2	**L1**	49	9
3	**L2**	38	12
4	**L3**	83	14
5	**L4**	84	5
6	**L5**	86 (85)	6
7	4,4'-*t*Bu$_2$bpy	17	31
8	4,4'-(MeO)$_2$bpy	12	17
9	5,5'-Me$_2$bpy	31	69
10	5,5'-Mes$_2$bpy	39	57
11	6,6'-Me$_2$bpy	0	0
12	phen	28	64
13	**L6**	59	29
14	**L7**	81	6

[a] Conditions: **1a** (0.5 mmol), **2a** (0.6 mmol), NiBr$_2$·DME (1 mol%), ligand (1.1 mol%), Zn (1 mmol), DMA (2 mL), 60 °C, 14 h. [b] Yields determined by ^{1}H NMR analysis. Isolated yield is shown in parentheses.

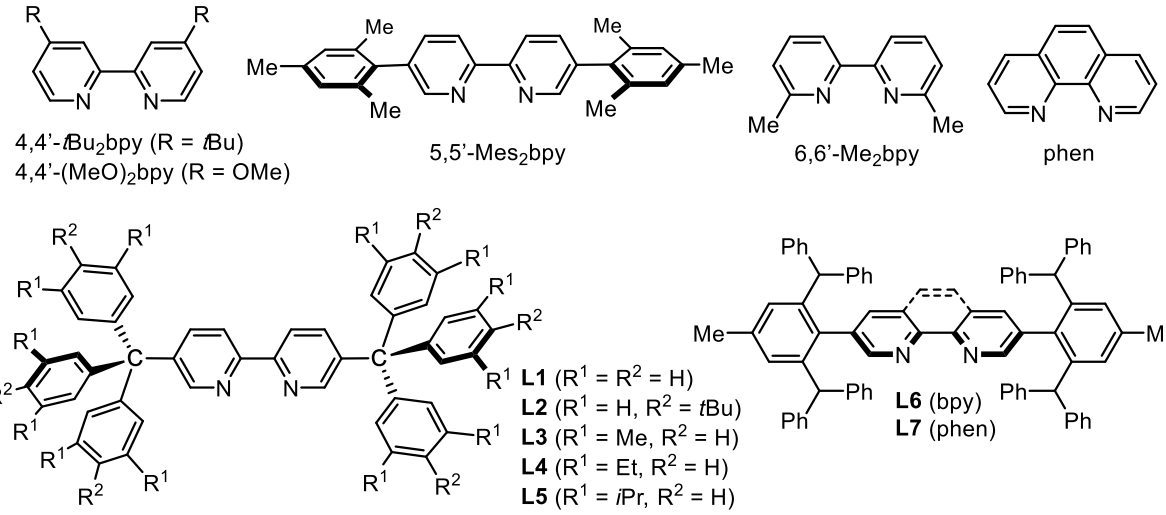

To further gain the insight in the ligand effect, ^{1}H NMR yield of the cross-coupling product and homo-coupling product were measured through the reaction (Figure 8). With common 5,5'-dMebpy ligand, large amount of homocoupling product was produced while only small amount of the desired product was produced during 6 hours of reaction time (Figure 8, red lines). In contrast, both of the dumbbell-shaped ligands **L3** and **L5** suppressed the formation of homo-coupling product while affording the desired cross-coupling product much faster (Figure 8, blue and green lines).

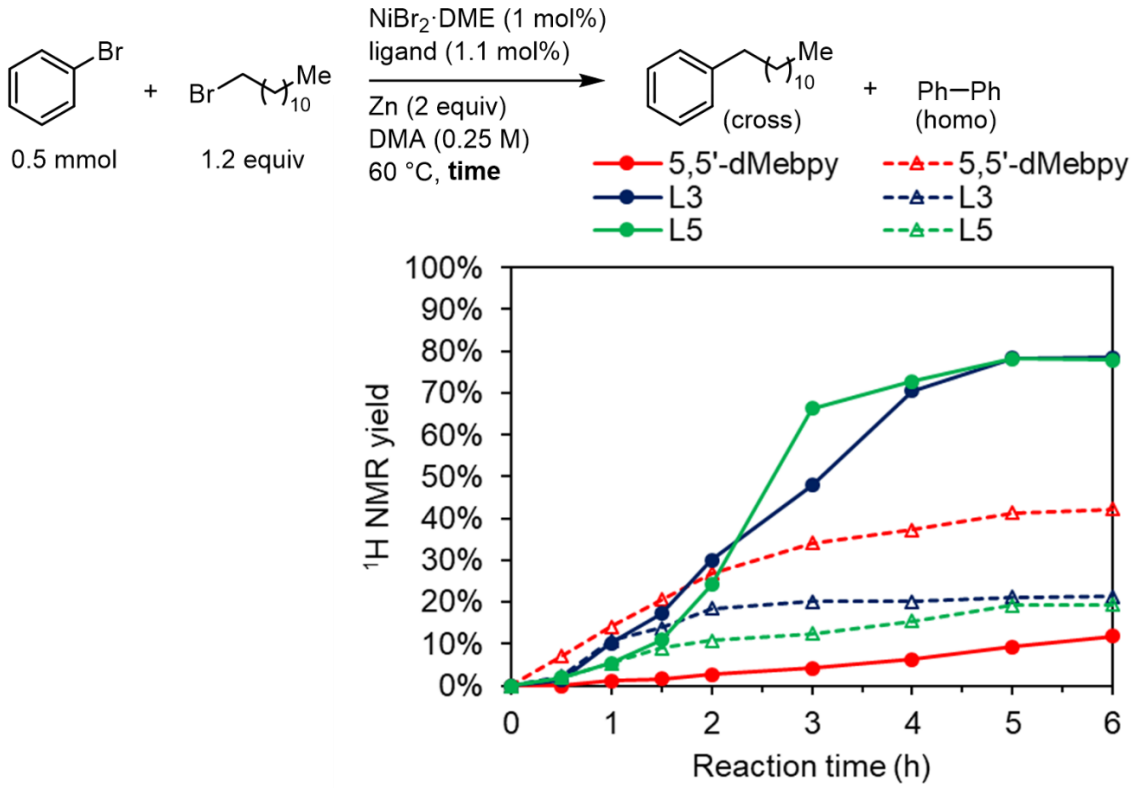

Figure 8. The time-yield profiles of the cross and homo coupling products with given ligands

The superior ligand effects of the dsbpys and dsphen (**L1–L7**) compared to the conventional bpy and phen ligands are attributable to the apparent monochelating nature of dsbpys/dsphen indicated by the UV-vis analysis of the Ni(II)-bpy coordination equilibria. The distal steric effects of the triarylmethyl substituents at the N-β-positions may also contribute to the suppression of the aryl homocoupling of the aryl bromides through inhibiting a bimolecular disproportionation reaction of the putative aryl bromide oxidative addition product [NiL(Ar)Br]. As shown in Figure 9, in the case of common bipyridine ligand, the two

[NiL(Ar)Br] species can easily interact with each other and undergo bimetallic disproportionation reaction. However, in the case of dsbpys having the 3,5-disubstituted trityl groups (**L3**–**L5**), this bimetallic interaction can be very difficult due to the steric repulsion between bulky substituents (Figure 10).

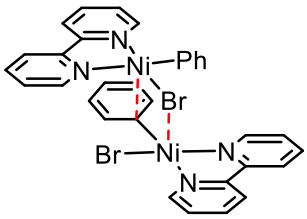

Figure 9. Bimetallic interaction between two [NiL(Ar)Br] species in the case of common bpy ligand

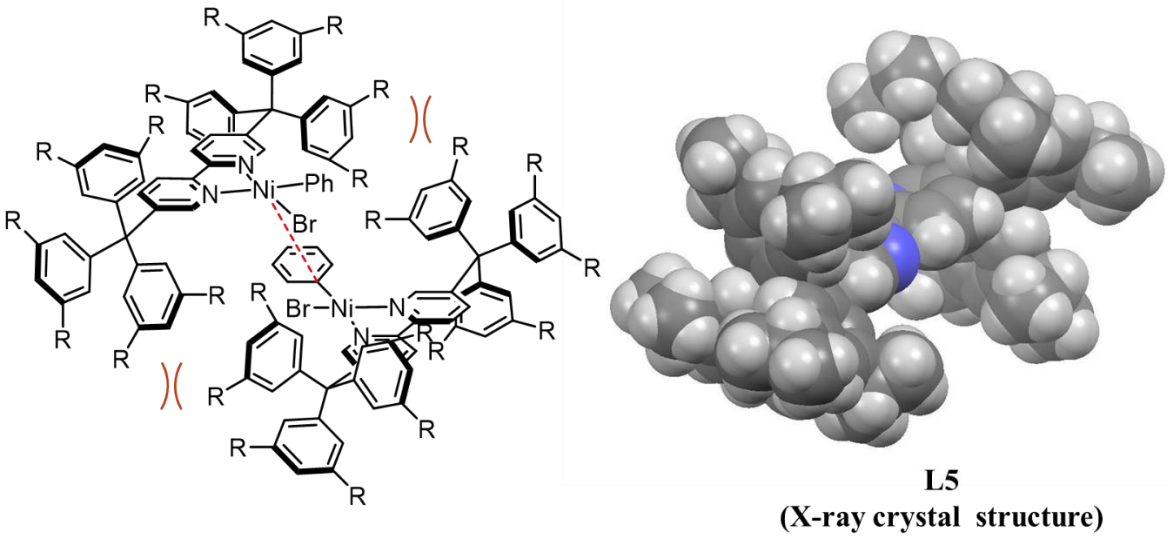

Figure 10. Bimetallic interaction between two [NiL(Ar)Br] species in the case of dsbpy ligands

As shown in Table 2, the Ni catalyst systems with high performing ligands **L3–L5** improved the efficacy of cross-electrophile coupling between several aryl bromides and alkyl bromides compared to that with bpy. Specifically, an electronically challenging aryl bromide 4-bromoanisole (**1f**) coupled with ethyl 4-bromobutanoate (**2b**) to afford **3b** in 82% yield using **L3**, while bpy gave **3b** in a low yield (25%) along with the biaryl homocoupling product (31%

based on **1f**). The reaction of an electron-deficient aryl bromide 4-bromobenzonitrile (**1g**) occurred most efficiently with **L5** (3c, 83%). While the cross-coupling was hampered by the ortho-substituent of *o*-tolyl bromide (**1h**), an acceptable yield was obtained with **L3** (3d, 47%). The dsbpys **L3–L5** allowed the cross-coupling of the alkenyl bromide, 2-bromopropene (**1i**), with benzyl 4-bromobutanoate (**2c**) in good yields (**3e**, 58–71%). Cyclic secondary alkyl bromides such as bromocyclopentane (**2d**) and 4-bromo-N-tosylpiperidine (**2e**) participated in the reaction using **L3–L5**, giving the corresponding products **3f** and **3g** in good to high yields. The dsphen ligand **L7** was also applied for the coupling product of **3c** and **3g**. The ligand showed moderate effectivity in this catalysis.

Table 2. Scope of aryl/alkenyl bromides (**1**) and alkyl bromides (**2**) with Ni catalyst systems[a]

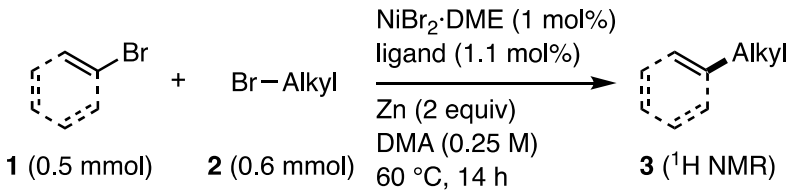

		Cross-electrophile coupling product **3** [%][b]					
		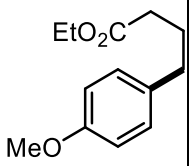 **3b**	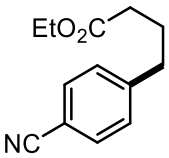 **3c**	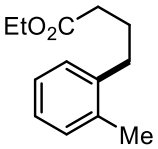 **3d**	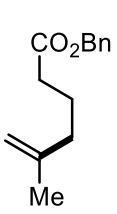 **3e**	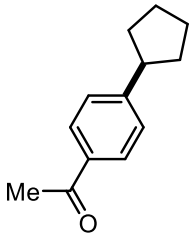 **3f**	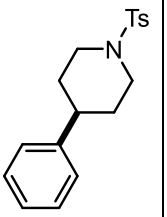 **3g**[c]
Ligand	bpy	25	44	14	34	44	36
	L3	82 (71)	51	47 (44)	58	85 (77)	63 (48)
	L4	75	62	41	68	79	60
	L5	47	83 (61)	29	71 (62)	71	56
	L7	-	57	-	-	-	54

[a] Conditions: **1** (0.5 mmol), **2** (0.6 mmol), $NiBr_2$·DME (1 mol%), ligand (1.1 mol%), Zn (1 mmol), DMA (2 mL), 60 °C, 14 h. [b] Yields determined by ^{1}H NMR analysis (orange, 80–100%; pink, 60–79%; green, 40–59%; blue, 0–39%). Isolated yields are shown in parentheses. [c] **1a** (0.75 mmol), **2e** (0.5 mmol). [d] The isolated product **3e** was contaminated with benzyl butyrate (3e/benzyl butyrate = 90:10, based on ^{1}H NMR analysis).

2. Ni/photoredox dual catalytic decarboxylative cross coupling

The another interesting selected reaction is Ni/photoredox synergistically catalyzed decarboxylative cross-coupling reaction developed by Dolye and MacMillan groups (Scheme 2).[7] This reaction is very important pioneering work on Ni/photoredox dual catalysis for the cross-coupling reactions. In this reaction, photoredox catalysis directly utilize cheap, abundant α-N alkyl carboxylic acids as a coupling partner in decarboxylative manner, while aryl halide coupling partner reacts with low valent (bpy)Ni catalysts. Although this reaction is impressively powerful molecular transformation, there is still limitation in aryl halide substrate scope. While electron deficient aryl bromides were well employed, the use of electron neutral or electron rich aryl bromides still remains a challenge with the reported system as shown in Scheme 2. In fact, the use of electron rich aryl bromides are notoriously challenging in another Ni/photoredox catalysis as well, such as aryl amination reaction.[8]

Scheme 2. Ni/photoredox dual catalytic decarboxylative cross-coupling

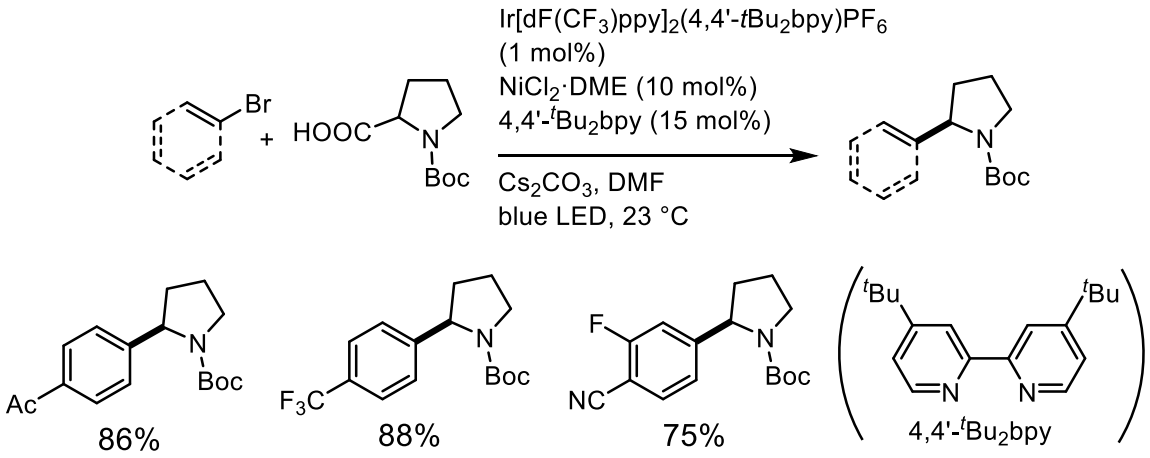

In the proposed reaciton mechanism, excited Ir photocatalyst decarboxlyates alkyl carboxylic acids to afford alkyl radicals (Figure 11). The reduced Ir photocatalyst then reduces Ni(I) catalyst to Ni(0). The Ni(0) then undergoes oxdative addtion with Ar-X to afford (bpy)Ni^{II}(Ar)X, and then the follwing radical trappping and reductive ellmination give the product. Thus, in order to undergo oxidative addtion, low valent nickel species such as Ni^{I} and Ni^{0} are nacessery. However, the oxidative addtion can be very difficult due to the bimetallic comproportionation pathways. As shown in Figure 12, the low valent (bpy)Ni^{I} species can

undergo comproportionation reaction with (bpy)Ni^{III} to give two (bpy)Ni^{II} species. As shown in Figure 13, this bimetallic compoportionation can easily undergo with common compact bpy ligands. However, I envisioned that the use of dsbpy ligand might prevent this problem by the distal steric effect (Figure 14), and eanble the use of challenging aryl bromide substrates.

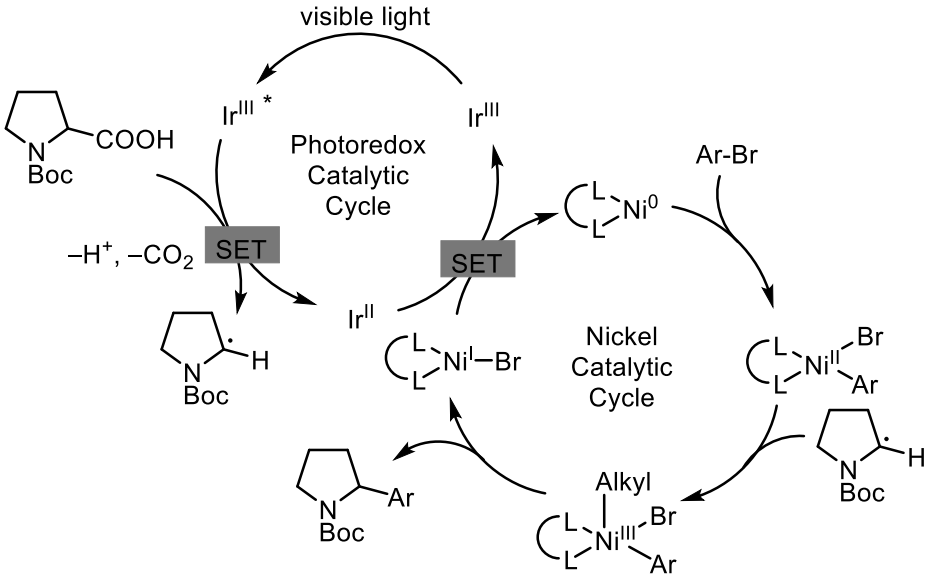

Figure 11. The proposed mechanism for Ni/photoredox dual catalytic decarboxylative cross-coupling

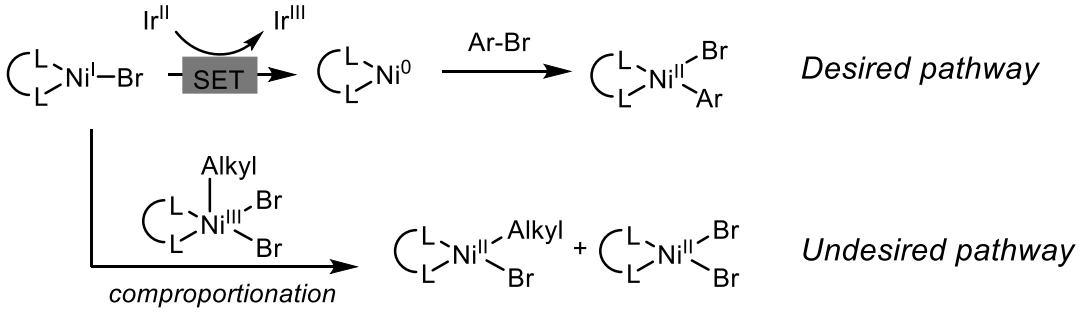

Figure 12. Difficulty in oxidative addition: undesired comproportionation pathway

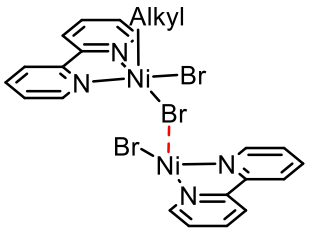

Figure 13. Comproportionation of (bpy)Ni^{I} and (bpy)Ni^{III}

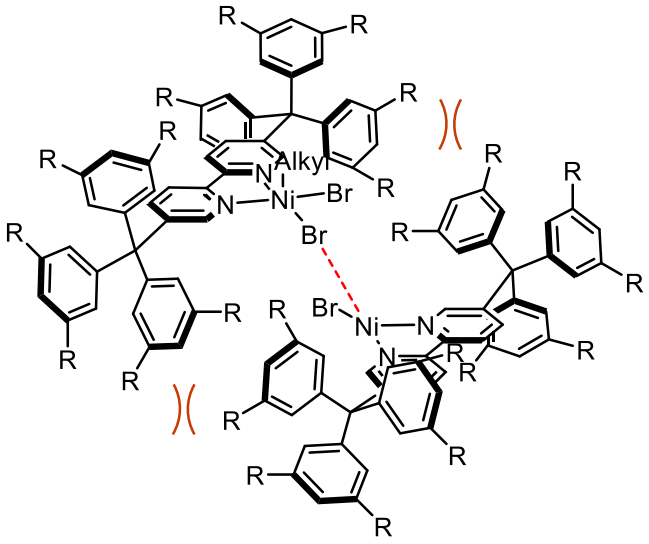

Figure 14. Comproportionation of (dsbpy)Ni^{I} and (dsbpy)Ni^{III}

As shown in Table 3, dumbbell-shaped bipyridine ligands **L3**–**L5** indeed showed better ligand performance than 4,4'-*t*Bu_2bpy in the reaction between electronically unbiased **1a** and N-Boc-proline (**5**) with 5 mol% Ni loading in the presence of Ir[dF(CF_3)ppy]$_2$(4,4'-tBu_2bpy)PF_6 (1 mol%) as a photocatalyst, giving **6a** in good-to-high yields.[9] More challenging substrate, electron rich aryl bromide **1f**, underwent efficient coupling reaction with **L3** to afford **6b** in 72% yield. Similar ligand effects were observed in the reaction of alkenyl bromide (**1i**) to produce **6c**. The bhp-substituted phen ligand **L7** also showed good performance comparable to dsbpys.

Table 3. Ni/photoredox-synergistically catalyzed decarboxylative cross-coupling of aryl /alkenyl bromides (**1**) and alkyl carboxylic acids (**5**).[a]

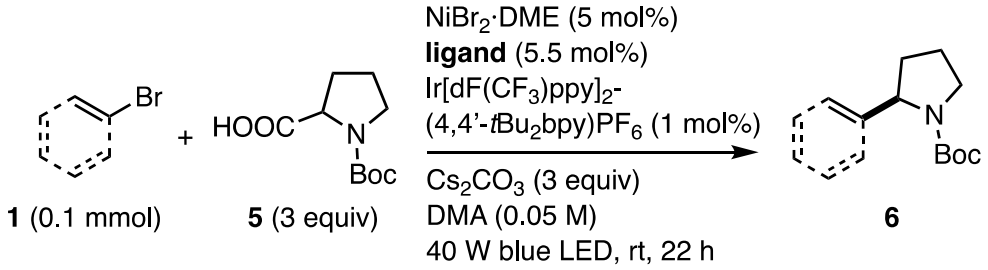

1 (0.1 mmol) **5** (3 equiv) **6**

		coupling product **6** [%][b]		
		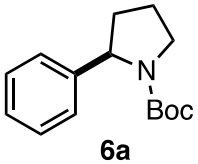 **6a**	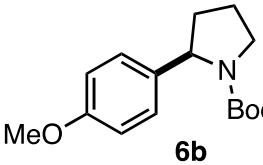 **6b**	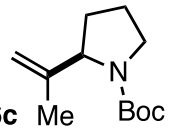 **6c**
Ligand	4,4'-*t*Bu2bpy	34	17	23
	L3	87 (77) [c]	72 (71) [c]	52 (45)[c]
	L4	84	59	49
	L5	74	41	36
	L7	79	58	42

[a] Conditions: **1** (0.1 mmol), **5** (0.3 mmol), $NiBr_2$·DME (5 mol%), ligand (5.5 mol%), Ir[dF(CF_3)ppy]$_2$(4,4'-*t*Bu$_2$bpy)PF_6 (1 mol%), DMA (2 mL), 40 W blue LED, room temperature, 22 h. [b] Yields determined by ^{1}H NMR analysis (orange, 80–100%; pink, 60–79%; green, 40–59%; blue, 0–39%). Isolated yields are shown in parentheses. [c] The isolated products **6a**–**6c** were existed as 2.2:1, 2:1, 1.3:1 mixtures of rotamers, respectively.

Conclusion

The newly synthesized dumbbell-shaped bipyridine and phenanthroline ligands (**L1**–**L7**) are applied to Ni-catalyzed cross-couplings. The ligands that sufficiently suppressed second ligand coordination (**L3**–**L5** and **L7**) showed improved ligand performance compared to conventional bipyridine and phenanthroline ligands. In the Ni-catalyzed cross-electrophile coupling between aryl bromides and alkyl bromides, the new ligands accomplished the reaction in much lower catalyst loading without additives. In the Ni/photoredox-synergistically catalyzed decarboxylative coupling between aryl bromides and alkyl carboxylic acids, the dsbpy and dsphen ligands enabled the expansion of the substrate scope to the aryl bromides that were

previously challenging. The superior ligand effects were attributed to the apparent monochelating nature of **L3**–**L5** and **L7**, while suppression of the notorious counterproductive bimetallic reactions such as Ni^{I}/Ni^{III} comproportionation and Ni^{II}/Ni^{II} disproportionantion may also play an important role. The author looks forward to the further application of the dsbpy and dsphen ligands in various transition metal catalysis.

Experimental section

General. NMR spectra were recorded on a JEOL ECX-II (400 MHz for ^{1}H NMR, 100.5 MHz for ^{13}C NMR). Chemical shift values are referenced to Me_4Si (^{1}H; 0 ppm), $CDCl_3$ (^{13}C; 77.16 ppm), C_6D_6 (^{1}H; 7.16 ppm, ^{13}C; 128.0 ppm). IR spectra were measured with a PerkinElmer Frontier instrument. TLC analyses were performed on commercial glass plates bearing a 0.25-mm layer of Merck Silica gel $60F_{254}$. Silica gel (Kanto Chemical Co., Ltd., Silica gel 60 N, spherical, neutral) was used for column chromatography. All reactions were carried out under nitrogen or argon atmosphere. Materials were obtained from commercial suppliers or prepared according to standard procedures unless otherwise noted.

General Procedure for Ni-catalyzed Cross-Electrophile Coupling between Aryl Bromides and Alkyl Bromides

In a nitrogen-filled glove box, $NiBr_2 \cdot DME$ (1.5 mg, 0.005 mmol, 1 mol%) and 2,2'-bipyridine ligand (0.0055 mmol, 1.1 mol%) was added to a 4-mL vial containing a magnetic stirring bar. 2 mL of DMA was added, and then the mixture was stirred for 5 min at room temperature. Aryl bromide (**1**, 0.5 mmol, 1 equiv.), alkyl bromide (**2**, 0.6 mmol, 1.2 equiv.), and zinc powder (65.4 mg, 1 mmol, 2.0 equiv.) were added to the solution. The vial was capped and removed from the glove box. The mixture was stirred at 60 °C for 14 h (aluminum block + IKA Plate (RCT digital), 750 rpm), and then cooled to room temperature. The reaction mixture was diluted with Et_2O, and then passed through a short plug of Celite and washed with Et_2O. The filtrated was quenched with 1M aqueous $NaHSO_4$, and then further diluted with Et_2O (40 mL). The organic layer was washed with water (2 x 30 mL), brine (20 mL), dried with $MgSO_4$, concentrated *in vacuo*. Internal standard (1,1,2,2-tetrabromoethane or 1,3,5-trimethoxybenzene)

was added to determine the ^{1}H NMR yield of the desired coupling product **3**. The crude product was purified by flash chromatography on silica gel.

General Procedure for Ni/photoredox-synergistically Catalyzed Decarboxylative Cros s-Coupling of Aryl Bromides and Alkyl Carboxylic Acids

In a nitrogen-filled glove box, Ir[dF(CF_3)ppy]$_2$(4,4'-*t*Bu_2bpy)PF_6 (1.1 mg, 0.001 mmol, 1 mol%), $NiBr_2$·DME (1.5 mg, 0.005 mmol, 5 mol%), 2,2'-bipyridine ligand (0.0055 mmol, 5.5 mol%), *N*-(*tert*-butoxycarbonyl)-*L*-proline (**5**, 64.6 mg, 0.3 mmol, 0.3 equiv.) was added to a 4-mL vial containing a magnetic stirring bar. 2 mL of DMA was added, and then the mixture was stirred for 5 min at room temperature. Aryl bromide (**1**, 0.1 mmol, 1 equiv.) and Cs_2CO_3 (97.7 mg. 0.3 mmol, 3.0 equiv.) were added to the solution. The vial was capped and removed from the glove box. The mixture was stirred at room temperature under blue LED irradiation for 22 h (40W, Kessil A160WE Tuna Blue + EvoluChem^{TM} photoredox box device). The reaction mixture was diluted with Et_2O (50 mL), and then the organic layer was washed with water (2 x 30 mL), brine (20 mL), dried with $MgSO_4$, concentrated *in vacuo*. Internal standard (1,1,2,2-tetrabromoethane) was added to determine the ^{1}H NMR yield of the coupling product **6**. The crude product was purified by flash chromatography on silica gel.

Compound Characterization Data

Docecylbenzene (3a)

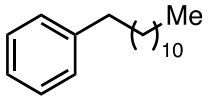

[Table 1, entry 6; with **L5**, 86% NMR yield] The product **3a** was isolated by flash chromatography on silica gel with elution (hexane 100%) as colorless oil (104.5 mg, 85% yield). **^{1}H NMR** (400 MHz, $CDCl_3$): δ 7.31–7.23 (m, 2H), 7.20–7.14 (m, 3H), 2.60 (t, J = 7.8 Hz, 2H), 1.66–1.55 (m, 2H), 1.38–1.18 (m, 18H), 0.88 (t, J = 7.3 Hz, 3H). **^{13}C NMR** (100.5 MHz, $CDCl_3$): δ 142.9, 128.4, 128.2, 125.5, 36.0, 31.9, 31.6, 29.70, 29.67, 29.62, 29.55, 29.4, 22.7, 14.1. Spectral data match those reported in the literature.[5]

Ethyl 4-(4-methoxyphenyl)butanoate (3b)

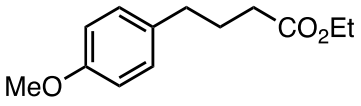

[Table 2; with **L3**, 82% NMR yield] The product **3b** was isolated by flash chromatography on silica gel with gradient elution (hexane/EtOAc, 100:0–95:5) as colorless oil (78.6 mg, 71% yield). **^{1}H NMR** (400 MHz, $CDCl_3$): δ 7.10 (d, J = 8.7 Hz, 2H), 6.83 (d, J = 8.7 Hz, 2H), 4.12 (q, J = 7.3 Hz, 2H), 2.59 (t, J = 7.3 Hz, 2H), 2.30 (t, J = 7.3 Hz, 2H), 1.92 (quin, J = 7.3 Hz, 2H), 1.25 (t, J = 7.3 Hz, 3H). **^{13}C NMR** (100.5 MHz, $CDCl_3$): δ 173.5, 157.8, 133.4, 129.3, 113.7, 60.1, 55.1, 34.1, 33.5, 26.7, 14.2. Spectral data match those reported in the literature.[10]

Ethyl 4-(4-cyanophenyl)butanoate (3c)

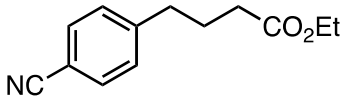

[Table 2; with **L5**, 83% NMR yield] The product **3c** was isolated by flash chromatography on silica gel with gradient elution (hexane/EtOAc, 100:0–95:5) as colorless oil (66.4 mg, 61% yield). **^{1}H NMR** (400 MHz, $CDCl_3$): δ 7.58 (d, J = 8.2 Hz, 2H), 7.29 (d, J = 8.2 Hz, 2H), 4.13 (q, J = 7.3 Hz, 2H), 2.72 (t, J = 7.8 Hz, 2H), 2.32 (t, J = 7.8 Hz, 2H), 1.96 (quin, J = 7.8 Hz, 2H), 1.26 (t, J = 7.3 Hz, 3H). **^{13}C NMR** (100.5 MHz, $CDCl_3$): δ 172.9, 147.0, 132.1, 129.2, 118.9, 109.8, 60.3, 35.1, 33.3, 25.9, 14.1. Spectral data match those reported in the literature.[5]

Ethyl 4-(*o*-tolyl)butanoate (3d)

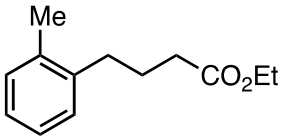

[Table 2; with **L3**, 47% NMR yield] The product **3d** was isolated by flash chromatography on silica gel with gradient elution (hexane/EtOAc, 100:0–95:5) as colorless oil (45.4 mg, 44% yield). **^{1}H NMR** (400 MHz, $CDCl_3$): δ 7.18–7.06 (m, 4H), 4.13 (q, J = 7.6 Hz, 2H), 2.64 (t, J = 7.6 Hz, 2H), 2.37 (t, J = 7.6 Hz, 2H), 2.31 (s, 3H), 1.91 (quin, J = 7.6 Hz, 2H), 1.26 (t, J = 7.6

Hz, 3H). **^{13}C NMR** (100.5 MHz, $CDCl_3$): δ 173.5, 139.6, 135.9, 130.2, 128.9, 126.0, 125.9, 60.2, 33.9, 32.5, 25.3, 19.2, 14.2. Spectral data match those reported in the literature.[5]

Benzyl 5-methylhex-5-enoate (3e)

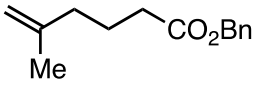

[Table 2; with **L5**, 71% NMR yield] The product **3e** was isolated by flash chromatography on silica gel with elution (hexane/EtOAc, 95:5) as colorless oil (74.0 mg contaminated with benzyl butyrate which was formed via dehaloprotonation of **1i**, **3e**/benzyl butyrate = 90/10 based on ^{1}H NMR analysis, 62% yield of **3e**). **^{1}H NMR** (400 MHz, $CDCl_3$): δ 7.38–7.30 (m, 5H), 5.12 (s, 3H), 4.72 (s, 1H), 4.67 (s, 1H), 2.36 (t, J = 7.3 Hz, 2H), 2.04 (t, J = 7.3 Hz, 2H), 1.80 (quin, J = 7.3 Hz, 2H), 1.70 (s, 3H). **^{13}C NMR** (100.5 MHz, $CDCl_3$): δ 173.4, 144.7, 136.0, 128.5, 128.1, 110.6, 66.1, 36.9, 33.6, 22.6, 22.1. **IR** (ATR): 3070, 3034, 2937, 1733, 1498, 1455, 1376, 1143, 994, 888, 735, 696 cm^{-1}. **HR-FDMS** (*m*/z): $[M]^+$ Calcd for $C_{14}H_{18}O_2$ 218.13068; found, 218.12962.

1-(4-Cyclopentylphenyl)ethan-1-one (3f)

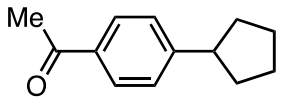

[Table 2; with **L3**, 85% NMR yield] The product **3f** was isolated by flash chromatography on silica gel with elution (hexane/EtOAc, 100:0–95:5) as colorless oil (72.4 mg, 77% yield). **^{1}H NMR** (400 MHz, $CDCl_3$): δ 7.89 (d, J = 8.7 Hz, 2H), 7.33 (d, J = 8.2 Hz, 2H), 3.11–2.99 (m, 1H), 2.59 (s, 3H), 2.15–2.04 (m, 2H), 1.89–1.78 (m, 2H), 1.78–1.66 (m, 2H), 1.66–1.55 (m, 2H). **^{13}C NMR** (100.5 MHz, $CDCl_3$): δ 197.8, 152.5, 134.8, 128.4, 127.2, 45.9, 34.4, 26.5, 25.5. Spectral data match those reported in the literature.[10]

4-Phenyl-1-tosylpiperidine (3g)

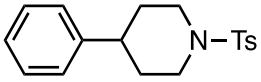

[Table 2; **1a** (0.75 mmol), **2e** (0.50 mmol) with **L3**, 63% NMR yield] The product **3g** was isolated by flash chromatography on silica gel with gradient elution (hexane/EtOAc, 95:5–85:15) and recrystallization with CH_2Cl_2/hexane as needle-like crystal (75.4 mg, 48% yield). **^{1}H NMR** (400 MHz, $CDCl_3$): δ 7.68 (d, J = 8.2 Hz, 2H), 7.35 (d, J = 8.2 Hz, 2H), 7.29 (dd, J = 7.8, 6.9 Hz, 2H), 7.21 (t, J = 7.3 Hz, 1H), 7.14 (d, J = 7.3 Hz, 2H), 3.93 (d, J = 11.5 Hz, 2H), 2.45 (s, 3H), 2.43–2.27 (m, 3H), 1.95–1.77 (m, 4H). **^{13}C NMR** (100.5 MHz, $CDCl_3$): δ 144.9, 143.5, 133.0, 130.0, 128.6, 127.7, 126.6, 46.8, 41.8, 32.5, 21.5. Spectral data match those reported in the literature.[11]

(±) *tert*-Butyl-2-phenylpyrrolidine-1-carboxylate (6a)

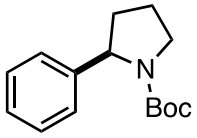

[Table 3; with **L3**, 87% NMR yield] The product **6a** was isolated by flash column chromatography on silica gel (hexane/EtOAc, 90:10) as colorless oil (19.0 mg, 77% yield, 2.2:1 rotameric mixture). **^{1}H NMR** (400 MHz, $CDCl_3$, rotameric mixture): δ 7.35–7.05 (m, 5H), 4.95 and 4.75 (brs, 1H, rotamer), 3.70–3.40 (m, 2H), 2.40–2.18 (m, 1H), 2.00–1.75 (m, 3H), 1.55–1.05 (m, 9H). **^{13}C NMR** (100.5 MHz, $CDCl_3$, rotameric mixture, resonances for the minor rotamer are enclosed in parentheses): δ 154.6, 145.1, (128.3) 128.1, 126.4, 125.5, 79.1, 61.3 (60.6), (47.3) 47.1, 36.0 (34.8), (28.5) 28.1, (23.4) 23.2. Spectral data match those reported in the literature.[12]

(±) *tert*-Butyl-2-(4-methoxyphenyl)pyrrolidine-1-carboxylate (6b)

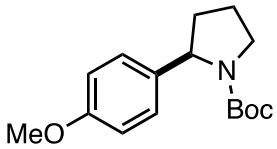

[Table 3; with **L3**, 72% NMR yield] The product **6b** was isolated by flash column chromatography on silica gel (hexane/EtOAc, 90:10) as colorless oil (19.6 mg, 71% yield, 2:1 rotameric mixture). **^{1}H NMR** (400 MHz, $CDCl_3$, rotameric mixture): δ 7.08 (d, J = 8.4 Hz, 2H), 6.83 (d, J = 8.4 Hz, 2H), 4.91 and 4.73 (brs, 1H, rotamer), 3.80 (s, 3H), 3.70–3.38 (m, 2H),

2.39–2.13 (m, 1H), 2.00–1.71 (m, 3H), 1.54–1.09 (m, 9H). **^{13}C NMR** (100.5 MHz, $CDCl_3$, rotameric mixture, resonances for the minor rotamer are enclosed in parentheses: δ 158.2, 154.6, 137.3, 126.6, (113.7) 113.4, 79.1, 60.7 (60.1), 55.2, (47.2) 47.0, 36.0 (34.8), (28.5) 28.2, (23.4) 23.1. Spectral data match those reported in the literature.[6]

(±) *tert*-Butyl-2-(prop-1-en-2-yl)pyrrolidine-1-carboxylate (6c)

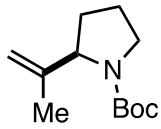

[Table 3; with **L3**, 52% NMR yield] The product **6c** was isolated by flash column chromatography on silica gel (hexane/EtOAc, 95:5) as colorless oil (9.5 mg, 45% yield, 1.3:1 rotameric mixture). **^{1}H NMR** (400 MHz, $CDCl_3$, rotameric mixture): δ 4.86–4.62 (m, 2H), 4.24 and 4.15 (brs, 1H, rotamer), 3.55–3.25 (m, 2H), 2.10–1.92 (m, 1H), 1.92–1.65 (m, 6H), 1.55–1.35 (m, 9H). **^{13}C NMR** (100.5 MHz, $CDCl_3$, rotameric mixture, resonances for the minor rotamer are enclosed in parentheses): δ 154.7 (154.4), 146.1 (145.3), 109.0, 79.0, 62.2 (61.9), (46.9) 46.5, 31.3 (30.4), (28.5) 28.4, (23.5) 22.9, (19.3) 19.1. Spectral data match those reported in the literature.[13]

References

[1] J. B. Diccianni, T. Diao, *Trends Chem.* **2019**, *1*, 830–844

[2] M. M. Beromi, G. W. Brudvig, N. Hazari, H. M. C. Lant, B. Q. Mercado, *ACIE*, **2019**, *58*, 6094–6098.

[3] B. J. Shields, B. Kudisch, G. D. Scholes, A. G. Doyle, *J. Am. Chem. Soc.* **2018**, 140, 3035–3039.

[4] P. Ma, S. Wang, H. Chen, *ACS Catal.* **2020**, *10*, 1–6.

[5] D. A. Everson, B. A. Jones, D. J. Weix *J. Am. Chem. Soc.* **2012**, *134*, 6146−6159.

[6] The use of *N,N′*-dimethylpropyleneurea (DMPU), which had proved to be an effective solvent in the Weix's report (ref 5), gave ligand effects similar to those with DMA. The reaction using **L5** in DMPU gave **3a** in 85% yield along with 3% of **4**. When bpy was used as a ligand, the formation of **4** (29%) was substantially suppressed although the

yield of **3a** was as moderate as 40%.

[7] Z. Zuo, D. T. Ahneman, L. Chu, J. A. Terrett, A. G. Doyle, D. W. C. MacMillan *Science* **2014**, *345*, 437–440.

[8] S. Gisbertz, S. Reischauer, B. Pieber, *Nature catalysis*, **2020**, *3*, 611–620.

[9] No ligand exchange was observed by ^{1}H NMR spectroscopy after Ir[dF(CF_3)ppy]$_2$(4,4'-*t*Bu$_2$bpy)PF_6 was treated with **L3** (1:1 ratio) in $CDCl_3$ at room temperature for 2 h.

[10] S. D. Dreher, P. G. Dormer, D. L. Sandrock, G. A. Molander, *J. Am. Chem. Soc.* **2008**, *130*, 9257–9259.

[11] R. R. Merchant, J. T. Edwards, T. Qin, M. M. Kruszyk, C. Bi, G. Che, D.-H. Bao, W. Qiao, L. Sun, M. R. Collins, O. O. Fadeyi, G. M. Gallego, J. J. Mousseau, P. Nuhant, P. S. Baran, *Science* **2018**, *360*, 75–80.

[12] S. Liang, X. Zhao, T. Yang, W. Yu, *Org. Lett.* **2020**, *22*, 1961–1965.

[13] C. Kong, N. Jana, T. G. Driver, *Org. Lett.* **2013**, *15*, 824–827.

Publication

[1] Y. Kim, T. Iwai, S. Fujii, K. Ueno, M. Sawamura, *Chem. Eur. J.*, *in press* (doi.org/10.1002/chem.202004053)

Acknowledgement

The studies described in this thesis have been carried out under the direction of Professor Masaya Sawamura at Graduate School of Chemical Science and Engineering, Hokkaido University from April 2018 to March 2021.

The author would like to express the deepest appreciation to Professor Masaya Sawamura for providing him this valuable research opportunity, helpful discussion, and kind encouragement. He is deeply grateful to Assistant Professor Tomohiro Iwai for his kind supports and precious discussions. He also wish to express his deepest appreciation to Associate Professor Yohei Shimizu, Assistant Professor Fernando Arteaga Arteaga, Specially Appointed Assistant Professor Kosuke Higashida and Specially Appointed Assistant Professor Ronald Lazo Reyes for their valuable advices, deep discussion, and kind supports.

The author is much grateful to Professor Keiji Tanino, Professor Hajime Ito for their insightful comments and considerable suggestions on this thesis.

Moreover, the author would like to express his appreciation to Professor Kosei Ueno and Assistant Professor Sho Fujii for the collaboration performing the important analytical studies in Chapter 1. He also thanks to Mr. Zhang, Mr. Ueda, Mr. You and other members in Prof. Sawamura's group for the continuous encouragements and the helpful supports.

Financial support from Hokkaido University Ambitious Leader's Program was indispensable and the author sincerely appreciates this support.

Finally, the author expresses his gratitude for his family, Ms. Sangsoon Lee, Mr. Imsoo Kim, Ms. Dayoung Kim for their warm encouragement.